TECHNISCHE
UNIVERSITÄT
DARMSTADT

Physik

Functional coatings with colorimetric properties: the influence of electrostatic interaction and hydrogen bonding on the assembly of gold nanoparticles in polymer brushes

vom Fachbereich Physik
der Technischen Universität Darmstadt

zur Erlangung des Grades
Doktor rerum naturalium
(Dr. rer. nat.)

Dissertation
von Dikran Boyaciyan

Erstgutachterin: Prof. Dr. Regine von Klitzing
Zweitgutachter: Prof. Dr. Markus Biesalski

Darmstadt 2018

Boyaciyan, Dikran: Functional coatings with colorimetric properties: the influence of electrostatic interaction and hydrogen bonding on the assembly of gold nanoparticles in polymer brushes
Darmstadt, Technische Universität Darmstadt
Jahr der Veröffentlichung der Dissertation auf TUprints: 2019
URN: urn:nbn:de:tuda-tuprints-83595
Tag der mündlichen Prüfung: 17.12.2018

TECHNISCHE
UNIVERSITÄT
DARMSTADT

Erklärung gemäß §9 Promotionsordnung

Hiermit versichere ich, dass ich die vorliegende Dissertation selbstständig angefertigt und keine anderen als die angegebenen Quellen und Hilfsmittel verwendet habe. Alle wörtlichen und paraphrasierten Zitate wurden angemessen kenntlich gemacht. Die Arbeit hat bisher noch nicht zu Prüfungszwecken gedient.

Datum und Unterschrift

Without commitment you will never start
but more importantly without consistency you will never finish.

– Denzel Washington –

Acknowledgements

First of all, I would like to thank Prof. Regine von Klitzing for the opportunity to do my Ph.D in her group, and for all the helpful discussions and her advice during my stay in her group.

I want to thank Prof. Jan Genzer for giving me the opportunity to come to his lab at NC State. Spending 6 month abroad was a wonderful experience during my Ph.D, not only from a scientific point of view but also personally.

I would also like to thank my colleagues who helped me during my neutron beamtime as well as with their knowledge in the interpretation of those neutron data, Larissa Braun, Oliver Löhmann, Dr. Stephanie Christau, Dr. Samantha Micciulla, Markus Trapp, and Luca Silvi.

I would like to acknowledge Patrick Krause, who was a student assistant during my stay at the TU Berlin. Further, Maren Lehmann and Markus Witt for helping me with the TEM measurements.

My gratitude goes to all of my colleagues who moved last year from Berlin to Darmstadt. It was quite tough but we could manage to move our whole lab and during this time we became all technicians, lab manager, and secretaries :-).

Thanks to the IRTG at the TU Berlin, namely Prof. Martin Schön, Dr. Daniela Fliegner, Petra Erdmann, and Beatrix Thiele. All this would not have been possible without you. Also I would like to thank the TU Darmstadt as well for financial support.

Big thank goes also to all of my friends, which is always fun to hang around and let forget about science.

And last but not least, I would like to express my deepest love and thanks to my family for their endless support during my studies and my life. Without your help I would not have made it this far.

Persönlicher Werdegang

Name : Dikran Boyaciyan (ehemals Kesal)

Geburtstadatum: 08.01.1988

Geburtsort: Berlin

Nationalität: deutsch

03/2017 – heute Promotionsstudium im Arbeitskreis von Regine von Klitzing, Festkörperphysik, TU Darmstadt, Deutschland

01/2015 – 02/2017 Promotionsstudium in Intl. Graduate Research Training Group 1524 (IRTG 1524, Stipendium) im Arbeitskreis von Regine von Klitzing, Stranski-Laboratorium für physikalische und theoretische Chemie, TU Berlin, Deutschland

05/2016 – 12/2016 Auslandsaufenthalt im Arbeitskreis von Jan Genzer, North Carolina State University, Raleigh, USA

Forschungsthema: "Impact of an Applied Electric Field on the Uptake of Gold Nanoparticles into Polymer Brushes"

03/2012 – 12/2014 Masterstudium in Chemie, TU Berlin. Schwerpunkt: Physikalische Chemie

05/2014 – 11/2014 Masterarbeit im Arbeitskreis von Tommy Nylander, Department of Chemistry at the Lund University, Lund, Schweden

Master thesis: "Interaction of Lipid Bilayer Systems on Nanowire Arrays"

10/2009 – 02/2012 Bachelorstudium in Chemie, TU Berlin

Bachelorarbeit: "Benetzung von strukturierten Oberflächen durch Tensidsysteme"

Abstract

The modification of surfaces with thin films is widely used to tailor physical and chemical properties of surfaces. This approach can provide "smart" surfaces with desired tunable properties. Polymer brushes represent a class of thin films, where the polymer chains are chemically end-grafted to the substrate. The chain functionality can be tailored by chemical composition, which allows the brushes to respond to external stimuli. In addition, polymer brushes may sterically stabilize colloids. Thus, polymer brushes are suitable candidates as a matrix for the incorporation of inorganic nanoparticles, like gold nanoparticles (AuNPs). AuNPs induce optical properties due to their surface plasmon resonance (SPR), which results in smart nanocomposite materials with tunable optical properties for the application as colorimetric sensors. The ability to control the particle amount and distribution within a brush matrix has a strong impact on fabrication of colorimetric sensors with optical properties on demand.

In order to achieve brush/AuNP composites with desired properties, the thesis focuses on the impact of electrostatic interaction and hydrogen bonding on the formation of brush/AuNP composite materials. Here, pH-sensitive AuNPs are embedded into strong cationic and non-ionic polymer brushes. The electrostatic interactions and hydrogen bondings are tuned by changing the surface charge of the AuNPs through variations of pH value, while the charges of the brushes are not affected.

The first part of the present thesis presents the assembly of pH-sensitive AuNPs into cationic polyelectrolyte brushes. In particular, the synergistic use of different characterization techniques clarify directly and indirectly effects of the electrostatic interaction on the structure, morphology and sensitivity of cationic brush/AuNP composites.

The second part discusses the influence of using a non-ionic polymer brush on the assembly of pH-sensitive AuNPs. It is shown, that the nature of polymer brush has a crucial impact on the stabilization of incorporated AuNPs. This work demonstrates a novel approach to incorporate negatively charged AuNPs into non-ionic polymer brushes by using an electric field.

Finally, the quality of brush/AuNP composites was experimental evaluated in terms of the long-term stability for the future prospect as colorimetric sensors.

The thesis presents a fundamental understanding of smart coatings, where the particle-particle interaction as well as particle-brush interaction can be simply controlled by variation in pH value and governs their structure and responsive behavior.

Zusammenfassung

Die Modifikation von Oberflächen mit dünnen Filmen kann genutzt werden um deren physikalische sowie chemische Eigenschaften nach Belieben zu ändern. Oberflächenmodifikationen dieser Art können zu "intelligenten" Materialien führen, welche breite Anwendung in der Wissenschaft findet. Polymerbürsten stellen eine Klasse von dünnen Filmen dar, bei denen Polymerketten chemisch auf ein Substrat aufgepfropft werden. Die Kettenfunktionalität kann je nach chemischen funktionellen Gruppen im Polymer maßgeschneidert werden und erlaubt der Polymerbürste auf äußere Umgebungsparameter zu reagieren. Zudem können Polymerbürsten auch genutzt werden um Kolloide sterisch und elektrostatisch zu stabilisieren. Daher sind Polymerbürsten hervorragende Kandidaten für die Einbettung von anorganischen Nanopartikeln wie z.B. von Goldnanopartikeln. Goldnanopartikel besitzen optische Eigenschaften, die auf ihre Oberflächenplasmonenresonanz zurückzuführen sind und der Polymermatrix optische Eigenschaften verleihen. Daraus resultieren "intelligente" Nanokompositmaterialien mit regelbaren optischen Eigenschaften, welche als kolorimetrische Sensoren verwendet werden können. Die optischen Eigenschaften lassen sich durch die Partikelmenge und Partikelverteilung innerhalb der Bürstenstruktur kontrollieren. Somit können verschiedenartige kolorimetrische Sensoren je nach Wunsch hergestellt werden.

Der Schwerpunkt dieser Arbeit liegt auf den Einfluss der Wechselwirkung zwischen Goldpartikel und Polymerbürste auf die Bildung von Polymerbürsten/Goldnanopartikel Kompositmaterialien. Hierzu wurden pH-sensitive Goldnanopartikel in stark positiv geladenen sowie ungeladenen Polymerbürsten eingebettet. Die elektrostatischen Wechselwirkungen wurden durch pH-Wert-Änderungen variiert. Die Änderung des pH-Werts wirkt sich auf die Oberflächenladung der Goldnanopartikel aus, aber hat keinen Einfluss auf die Ladungen der Polymerbürste.

Der erste Teil der Arbeit zeigt den erfolgreichen Einbau von pH-sensitiven Goldnanopartikeln in kationische starke Polyelektrolytbürsten. Mit Hilfe von verschiedenen Charakterisierungstechniken konnten die direkten und indirekten Effekte der elektrostatischen Wechselwirkung auf die Struktur und Morphologie der kationischen Bürsten/Goldnanopartikel Komposite geklärt werden. Zudem wurde das Quellverhalten bei Variation der Umgebungsparameter untersucht.

Der zweite Teil dieser Arbeit beschreibt die Einlagerung von pH-sensitiven Goldnanopartikeln in ungeladenen Polymerbürsten. Es konnte gezeigt werden, dass der Polymerbürstentyp eine wesentliche Auswirkung auf die Stabilisierung von eingebetteten Goldnanopartikeln hat. Darüber hinaus wurde ein neuer Ansatz durchgeführt um die elektrostatischen Wechselwirkungen zwischen Goldnanopartikel und Polymerbürste zu verbessern. Hierbei

wurde ein elektrisches Feld verwendet um die negativ geladenen Goldnanopartikel in die ungeladene Polymerbürste einzubauen.

Als letzes wurde die Qualität der Polymerbürste/Goldnanopartikel Komposite hinsichtlich ihrer Langzeitstabilität experimentell bewertet, um zu überprüfen, ob sich die Komposite als kolorimetrische Sensoren einsetzten lassen.

Die Arbeit präsentiert ein fundamentales Verständnis von "intelligenten" Beschichtungen in denen die Partikel-Partikel Wechselwirkung sowie Partikel-Polymerbürsten Wechselwirkung durch eine Änderung des pH-Wertes kontrolliert werden kann. Hiermit lässt sich nicht nur die Struktur dieser Komposite sondern auch die Antwort auf äußere Umgebungsparameter kontrollieren.

Contents

List of symbols and abbreviations

Symbols and Abbreviations

AuNP	Gold nanoparticle
PMETAC	Poly(2-(methacryloyloxy)ethyltrimethylammonium chloride)
PNIPAM	Poly(N-isopropylacrylamide)
PDMAEMA	Poly(N,N-dimethylaminoethyl)methacrylate
PMMA	Poly(methyl methacrylate)
BTPAm	2-bromo-2-methyl-N-(3-(triethoxysilyl)propyl)propan- amide
e-BMPUS	11-(2-bromo-2-methyl) propionyloxy) undecyl trichlorosilane
SI-ATRP	Surface-initiated atom transfer radical polymerization
MPA	3-Mercaptopropionic acid
Si	Silicon
NR	Neutron reflectivity
XRR	X-ray reflectivity
AFM	Atomic-force microscopy
TEM	Transmission electron microscopy
SEM	Scanning Electron Microscopy
SLD	Scattering length density
SPR	Surface plasmon resonance
UV/Vis	Ultraviolet/visible
UVO	Ultraviolet/ozone
LCST	Lower critical solution temperature
R	Reflectivity
F	Free energy
N	Degree of polymerization
R_g	Radius of gyration
Σ	Reduced tethered density
σ_{ext}	Extinction cross-section
ϵ	Dielectric constant
rh	Relative humidity
ρ_e	Electron density
σ	Grafting density
q_z	Perpendicular momentum transfer
Θ_i	Volume fraction of component i
σ_{RMS}	Root-mean-square roughness
h	Thickness
λ	Wavelength

*Non-essential and empirical parameters are not included

Chapter 1

Introduction

Surface modification with polymers is useful for developing nanomaterials with customized properties. Prominent examples are polymer brushes consisting of polymer chains, which are chemically end-grafted to a substrate. They can be applied to flat, spherical, or porous substrates. The surface properties can be easily tailored by changing the chain functionality. Their potential, in particular, lies in their sensitivity to external stimuli, which allows them to be suitable for numerous technological applications. Due to the optical transparency of the polymer brushes, one promising application are colorimetric sensors realized by embedding optically functional nanoparticles into stimuli-responsive polymer brushes. For instance, Gold nanoparticles (AuNPs) exhibit a surface plasmon resonance (SPR), so that environmental changes can be detected spectroscopically. To enable the use of polymer brushes as colorimetric sensors, it is crucial to know how to control the loading capacity and distribution of AuNPs in polymer brushes, which in turn trigger different optical responses. Furthermore, the long-term stability of those composite materials is also of interest.

The focus of this thesis is to understand (1) the effect of electrostatic interaction and hydrogen bonding on the uptake and distribution of pH-sensitive AuNPs in cationic and non-ionic polymer brushes, (2) the responsive properties after the incorporation of AuNPs in cationic and non-ionic polymer brushes and (3) the stability of polymer brush/AuNP composites for their use as colorimetric sensors.

The thesis is divided into three main parts. The first part (Chapter 4 - 7) of the present thesis deals with the uptake and distribution of pH-sensitive AuNPs into cationic polyelectrolyte brushes. The second part (Chapter 8 and 9) investigates the impact of using a non-ionic polymer brush on the assembly of the same pH-sensitive AuNPs. And the third part (Chapter 7 and Chapter 9) discusses the qualitiy of the prepared brush/AuNP composites in terms of the long-term stability. In particular, Chapter 4 discusses the effect of electrostatic interaction between pH-sensitive AuNPs and cationic poly-[2-(Methacryloyloxy) ethyl] trimethylammonium chloride (PMETAC) brushes on the loading capacity at different pH values. Next, Chapter 5 addresses the pH-triggered distribution and relocation of pH-sensitive AuNPs in cationic PMETAC brushes. PMETAC/AuNPs composite materials are investigated in aqueous conditions and at different humidites using neutron and X-ray reflectometry (NR and XRR), respectively. Here, NR measurements are conducted in D_2O and analyzed using a step-like fitting model. Chapter 6 elucidates the internal structure of PMETAC/AuNP composites by using NR with contrast variation. The use of

self-consistent reflectivity analysis based on the analytical parametrization of the volume fraction profiles of all chemical components provides the volume fraction of all tested chemical compositions. This approach yields more detailed information on the internal structure of the composites, which is useful for the future design of PMETAC/AuNP composites. Regarding the optical response, the effect of different pH values on PMETAC/AuNP composites as a post-treatment for shifting the SPR band is subject of Chapter 7. Furthermore, the future prospect for the long-term use as colorimetric sensors was tested. The last two Chapters (8 and 9) addresses the question what influence has a change in the nature of the polymer brush material by using a non-ionic poly(N-isopropylacrylamide) (PNIPAM) brush on the assembly formation of the same pH-sensitive AuNPs that has been used before. In Chapter 8, the pH value during the incubation of PNIPAM brushes in AuNP suspension is changed in a systematic manner from pH 4 to pH 8. The uptake and distribution are investigated by atomic-force microscopy (AFM), UV/Vis, and scanning electron microscopy (SEM). Since PNIPAM does not bear any charges while AuNPs are pH-sensitive, it is very important to consider the interaction strength that alters with a change in the pH value. It is expected that at high pH AuNPs tend to be rather negatively charged and do not interact with the uncharged PNIPAM brush. Regarding this issue, the assembly of negatively charged AuNPs at pH 8 in non-ionic PNIPAM brushes is studied lastly under an applied electric field in Chapter 9. In order to enhance the uptake and penetration of AuNPs into the PNIPAM brush matrix, artificial charges along the substrate were created by an electric field to drag the AuNPs inside the brush.

Chapter 2

Scientific background

The scope of this chapter is to present a broad scientific background about the materials that have been used in this thesis. Here, polymer brushes (neutral and charged) and AuNPs will be discussed separately from a theoretical and experimental point of view. The last section of this chapter discusses the theoretical predictions as well as experimental work of the assembly of inorganic nanoparticles in polymer brushes and also their use for sensor applications.

2.1 Polymer Brushes

Polymer brushes are polymers tethered to a surface or interface by one end, which at sufficiently high grafting densities show a stretched conformation[1–4]. This stretching is often responsive to environmental conditions and that makes them a suitable candidate for the design of smart coatings[5–9]. In general, these coatings can be applied to surfaces, regardless of their curvature[10–14] or porosity[15–17] and their properties can be easily tailored by changing the chain functionality of the polymer[18–20]. Polymer brushes can be synthesized through the surface-initiated atom transfer radical polymerization (SI-ATRP)[21,22], which is a controlled radical polymerization technique (detailed synthesis procedure is explained in Section 3.2.2). Matyjaszewski and coworkers introduced ATRP in 1995[23] and its preferred use is based on the fact that ATRP performs at room temperature[24] and in aqueous solution[25–27]. Polymerization of chains from surfaces is similar to bulk polymerization, except that the initiator is deposited onto the substrate surface rather than floating freely in solution. This approach has been termed "grafting from" polymerization. Alternatively, polymer in bulk or in solution contain a specific functionality (usually at the chain end) that adsorbs chemically onto the substrate from that functional group. Since the chains move from the solution to the surface, this approach is called "grafting to" method. The choice for one grafting technique over the other depends on the application of the brush. Since the "grafting from" method produces denser brushes, the polymer chains tend to have a greater polydispersity[28,29].

Regardless of the polymer brush synthesis technique, the chain conformation of surface-initiated brushes is distinctly different from chains in solution due to the presence of adjacent polymer chains. Polymer brushes exhibit many novel and various properties compared to chains in solution and this make them an interesting field for novel properties[30–32]. The

brush conformation of neutral brushes with respect to the grafting density and solvent quality will be discussed in the next section.

2.1.1 Neutral brushes

Theoretical fundamentals

The first theoretical description of the brush structure was derived in the work of Alexander[33]. For uniformly absorbed polymers, the film thickness h is smaller than the free polymer radius of gyration R_g[34]. The thickness of end-grafted polymers, however, have the opposite behavior compared to uniformly absorbed polymers at increased grafting density, where the chain-chain interaction dominates. The distance between tethering points is smaller than the size of the polymer chain and it reflects the start of the interaction between grafted chains. Applying the "Flory theory" for polymer chains in solution to polymer brushes, the brush conformation (brush free energy, F_{brush}) is derived as the balance between the elastic energy of an entropic spring (difference between stretched and unstretched polymer chains), F_{el}, and an excluded volume repulsion between segments (interaction energy), F_{int}. Polymer chains are considered to be ideal and their elastic energy increases quadratically with their end-to-end distance, which is represented by the brush film thickness. In contrast, the excluded volume originates from uniformely distributed monomer segments and is proportional to their volume fraction. The total free energy of a single polymer chain in the brush can be written as follows

$$F \;=\; F_{el} + F_{int} \;=\; k_b T \left[\frac{3h^2}{2Na^2} + \frac{v_{ex} N^2 \sigma}{h} \right] \tag{2.1}$$

in which a is the monomer diameter, v_{ex} is the excluded volume, N is the degree of polymerization, and σ is the grafting density (number of chains per area). By minimization with respect to the thickness (See Figure 2.1), following relationship can be obtained for the height h of neutral brushes

$$h \;\propto\; N\sigma^{\nu} \tag{2.2}$$

in which ν is the power law exponent and scales with 1/3 for brushes in a good solvent. A similar relationship was also obtained by de Gennes through simple scaling analysis where polymers in the brush were considered as a series of tension blobs with their steric

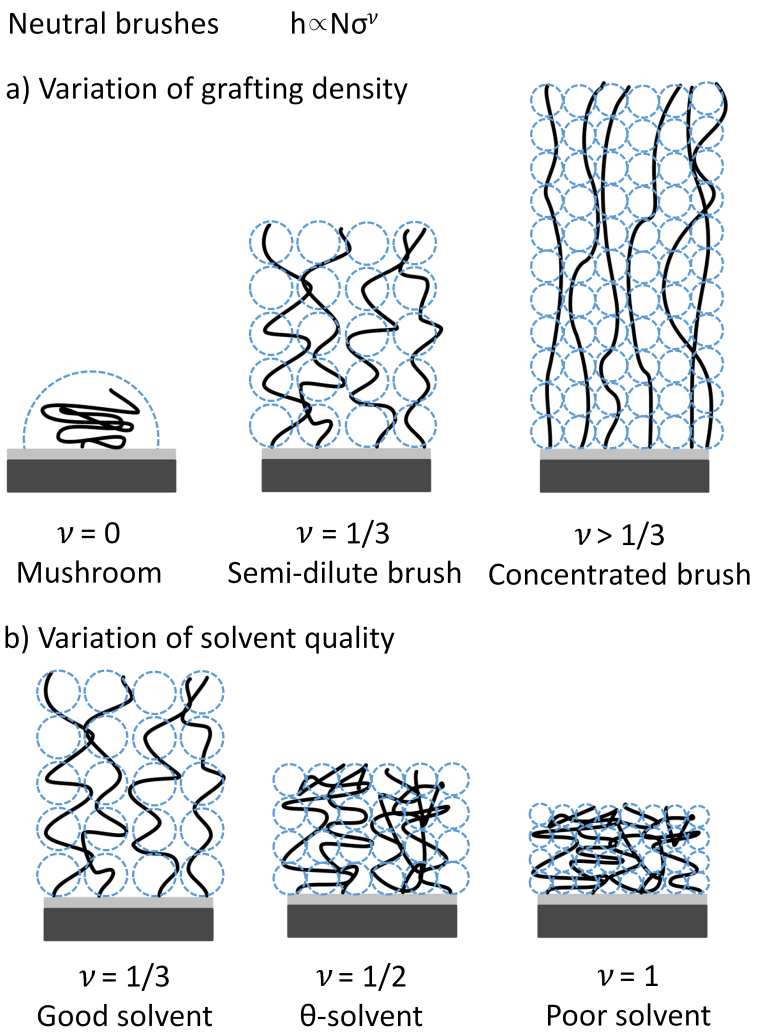

Figure 2.1: Scheme of scaling laws of neutral brushes with variation of the power law exponent ν at different conditions.

interaction determining the conformation of the brushes[35]. This led to correlation length of polymer chains in the brush to be the distance between grafting points which is equal to $\sigma^{-1/2}$ and is the same in the work of Alexander[33]. This description is then referred to as an Alexander-de Gennes brush, and it is the most basic model for a brush. One important difference between polymer brushes to free polymers is that the brush dimension is proportional to N instead of $N^{1/2}$ in its free form (gaussian coil). For the chains in the brush, their length could be much larger than R_g due to steric deformation leading to properties that are distinct from free polymers.

Similarly, the thickness scaling laws for polymer brushes in a θ-theta solvent and poor solvent were also derived[36–38]. The power law dependence of the thickness on grafting

density increases from 1/3 to 1/2 to 1 as the solvent quality decreases from good to θ-solvent to poor solvent. In contrast, the dependence on the molecular weight remains constant at N. A similar increase on the dependence could be obtained when the grafting density is further increased from moderate grafting density to high grafting density. At high surface coverage, the excluded-volume effect between segments becomes fully screened like concentrated polymer solutions, and higher order interactions become important. In some cases, the brush height scaling relationship could exhibit a higher power law exponent dependence than 1/3, and it may even be as high as 1 [36,39,40]. Such brushes are defined as a "concentrated brush" in contrast to the "semidilute brush" where excluded volume repulsion dominates.

Alexander-de Gennes brush theory also depicts the brush density profile. In their model a step-like density profile of the polymer brush was assumed, which leads to a constant density inside the polymer brush. Also it was assumed that all polymer chains are equally stretched resulting in the polymer chain ends to be at an equal distance to the surface.

A more detailed model for polymer brushes was described independently by Milner et al. [41–43], Skvortsov et al. [44], and Zhulina et al. [45] using self-consistent field theory. As a result, the brush density profile is a parabola and the chain free-end would not have its maximum concentration at the edge of the brushes. The brushes would have stronger excluded volume repulsion in the deeper layers compared to the Alexander-de Gennes model. More detailed comparison between these two models has been discussed elsewhere [46] and will not be addressed here.

Experimental studies on brush conformation

A commonly used literature parameter for the quantitative experimental characterization of the transition from the low grafting density "mushroom" state to the "brush" state is the reduced tethered density Σ [47]. It is expressed as

$$\Sigma = \sigma \pi R_g^2 \tag{2.3}$$

where R_g is radius of gyration of a tethered chain at specific experimental conditions of solvent and temperature. The definition of the grafting density, σ, is determined by $\sigma = (h\rho N_A)/M_n$ (h, brush thickness; ρ, bulk density of the brush composition; and N_A, Avogadro's number). The physical interpretation of Σ is the number of chains that occupy

an area that a free non-overlapping polymer chain would normally fill under the same experimental conditions.

Based on experimental results, the "mushroom" or weakly interacting regime is found for $\Sigma < 1$, the crossover regime is at $\Sigma \approx 1$, and the highly stretched regime is at $\Sigma > 1$. However, the "true brush" regime is typically characterized by around $\Sigma > 5$, which is a rough average of several studies. Just to note, on real systems the transition between single grafted chains and a polymer brush is less sharp because of the statistical characteristic of grafting and polydispersity of the tethered chains[48,49].

2.1.2 Charged brushes

Charged brushes, which are also known as polyelectrolyte brushes, have different properties compared to neutral brushes. In addition, interactions due to charges must be considered, which increases the complexity of polyelectrolyte brushes. Furthermore, the interactions can be altered when the surrounding environment of the polyelectrolyte brushes is changed[50]. If the charges on the brush are not permanently associated with certain chemical groups, the pH of its surrounding can control the charge ratio of the brushes and determine their behavior. Those polyelectrolyte brushes are referred to as "weak" polyelectrolyte brushes. In comparison, "strong" polyelectrolyte brushes cannot be influenced by pH, since the charges along the chain are permanent and are associated with strong acid/base groups. This section will focus only on the strong polyelectrolyte brushes. In salt-free solution, the brush thickness is independent of the grafting density and only proportional to the molecular weight and the square root of the fraction of charged monomers f [51]. This so-called "osmotic brush" results from an increased osmotic pressure within the brush caused by the counterions[52] (Figure 2.2). The equation describing the height of these brushes is expressed as

$$h \propto N f^{1/2}. \tag{2.4}$$

Adding electrolytes to the polyelectrolyte brushes turns them into the so-called "salted brushes" where the charges are screened (Figure 2.2). The transformation happens when the electrolyte concentration of the solution, C_s, equals the concentration inside the polyelectrolyte brushes, where the osmotic pressure is decreased by the penetration of electrolytes[52]. The scaling of the height of salted brushes is expressed by

$$h \propto N\sigma^{1/3}C_s^{-1/3}. \tag{2.5}$$

To model brushes with low or moderate charge densities and brushes outside the high grafting density regime, the Pincus brush was developed (Figure 2.2). Under such conditions it cannot maintain its charge neutrality, hence charge repulsion is dominant. It is described as

$$h \propto N^3\sigma f^2. \tag{2.6}$$

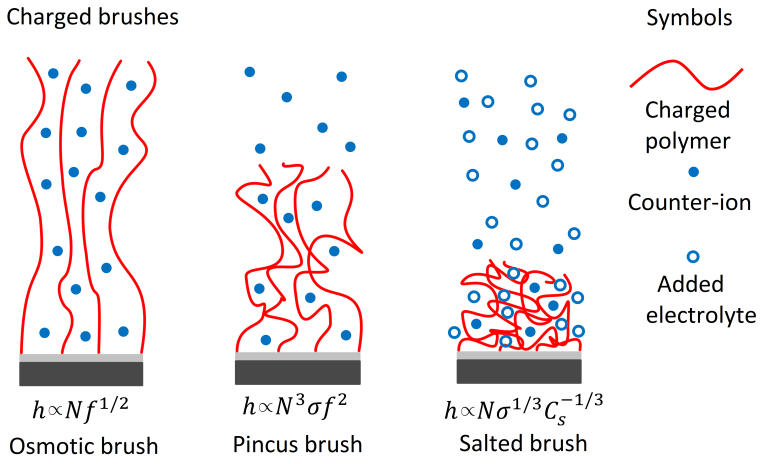

Figure 2.2: Scaling laws for charged bruses under different conditions.

2.1.3 Sensitivity of polymer brushes to external stimuli

When it comes to application of polymer brushes, the conformation of brushes plays an important role. Assuming polymer brushes in a good solvent and with a sufficient grafting density for chain extension, the conformation can also be controlled with respect to their sensitivity to external stimuli (Figure 2.3). The sensitivity can be tailored by using different chemical compositions and thus triggers the brushes responding to different external stimuli like temperature[53–55], pH[56–58], ionic strength[59–62] or solvent[63–65]. Due to their responsive nature, brushes are highly applicable to be used as "smart" materials. They can be found in many applications for coatings, for instance as antifouling surfaces in biotechnological applications[30–32]. They are also potential candidates for drug delivery systems[66–68] or can regulate interactions between a surface and liquids, solids, proteins, or cells[69,70].

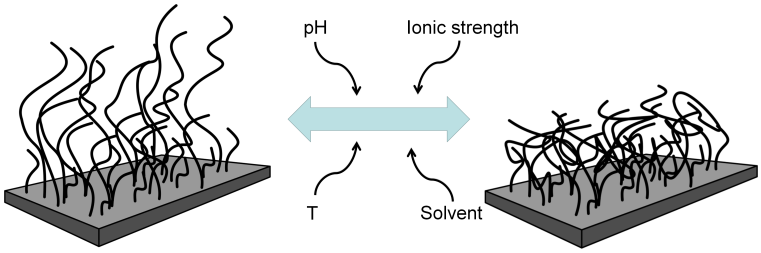

Figure 2.3: Polymer brushes are end-grafted polymer chains. Depending on the polymer chemistry, they can respond to different external stimuli by conformational changes.

Besides the sensitivity, polymer brushes are capable of serving as a matrix for the incorporation of inorganic nanoparticles. In fact, they increase the sterically stabilization of colloids if the interaction between polymer and particles is strong[71]. Using gold nanoparticles (AuNPs) results in smart nanocomposite materials with tunable optical properties for application as sensors, since AuNPs can interact with light[72]. The next section discusses the preparation and properties of AuNPs.

2.2 Gold Nanoparticles (AuNPs)

Nanoparticles are nowadays widely used in the material science for a huge variety of applications[73,74] with respect to their material and shape. However, this section will only deal with the preparation and properties of spherical AuNPs.

2.2.1 Preparation of AuNPs

Regarding the synthesis of colloidal AuNP suspensions several techniques are established. An early one is the method by Turkevich et al.[75] leading to citrate capped AuNPs, where the citrate acts as both reducing and stabilizing agent. Frens further refined this method by varying the gold-to-citrate ratio to control particle size[76]. Brust and Schriffin[77] in 1994, on the other hand, achieved a breakthrough in AuNP synthesis by synthesizing organic soluble alkanethiol-stabilized AuNPs through a biphasic reduction protocol using tetraoctylammonium bromide (TOAB) as the phase transfer reagent and sodium borohydride ($NaBH_4$) as the reducing agent. In this thesis, AuNPs were synthesized by slightly modifying the Turkevich method in combination with a ligand exchange of the capping (the synthesis procedure will be discussed in the Experimental section 3.2.3). Both methods are based on the reduction of $HAuCl_4$, which finally leads to the formation

of small Au seeds, that can initiate the formation of nanocrystals. Both follow a bottom-up approach, hence the final AuNP is the result of the fusion of smaller building blocks.

An essential property that nanoparticle suspensions in general must possess is colloidal stability. Otherwise nanoparticles would start to agglomerate irreversibly and the physicochemical properties would change entirely. As agglomeration would be the result of an attractive interaction (i.e. van der Waals forces) between the surfaces of individual nanoparticles, it can be prevented by modification of the surface. This modification can act in different manner and induce repulsion, either by electrostatic interactions or sterical exclusion. The attachment of such coatings usually is achieved via electrostatic and/or hydrophobic interaction or covalent binding. The citrate-capping is just physiosorbed to the surface and it stabilizes the AuNPs via electrostatic repulsion. However, physiosorbed molecules are not long-term stable. In order to enhance the stability of AuNPs, the most common strategy is to attach molecules with a thiol bearing end group. Here, 3-mercaptopropionic acid (MPA) was used. Thiol has a high affinity to bind to gold and tend to have a higher bond-dissociation energy than citrate. The carboxyl bearing end group in MPA increases the hydrophilicity, hence water solubility is achieved. Furthermore, MPA-capped AuNPs are pH-sensitive, therefore surface charges can be regulated with respect to pH value and ionic strength.

2.2.2 Properties of AuNPs

Spherical AuNPs possess useful properties such as size- and shape-related optoelectronicity[78], large surface-to-volume ratio and low toxicity[79]. The huge advantage of AuNPs are that they can interact with light through the localized surface plasmon resonance (LSPR). Spherical AuNPs exhibit a range of colors in aqueous solution as the core sizes increases from 1 to 100 nm, and generally show a size-dependent absorption peak from 500 to 550 nm. This absorption band arises from the collective oscillation of the conductive electrons due to the resonant excitation by the incident photons (Figure 2.4) which is called a "surface plasmon band"[80]. This phenomenon is not only influenced by size, but also by shape, dielectric environment (such as solvent or the incorporation into a polymer matrix), surface ligand, core charge, temperature and is even sensitive to the proximity of other AuNPs[81,82].

To describe the displayed color of the AuNPs quantitatively, Gustav Mie[83] derived a generic solution by considering the scattering of an electromagnetic wave from the nanoparticles. The Mie theory is the exact solution to Maxwell's electromagnetic field equations for a

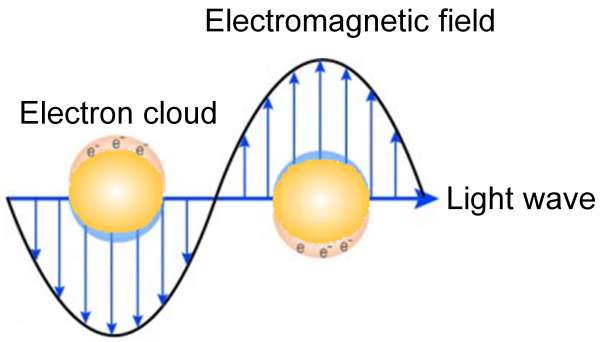

Figure 2.4: Schematic representation of the oscillation of conduction electrons across the AuNP in the electromagnetic field of the incident light.

plane wave interacting with a homogeneous sphere of radius R with the same dielectric constant as bulk metal and describes the optical properties of metallic spherical particles. It can be applied to spherical particles of any size and composed of an absorbing or non-absorbing materials and can be used to predict the extinction. The extinction cross-section (σ_{ext}) of the spheres is the sum of scattering and absorption and thus related to the measured transmittance and absorbance. In the limit of $2R \ll \lambda$ (particle diameter is much smaller than wavelength of the radiation then the incident electric field can be considered homogeneous within the particle's volume), only the electric dipole term contributes significantly to the extinction cross-section. The Mie theory, then, reduces to the following relationship:

$$\sigma_{ext} = \frac{18\pi(\epsilon_m)^{3/2}}{\lambda} V_{NP} \frac{\epsilon_2}{(\epsilon_1 + 2\epsilon_m)^2 + \epsilon_2^2}. \tag{2.7}$$

In this equation, ϵ_m is the dielectric constant of the surrounding medium and $\epsilon = \epsilon_1 + i\epsilon_2$ is the complex dielectric constant of the particle. A SPR peak occurs whenever the condition of $\epsilon_1 = -2\epsilon_m$ is satisfied. It is also evident that σ_{ext} scales with the particle volume V_{NP}.

Although Mie theory has traditionally been developed for the calculation of extinction spectra of single particles of highly symmetric shape and appropriate size range, in reality, particles in suspension interact with their surrounding as well as with neighboring particles, leading to plasmon coupling and to different SPR absorption bands[84]. It has been proved theoretically and experimentally that when the individual spherical AuNPs come into close proximity to one another, electromagnetic coupling becomes effective for particle-particle distances smaller than five times the particle radius ($d \leq 5R$, where d is the center-to-center distance and R is the radius of the particles)[85]. As a consequence, their plasmon resonance

is red-shifted (Figure 2.5)[86]. The plasmon coupling is attributed to the dipole-dipole interaction between AuNPs[87].

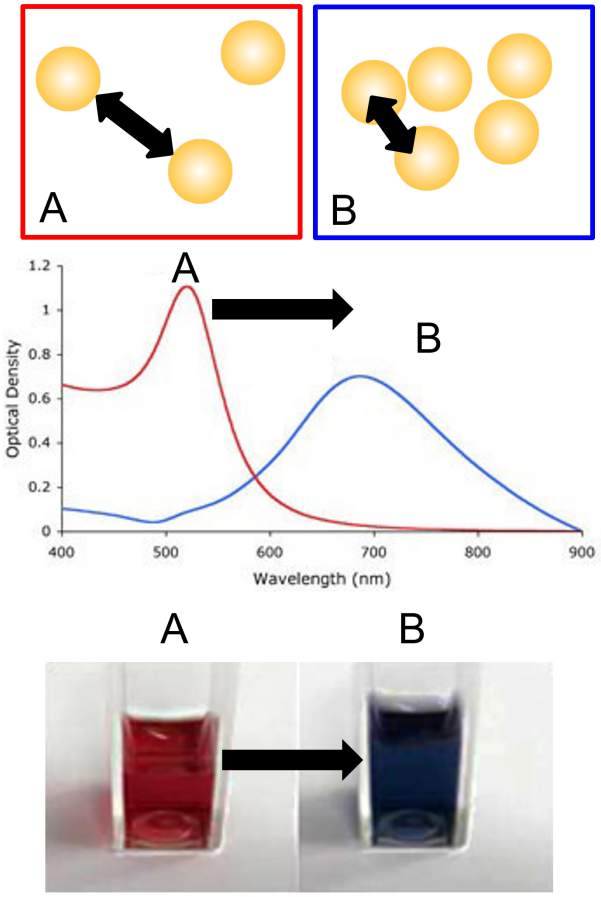

Figure 2.5: Decrease in the interparticle distance of AuNPs in suspension leads to a shift of the absorption band to longer wavelength.

2.3 Polymer brush/AuNP composite materials

Polymer brush/AuNP composites combine the responsive properties of the brush with the physico-chemical properties of the particles[88–91]. AuNPs can act in two ways: They can be considered as colorimetric sensors to detect changes in the polymer brush matrix or they can be used to trigger the structure of the polymer brush matrix, i. e. via acting as hot spots.

Regarding the self-assembly of spherical particles within brush matrices, it is crucial to understand how certain parameters affect the structure of the composites, and even more important, how to tune that structure. Here, the mutual effect of particle and brush

parameters are discussed theoretically as well as experimentally and with respect to sensor applications.

2.3.1 Theoretical predictions

It was predicted, that insertion of small, impenetrable objects will lead to a repulsive pressure inside the brush. The induced pressure is decaying exponentially away from the region of insertion and shows that the amount of particle incorporation and depth is limited[92].

With regard to the particle amount and for a given brush molecular weight, Currie et al.[93,94] showed that the number of adsorbed particles increases as grafting density σ increases in the low grafting density regime. This behavior results from the increased attachment sites for the particles along the polymer backbone that become available as σ is increased. As predicted theoretically, particle loading inside the brush causes an increase in the osmotic pressure exerted by the grafted polymers. At some grafting density (σ_{max}), a balance is achieved between the enthalpy gain associated with the particle attachment to the grafted polymers and entropy loss due to the osmotic swelling. At this point, the particle loading inside the brush is at its highest. Further increase in σ results in the expulsion of particles from the deeper areas inside the brush; the particles are only allowed to adsorb near the outermost layer of the brush, resulting in reduction in total particle loading.

Kim and O'Shaughnessy, on the other hand, studied the particle distribution theoretically with respect to their size within a brush of chains of length N grafted at density σ. For polymer-soluble particles, the authors showed that particles smaller than the particle threshold size $b^* \sim \sigma^{-2/3}$ disperse freely in the brush, which is dominated by entropy, while larger particles penetrate into the soft surface region of the brush to a certain depth $\delta \approx h(b^*/b)^3$ where h is the brush height and complete expulsion occurs for sizes above $b_{max} \sim (N/\sigma)^{1/4}$ [95,96].

Brush-particle interactions have been theoretically studied by Halperin, Kröger and Zhulina[97]. Attractive interactions can lead to adsorption of the particles at the substrate, leading to primary adsorption, and arises from attractive substrate-particle interactions, while at the same time the monomer-particle interactions are repulsive. Furthermore, the particles can adsorb in the polymer matrix and to a ternary adsorption in which weak-monomer-particle attractions are present.

The ternary adsorption onto brushes has been studied for spherical proteins by the same authors[98]. They introduced the osmotic penalty $F_{osm} = N \cdot V_p \cdot \Pi_{osm}$, associated with the insertion into the brush for N proteins with a volume of V_p. Here, Π_{osm} denotes to the osmotic pressure inside the brush, which scales approximately linearly with the brush volume fraction. Π_{osm} is also different based on the type of polymer brush (strong vs. weak polyelectrolyte brushes) due to different ion concentrations inside the brush[99]. This penalty is much higher for aggregates ($N > 1$) than for the individual particles.

Opfermann et al.[100] showed that the polymer brush morphology is affected by the particle concentration. For sufficiently strong polymer-nanoparticle interactions, increasing nanoparticle concentration causes the polymer layer to compress. At higher concentrations, the trend is reversed and further addition of nanoparticles results in swelling of the layer.

2.3.2 Experimental studies

The control over the self-assembly of particles within brushes has been also approached experimentally.

Christau *et al.*[90] studied the effect of brush thickness on AuNP uptake. They found an increased particle uptake with increasing polymer molecular weight due to increased surface roughness. Furthermore, they reported that the type of assembly was not affected by the brush thickness. In particular, the majority of AuNPs were attached on top of the brush and only a low amount of particles were found to penetrate the brush. Further studies by Christau *et al.*[91] elaborated that changing the grafting density has a dramatic impact on the assembly of AuNPs within polymer brushes, with maximum particle uptake for intermediate grafting densities. The particle distribution was rather homogeneous within the whole brush (3D assembly). A rather 2D assembly was found for high grafting densities, where the high osmotic pressure in the brush and steric hindrance limited the particle attachment and penetration. Recent observations have shown that the type of particle assembly (2D or 3D) has a strong effect on collective properties. For example, pronounced IR transparency and electrical insulation were found for AuNPs assembled as a layer (2D), and a decrease in electrical resistance was found for AuNPs assembled in 3D[101,102].

Another study of Christau et al.[103] showed that the assembly of AuNPs in non-ionic poly(N-isopropylacrylamide) (PNIPAM) brushes depends strongly on the particle surface functionalization. Two different AuNP types were used to control the assembly: Hydrophilic

citrate-coated AuNPs and more hydrophobic 12-mercaptododecanoic acid (MDA)-coated AuNPs with a diameter of about 4 nm diameter. Due to the different hydrophobicity of the particles different solvents (water and toluene) were used during incubation, which led to different polymer conformation and different particle distribution. The interaction between particle and brush is driven via hydrogen bonding with the PNIPAM brush.

Another approach was found by Bhat et al.[104] where electrostatic attraction forces negatively charged AuNPs into positively charged poly(acryl amide) (PAAm) brushes. Here, they controlled a 2D and 3D assembly by changing the molecular weight of PAAm brushes. A surface layer of AuNPs on top of the PAAm brush (2D) was obtained for shorter polymer chains and a homogeneous distribution of AuNPs in PAAm brushes (3D) was obtained for longer polymer chains. Furthermore, the strength of the charge density of the AuNPs has a high impact on the particle distribution within the polymer brush.

With regard to the ability of polymer brushes to act as nanoparticle stabilizers, Zhang et al.[105] grafted pH-responsive poly(4-vinylpyridine) (P4VP) on cellulose nanocrystals (CNC) and subsequently used to stabilize AuNPs as efficient nanocatalysts for the reduction of 4-nitrophenol (4NP). The presence of P4VP brushes on the CNC surface stabilized the AuNPs compared to AuNPs deposited directly on pristine CNC. Thus, the catalytic activity was more than 2 times higher due to an enhanced stabilization, which stems from the strong interactions between brush and particle.

To summarize, the theoretical predictions are in good agreement with experimental studies showing that the choice of particle size, brush grafting density, brush molecular weight, solvent quality, and brush-particle interaction have a strong impact on the structure of the brush/particle composites.

2.3.3 Polymer brush/AuNP composites for sensor applications

Incorporation of AuNPs into the optically transparent polymer brush induces optical properties due to the SPR yielding in colorimetric sensors. Namely, when the conformation of the brush responds to a chemical stimulus (the analyte), it triggers a change in the proximity of the AuNPs, in turn resulting in a spectral shift.

Fortin et al.[106] grafted polymer brushes inside polypropylene hollow fibers in order to monitor the glucose level of the environment. Poly(methacrylic acid) (PMAA) brushes were functionalized with phenylboronic acid (PBA) that can bind to glucose. The binding process can be monitored by a thickness change of the polymer film. The experiments revealed

that a glucose concentration down to 10 mM can be detected. Therefore, polypropylene hollow fibers modified with polymer brushes can be considered for sensing blood glucose levels of diabetic patients.

Tokarev et al.[107] reconstructed a pH sensor based on AuNPs on PDMAEMA grown on poly(glycidylmethacrylate) (PGMA) treated Au island on transparent glass substrates. PDMAEMA was used, due to its pK_a value, which is close to neutral pH, allowed the sensing of pH changes in the near-physiological range of pH 5-9. When PDMAEMA swells at low pH (pH 5), the AuNPs and Au islands are generally spaced far apart. However, as the pH value is increased up to 9, PDMAEMA collapses, causing the Au structures to approach each other resulting in a red-shift. They also demonstrated the feasibility of the PDMAEMA-based plasmonic device for monitoring the enzymatic oxidation of glucose by glucose oxidase. Since this enzymatic process yielded gluconic acid, the reaction medium became more acidic, which was detected in a SPR shift. The response of the plasmonic device was found to depend on the concentration of the enzyme and a shift of up to 10 nm was achieved.

Ferhan et al.[108] used polymer brushes for the incorporation of AuNPs for the spectroscopic detection of lead ions. Poly(oligo(ethylene glycol) methacrylate) (POEGMA) brushes were grown on glass and loaded with AuNPs. As a post-functionalization, AuNPs were coated with thiosulfate. By exposing POEGMA/AuNP composites to lead ions, formation of nanoparticles with Au-PB alloy surface occurs, which leads to a reduced interaction with the polymer brush and particle release from the brush matrix, which in turn was detected by a decrease in UV/Vis absorbance.

For some applications it is more useful to detect temperature changes in the surrounding environment. One prominent candidate is the non-ionic PNIPAM, which has its lower critical solution (LCST) temperature at ~ 32 °C in water. PNIPAM's LCST can be tuned to body temperature (37 °C) by adding co-monomers and this is interesting for medical applications. Gupta et al.[109] used PNIPAM brushes as a template for the immobilization of AuNPs for the fabrication of temperature-sensitive nanosensors. Carboxylic functionalized AuNPs with particle sizes of 5 to 6 nm were embedded in PNIPAM brushes with a dry thickness of around 70 nm. Attraction between particle and brush is realized by hydrogen binding between the amide group of PNIPAM chains and the carboxylate group of the AuNPs capping. The shift in the SPR absorption band was triggered by altering the temperature. Temperature increase above the LCST results in a collapse of the PNIPAM brush, which in turn shifts the SPR absorption band to longer wavelength. Red-shift indicates that the AuNPs come closer together. A shift of around 12 nm has been found for

heating an cooling cycles. It was also observed that the shift is reversible, demonstrating the versatile use as nanosensor.

Chapter 3

Experimental section

3.1 Materials

2-(methacryloyloxy)ethyltrimethylammonium chloride (METAC), 2,2'-Bipyridine, N- Isopropylacrylamide (NIPAM), N,N,N',N",N"- pentamethyldiethylenetriamine (PMDETA), copper(I) chloride (CuCl), copper(II)chloride ($CuCl_2$), gold(III)chloro trihydrate ($HAuCl_4 \times 3\ H_2O$), sodium borohydride ($NaBH_4$), sodium citrate trihydrate, 3-mercaptopropionic acid (MPA), thioctic acid, sulfuric acid (H_2SO_4), hydrogen peroxide (H_2O_2), aminopropyltriethoxysilane (APTES), 2-bromoisobutyrylbromide (BIBB), triethylamine (TEA), molecular sieve 4 Å , sodium hydroxide (NaOH), formic acid, succinic acid, potassium hydroxide (KOH), trishydroxymethylaminomethane (TRIS), hydrogen chloride (HCl), ethanol (EtOH), methanol (MeOH), and toluene were purchased from Sigma-Aldrich (St. Louis, MO, USA) and used without further purification. Silicon substrates (<100> orientation, Boron/p-doped, polished) were purchased from MicroChemicals GmbH (Ulm, Germany) and cut into pieces of 1 cm × 2 cm and were used for ellipsometry measurements, atomic force microscopy measurements, and X-ray reflectometry measurements, and SEM measurements. Glass substrates (Fused Silica JG52, polished) with dimensions of 1 cm × 2 cm were purchased from MicroChemicals GmbH and were used for UV/Vis spectroscopic measurements. Silicon blocks with dimensions of 5 cm × 8 cm × 1.5 cm with a roughness less than 0.2 nm were used for neutron reflectometry measurements and purchased from Siltronic AG (München, Germany).

3.2 Synthesis and preparation

3.2.1 Synthesis of ATRP initiator BTPAm

As the initiator, 2-bromo-2-methyl-N-(3-(triethoxysilyl)propyl)propan- amide (BTPAm) was used. BTPAm was prepared according to literature procedure[110] by a coupling reaction between aminopropyltriethoxysilane (APTES) with 2-bromoisobutyrylbromide (BIBB) through an amidiziation reaction (Figure 3.1).

A solution of BIBB (0.825 ml, 6.6 mmol) in dry toluene (25 ml) was slowly added into a cold solution (0 °C) of APTES (1.485 ml, 6.6 mmol) in dry toluene (20 ml) with TEA (1.11 ml, 7.4 mmol). The mixture was magnetically stirred for 2 h at 0 °C under nitrogen

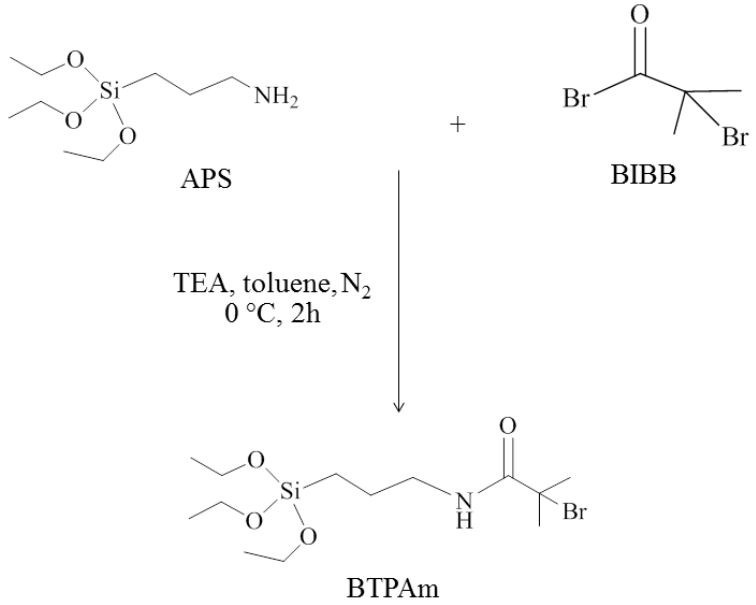

Figure 3.1: Coupling reaction between APTES and BIBB to obtain BTPAm.

atmosphere and then for another 24 h at room temperature. TEA salt, which was the reaction by-product, was precipitated out during the reaction. It was removed by filtration and the filtrate was evaporated under reduced pressure to remove the unreacted TEA. BTPAm was recovered as a yellowish oil.

3.2.2 Polymer brush synthesis

The polymer brushes have been synthesized via the "grafting from" method through SI-ATRP. In order to yield polymer brushes, two synthesis steps are needed. As a first step, an initiator-coated self-assembled monolayer (SAM) has to be generated (Figure 3.2). The initiator molecule used for this technique is attached from one end to the substrate where the other end is used to initiate the polymerization.

As a second step, the surface-initiated polymerization is carried out. The general mechanism of SI-ATRP is illustrated in Figure 3.3.

For both, immobilizing the initiator and the synthesis of the brush, a specific reactor was used, which was developed by Christau and co-workers[90]. The advantage of this reactor is that various samples can be prepared at the same time in order to achieve the same conditions for all samples.

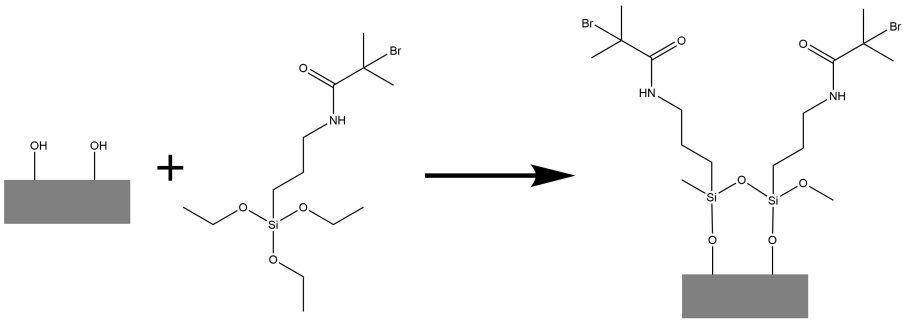

Figure 3.2: Schematic sketch of the monolayer formation of the initiator (BTPAm). The freshly cleaned silicon substrate bears hydroxyl terminating groups, which increases the surface hydrophilicity and the reactivity. The hydroxyl groups reacts chemically with the silane group of the initiator and the halogen group at the other end is used for starting the polymerization.

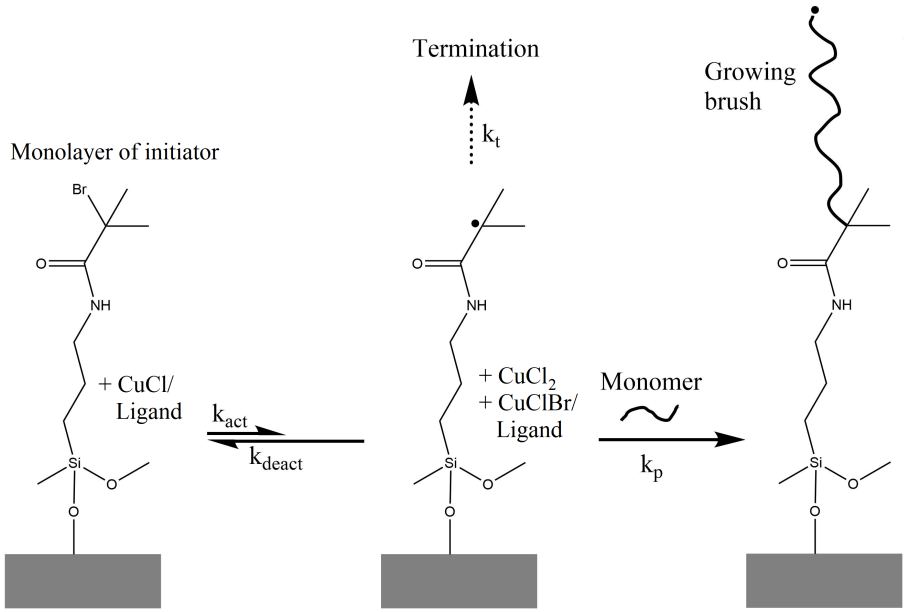

Figure 3.3: General mechanism of the surface-initiated atom transfer radical polymerization (SI-ATRP) for growing the polymer brush from the BTPAm-coated substrate. CuCl is involved as an activating metal species while $CuCl_2$ is involved as the deactivating species. k are the rate constants for activation, deactivation, termination, and polymerization step.

Immobilization of the initiator

The substrates (silica or glass) were etched for 30 min using piranha solution (H_2SO_4/H_2O_2 1:1 *v/v*%). This procedure generates hydroxyl groups on the surface to achieve covalent bonding between surface and the initiator. After etching the samples, they were rinsed with Milli-Q water and the freshly cleaned substrates were placed into the reactor containing 10 mM solution of BTPAm in anhydrous toluene (Figure 3.2). The reactor was sealed and the reaction was carried out for 24 h at room temperature. After the reaction, the initiator-coated samples were rinsed with toluene, sonicated for 20 min in ethanol and then dried under a stream of N_2.

Besides BTPAm, (11-(2-bromo-2-methyl) propionyloxy) undecyl trichlorosilane) (e-BMPUS) was also used as an initiator. The polymer brushes that were synthesized with e-BMPUS are used for the investigation in Chapter 9. The results in Chapter 9 are obtained during the research visit at the NCSU in Raleigh, USA, which was part of my Ph.D. e-BMPUS has been used, because it is commercially available.

Before generating a monolayer of e-BMPUS onto the substrate, the substrates were cleaned by ultraviolet/ozone (UVO). The freshly cleaned substrates were immersed into a solution of e-BMPUS in dry toluene (10 μl/10 ml e-BMPUS/dry Toluene) overnight at -11 °C to generate a monolayer of e-BMPUS on the substrate. After deposition was complete, the substrates were sonicated in toluene for 20 min, rinsed with EtOH and dried under a stream of nitrogen.

PMETAC brush synthesis

The polymerization of 2-(methacryloyloxy)ethyltrimethylammonium chloride (METAC) through SI-ATRP followed literature procedure[111], but the literature recipe was modified by changing the $CuCl/CuCl_2$ and changing the concentration of the monomer METAC in order to decrease the polymerization time. In a typical reaction protocol, METAC with various amounts (20 mL, 85 mmol; 35 mL, 150 mmol; 47 mL, 200 mmol) was mixed with 2,2'-bipyridyl (844 mg, 5.4 mmol) in 20 mL of Milli-Q water/MeOH (1:4 *v/v*) in the reactor. The mixture was flushed with N_2 for 30 min. Then, CuCl and $CuCl_2$ of different amounts (ratio of 10:1: 217.8 mg, 2.2 mmol and 30 mg, 0.22 mmol or 15:1: 326.7 mg, 3.3 mmol and 30 mg) was added quickly to the mixture. The mixture was further stirred and degassed for another 30 min. The BTPAm-coated samples were placed in the reactor in nitrogen atmosphere. The polymerization was carried out for a given polymerization time

at room temperature. By exposing the samples to air, the polymerization can be stopped afterwards. The samples were sonicated in water for 10 min, then in MeOH for another 10 min and dried with N_2.

PNIPAM brush synthesis

The synthesis of PNIPAM brushes is adapted from literature[112]. NIPAM monomer (2 g, 17.67 mmol) was dissolved in 35 mL of Milli-Q water/MeOH (1:1 v/v), and the mixture was stirred (500 - 600 rpm) under rigorous nitrogen bubbling for 30 min. Then, PMDETA (150 μl, 0.718 μmol) and CuCl (0.0195g, 0.197 mmol) were added at once. After stirring for another 30 min under nitrogen bubbling, the BTPAm-coated (or e-BMPUS) substrates were added, and the reaction was carried out for 8 min in a nitrogen atmosphere. Afterwards the samples were removed quickly, sonicated for 10 min in ultrapure water, then in MeOH for another 10 min and dried under a stream of nitrogen.

PMMA brush synthesis

PMMA brush synthesis was adapted from literature[113]. MMA (21.6 ml), Bipy (624 mg) were added to a solution of methanol (24 ml) and water (8 ml). The solution was degassed with argon gas for 30 min. CuBr (288 mg) were added to the solution and was further degassed for another 30 min. Silicon substrates functionalized with e-BMPUS were placed into the reactor for starting the polymerization. After polymerization the substrates were taken out from the solution and sonicated in acetone for 20 min, followed by drying with N_2.

3.2.3 AuNP synthesis

3-Mercaptopropionic acid-capped (MPA) AuNPs were synthesized by modifying a multi-step procedure based on a ligand exchange reaction[114]. As a first step, citrate stabilized AuNPs were prepared. Here, a solution of gold(III) chloride hydrate ($HAuCl_4 \cdot xH_2O$) (0.25 mL, 0.1 M) was added to 99.5 mL of Milli-Q water and was stirred with a solution of trisodium citrate dihydrate ($C_6H_5Na_3O_7{\cdot}2H_2O$) (0.25 mL, 0.1 M) to the previous solution. While the mixture was stirred, a solution of sodium borohydride ($NaBH_4$) (2 mL, 0.1 M) was added at once. The solution turned red immediately. The AuNP suspension was stirred for another 2 h. In order to gain MPA-capped AuNPs, the citrate molecules on the

AuNP surface were displaced by thioctic acid. For this purpose, thioctic acid (6 mg, 0.029 mmol) was dissolved in 1 mL ethanol and added to the previously synthesized citrate reduced AuNPs while the suspension was stirred. The color of suspension turned from red to purple. NaOH solution was added dropwise to the purple suspension until the suspension color changed to red again. The mixture was stirred overnight so that the reaction could reach equilibrium. The last step was the functionalization of the AuNPs with MPA by adding 2.18 μL (0.025 mmol) to the suspension and letting it stir overnight. In order to get rid of the excess ligand, the AuNPs were precipitated by adding ethanol to the AuNP suspension. The suspension was centrifuged at 7000 rpm for 20 min. The supernatant was discarded while the pellet was resuspended in Milli-Q water with a pH of 13 prior to use (see Figure 3.4). MPA-AuNP suspensions have a pK_a of 4.3[115] (see Figure 3.5).

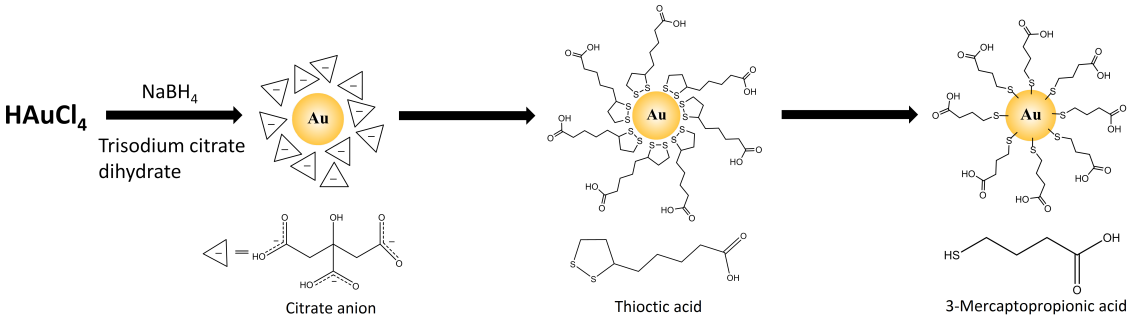

Figure 3.4: Schematic sketch of the three-step synthesis of AuNPs through ligand exchange reaction. As a first step $HAuCl_4$ is reduced by $NaBH_4$ in presents of trisodium citrate dihydrate to obtain citrate stabilized AuNPs. The citrate capping is exchanged by thioctic acid and afterwards by 3-mercaptopropionic acid to get the desired MPA-capped AuNPs.

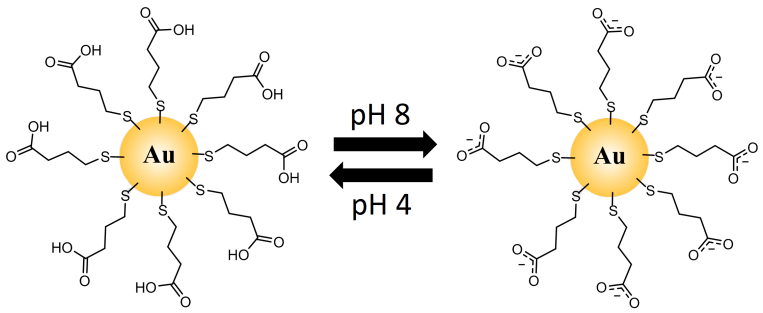

Figure 3.5: Varying the charge of the MPA capping by changing the pH. pK_a of MPA-capped AuNPs is 4.3. Exposing MPA-capped AuNPs to pH 8 leads to a negatively charged surface due to the deprotonation of the carboxylic acid groups while exposing MPA-capped AuNPs to pH 4 leads to uncharged AuNPs due to the protonation of the carboxylic acid groups.

The diameter of the particles were found to be 4.8 $\pm$ 1.1 nm, as determined by transmission

electron microscopy (TEM) and using ImageJ (National Institutes of Health, Rockville Maryland, USA) for the size determination (see Figure 3.6).

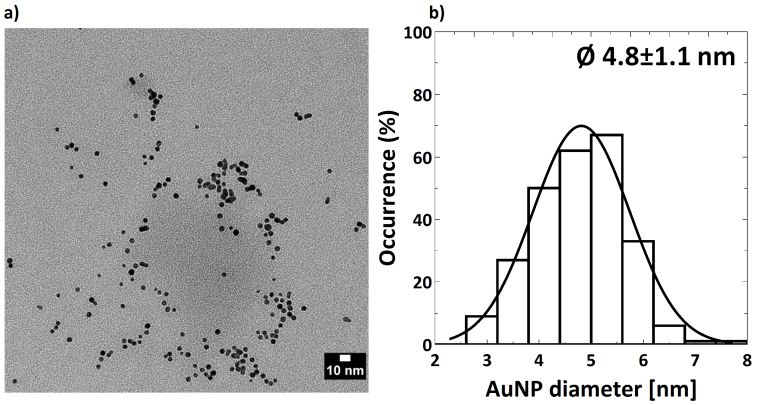

Figure 3.6: Transmission electron microscopy (TEM) image of MPA-capped AuNPs a) and the particle size distribution b). The diameter of AuNPs are 4.8 ± 1.1 nm and was determined by averaging the size of 200 particles from the TEM images using ImageJ.

3.2.4 Buffer solution preparation

Buffer solutions were used to obtain the desired pH because they maintain a relatively constant pH over a long period. Low ionic strength (∼0.05 M) buffer solutions were selected to guarantee that no salt effects disturb the brush/AuNP composites in aqueous solution. Buffer solutions ranging from pH 4 to pH 8 were prepared by two different buffer systems (citric acid monohydrate (Na-citrate)/KOH and trishydroxymethylaminomethan (TRIS)/HCl) with an ionic strength of around 0.05 M. Na-citrate/KOH buffer system was used to prepare solutions with a pH of 4, 5, and 6 while TRIS/HCl buffer system was used to prepare solutions with a pH of 7 and 8.

3.2.5 Preparation of brush/AuNP composite materials

Brush/AuNP composites can be achieved by incubating the polymer brush into the AuNP suspension. The samples were incubated at different pH by mixing AuNP stock suspension with buffer solution at a 1:9 AuNP/buffer ratio. The incubation time was set to 24 h (Chapter 4) and 6 h (Chapter 5-9). The AuNP suspension had a concentration of 0.16 mg/ml. After incubation, the samples were taken out, sonicated in Milli-Q water for 1 min and dried under a nitrogen stream.

3.2.6 Polymer brushes in presence of an electric field

For the experiments in Chapter 9, polymer brushes were immersed in ultrapure water and AuNP suspension, respectively. A copper wire was attached to the rear of the brush-bearing silicon substrate to act as the working-electrode using silver epoxy, and the sample was placed in a petri dish made of plastic. Between the silicon substrate and the petri dish, rubber was used as an insulator. Twenty milliliters of ultrapure water or AuNP suspension was added into the petri dish. A counter-electrode consisting of a 6 mm length of gold wire was placed parallel to the sample surface at a distance of 3 mm. The crucial point was that the liquid medium should not come in contact with the copper wire otherwise the current would not flow through the silicon substrate in order to act as an working-electrode. In the convention used throughout Chapter 9, positive bias refers to the positive terminal of the voltage supply being connected to the brush substrate and vice versa (see Figure 3.7).

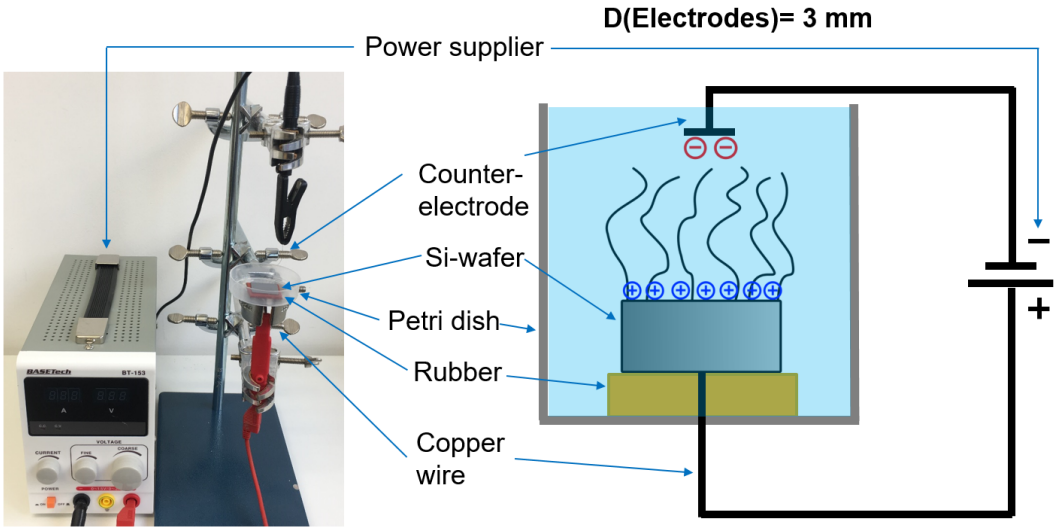

Figure 3.7: Experimental setup of applying an electric field.

3.3 Instruments and measurement procedure

3.3.1 Ellipsometry

The ellipsometric measurements were carried out with a polarizer-compensator sample analyzer (PCSA) ellipsometer (Optrel GbR, Sinzing, Germany) at a wavelength of 632.8 nm in null ellipsometry mode. The measurements were carried out at an angle of incidence of 70° for measurements under controlled humidity and ambient conditions, and at an

angle of incidence of 60° for measurements in water. A home-built humidity cell was used to perform measurements at different humidities as introduced earlier[116]. The data were fitted with Elli v3.1 (Optrel, Sinzing, Germany) based on an one-layer-model for the polymer brushes shown in Table 3.1.

Table 3.1: One-layer-model for fitting polymer brushes on a silicon wafer against air or water. Parameters are refractive index n, absorption coefficient k and the thickness of the layer, respectively. Arrays with an infinity symbol imply bulk properties with quasi-infinity thickness. Arrays with "fit" indicate the fitting parameters.

Layer	n	k	Thickness [nm]
air/water	1/1.33	0	∞
brush	fit	0	fit
SiO_x	1.50	0	1.50
Si	3.885	-0.020	∞

3.3.2 Atomic-force microscopy (AFM)

Scanning measurements were carried out with a Cypher AFM (Asylum Research, Santa Barbara, CA, USA) at a scan rate of 1 Hz. For measurements in air, silicon cantilevers with a reflective coating of aluminum (AC160TS, Olympus, Tokyo, Japan) were used. The cantilever had a length of 160 μm, a resonant frequency of 300 kHz and a force constant of 26 N/m. Measurements in water were performed with Cr/Au-coated silicon cantilevers (OMCL-TR series, Olympus, Tokyo, Japan) with a triangular shape, a resonant frequency of 11 kHz and a spring constant of 0.02 N/m. All measurements were done at room temperature. The data were analyzed with IgorPro (Wavemetrics, Inc., Portland, OR, USA). The roughness was determined by the average of the root mean square roughness (rms) of 3 areas of (20 × 20) μm^2. The rms was calculated using the formula:

$$\sigma = \sqrt{\left(\frac{1}{N}\sum y_i^2\right)}, \tag{3.1}$$

where N is the number of data points and y_i the respective height of each data point. All images were planar fitted and flatted to correct any tilting of the samples.

The full-indentation method were used to measure the thickness in water, which has been already introduced by Üzüm *et al.*[117] for polyelectrolyte multilayers and were applied on polymer brushes doped with AuNPs by Yenice *et al.*[89]. An AFM force measurement setup was used for indentation in z-direction. The experiments were carried out in water at room

temperature on an MFP-3D AFM (Asylum Research, Santa Barbara, CA, USA). Cr-Au coated silicon cantilevers (HQ:CSC38/CR-Au, MikroMasch, Sofia, Bulgaria) with a spring constant of 0.05 N/m were used. Each sample measurement consists of 12 individual force curves taken at different lateral positions on the sample. Details are described in ref[89,117].

3.3.3 Transmission electron microscopy (TEM)

TEM measurements were performed on a FEI Tecnai G^2 20 S-TWIN (FEI, Hillsboro, OR, USA). TEM copper grids with a carbon film were used (200 mesh, Science Service, Munich, Germany). Electric charge was removed by glow discharge for 15 s. Subsequently, 5 μL of the sample solution were deposited onto the grids. After 1 min incubation the excess liquid and AuNPs were blotted with filter paper. The grids were then dried at room temperature and placed inside the TEM.

3.3.4 Gravimetric analysis

Gravimetrical measurements were performed to determine the amount of AuNPs in the stock suspension. To do this, 1 mL of the AuNP stock suspension was poured into a porcelain crucible. The vessel was placed in a muffle furnace and a defined temperature program was run to guarantee that everything was decomposed except the gold. The amount of gold of the used AuNP stock suspension volume can be determined by weighing the vessel before pouring AuNP stock suspension and after the decomposition of the AuNP stock suspension which has been done three times. The concentration of AuNP stock suspension was found to be 2.45 nmol/ml (detailed calculations will be described in Chapter 4).

3.3.5 Scanning Electron Microscopy (SEM)

SEM images were recorded after attachment of MPA-capped AuNPs in polymer brushes at the Zentrum für Elektronenmikroskopie (ZELMI) at the TU Berlin using a Zeiss DSM 982 GEMINI (Oberkochen, Germany). SEM was operated at acceleration voltages of 10 kV for imaging in top view and the crosssections.

3.3.6 UV/Vis spectroscopy

Numerical values are obtained in a UV/Vis spectroscopy experiment by the application of Lamber-Beer's law:

$$A = log\frac{I_0}{I} = cl\epsilon, \tag{3.2}$$

where l is the length of the cuvette the light passes through, ϵ is the extinction coefficient, c the concentration, A the absorbance and I_0, I is the intensity of the measuring beam before/after passing through the sample. It clearly shows that A scales proportional to the concentration of the solution.

Spectroscopic measurements were performed in a wavelength range of 400–800 nm at room temperature in aqueous solution using a UV/Vis spectrophotometer (PerkinElmer Inc., Waltham, MA, USA). In order to record UV/Vis spectra and measure the transmittance of brush/AuNP composites, the substrate from silicon wafer to fused silica wafer (Microchemicals GmbH, Ulm, Germany) was changed.

3.3.7 Reflectometry

Reflectometry is a scattering technique and uses the reflection of electromagnetic waves (light, X-ray photons, neutrons) at surfaces or interfaces between two media to detect or characterize features of the system. It is a non-destructive method to determine thickness, roughness and the composition of the system. Using reflectometry in the specular mode at an interface, an electromagnetic wave beam hits the surface of a sample with an angle θ_i and wave vector $\vec{k}_i$ and is reflected with an angle $\theta_r = \theta_i$ and wave vector $\vec{k}_r$. The reflection process is described by the momentum transfer $\vec{Q} = \vec{k}_r - \vec{k}_i$ (Figure 3.8) under the assumption of elastic scattering $\left|\vec{k}_i\right| = \left|\vec{k}_r\right| = 2\pi/\lambda$.

The specular reflectometry is calculated using Abeles formulation[118] as a function of the momentum transfer Q_z perpendicular to the surface,

$$Q_z = \frac{4\pi}{\lambda} \cdot sin\theta. \tag{3.3}$$

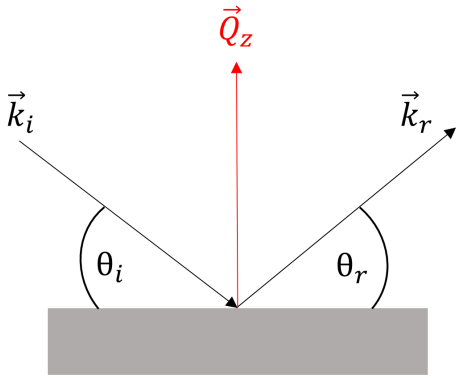

Figure 3.8: Elastic scattering on a planar surface.

The typical parameter used to describe reflection from a surface is the normalized intensity, or specular reflectivity R, which is the ratio of reflected intensity I_R over incident intensity I_o

$$R(Q) = \frac{I_R(Q)}{I_o}. \tag{3.4}$$

The measured specular reflectivity depends on the scattering length density (SLD) of the material, which is different for X-rays and neutrons, since X-rays interact with the electrons of the materials while neutrons interact with the nuclei.

X-ray reflectometry (XRR)

The SLD of X-rays is given by

$$\rho_e = \frac{SLD_{X-ray}}{r_e} \tag{3.5}$$

where r_e is the classical electron radius (2.8179×10^{-5} Å). XRR measurements were carried out on a Bruker-AXS D8 Discover XRD diffraction system (Bruker AXS GmbH, Karlsruhe, Germany) long-fine focus KFLCu2K tube at $\lambda_{\mathrm{Cu\ K}\alpha} = 0.1542$ nm in a home-built humidity cell. To control the humidity, silica gel was used as a desiccant for having a relative humidity of 4-7 % and cotton pads soaked with water were used to adjust a relative humidity of >92 %. For measurements at ambient conditions (≈30 %rh), the lit of the home-built humidity cell was taken off and no materials were used to regulate the humidity.

X-ray data were fitted with IgorPro (Wavemetrics, Inc., Portland, OR, USA) package Motofit[119]. For data fitting a layer model was used to derive thickness, roughness, and the SLD. Air as the fronting continuum (SLD = 0 Å^{-2}), silicon as the backing continuum (SLD = 20.1 × 10^{-6} Å^{-2}), and a SiO_x layer (h = 15 Å, SLD = 18.9 × 10^{-6} Å^{-2}) was used. The neat polymer brush was fitted with one layer (one-layer model). For the brush/AuNP composites, a three-layer model as well as an one-layer model was used (For more details see Chapter 5 and Chapter 9). The layer-model yields information about the film thickness, film roughness and electron density. Since the electron density of gold is much higher than of the polymer brush, an increase in the electron density should indicate particle uptake.

Neutron reflectometry (NR)

The SLD of neutron is given by

$$SLD_{Neutron} = \frac{1}{V}\sum_{i=1}^{M} b_i \tag{3.6}$$

where b_i is the coherent scattering length of atom i in volume V, and the total number of atoms is M.

NR measurements were carried out with two different analysis approaches and different water contrasts by mixing H_2O and D_2O (Chapter 5 and 6) to achieve a good understanding of the internal structure of brush/AuNP composite. The NR measurements in Chapter 5 were carried out at the time-of-flight reflectometer BioRef (V 18) at the Helmholtz-Zentrum Berlin (Berlin, Germany)[120,121] just in D_2O at 22 °C with a resolution mode of $\delta\lambda/\lambda = 5$ %. Reflectivity curves were measured with two angular settings of 0.5° and 2°. With a wavelength band of 3-11 Å, the Q-space from 0.005 to 0.12 Å^{-1} was covered. The measuring time per run varied between 2:15 h and 4:30 h and the data were fitted with a step-like fitting model. While the NR measurements in Chapter 6 were carried out at the reflectometer V6 at Helmholtz-Zentrum Berlin (Berlin, Germany)[122]. All measurements at V6 were carried out using solid/liquid cells at a controlled temperature of T = 25 °C in H_2O (ρ_W = -0.56 × 10^{-6} Å^{-2}), 4-matched water 4MW (ρ_W = 4.00 × 10^{-6} Å^{-2}), and D_2O (ρ_W = 6.36 × 10^{-6} Å^{-2}). The monochromatic incident beam had a wavelength of λ = 4.66 Å . The value of Q_z ranged from 0.005 Å^{-1} to 0.10 Å^{-1}. The wavelength resolution was $\delta\lambda/\lambda$ = 2 %, resulting in a finite Q_z-resolution, which was taken into consideration for the data analysis by convolution with Gaussian functions[123–125]. The measuring time per run varied between 12 h and 18 h and the data were fitted with a self-consistent model.

Surface grafted polymer brushes have a high polydispersity , which becomes pronounced in water and complicates fitting procedure and final data analysis. The higher polydispersity has to be considered more in detail for NR than for XRR measurements. Therefore, two different analysis models were employed in which the second model is an improvement of the first model.

1) Step-like fitting model

To account for the polydispersity of the brush, a step-like fitting model was used to analyze the NR measurements in Chapter 5. The reflectivity data, obtained at the BioRef, were fitted using Motofit[119] and the model was employed by Christau et al.[103] (Figure 3.9). This was done by using Si (SLD = 2.07 $\times$ 10^{-6} $\dot{A}^{-2}$) and D_2O (SLD = 6.36 $\times$ 10^{-6} $Å^{-2}$) as a continuum, and a SiO_x layer (h = 15 Å, SLD = 3.47 $\times$ 10^{-6} $Å^{-2}$). A second layer was used as a basic layer with varying thickness and SLD. Following the basic layer a stack of 28 layers with a fixed layer thickness of 5 nm but varying SLD was used to fit the data. The inter-layer roughness was set to zero. The constraint for the varied SLD was that the SLD values have to increase towards the sub-phase until it reaches the SLD of 6.36 $\times$ 10^{-6} $Å^{-2}$ (SLD of D_2O). The multi-layer model was used for modeling the gradual profile of the brush and the decreasing brush density in z-direction towards the sub-phase. In reality, there should be roughness associated with those layers, which would make the profile of the brush more gradual. However, that would introduce another fitting parameter, which is why layers of 5 nm thickness was chosen to model the brush profile with less cpu time for the fitting procedure.

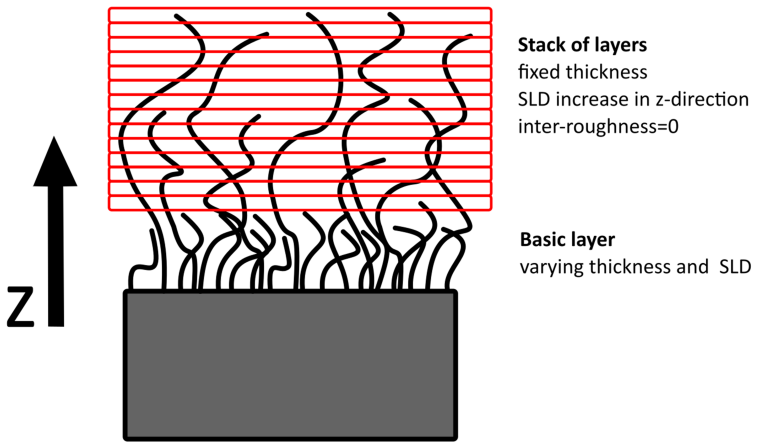

Figure 3.9: A step-like fitting model has been used in order to model the polydispersity of the brush by having small layers which have the same thickness but varying scattering length density (SLD).

2) Self-consistent model

The second analysis approach (Chapter 6) was used to analyze the NR measurements in Chapter 6, which were obtained at V6. It was done with the help of a self-consistent model based on the analytical parametrization of the volume fraction profiles of all chemical components. The reflectivity curves $R(q_z)$ depend on the interfacial scattering length density (SLD) profiles $\rho(z)$, where z denotes the position on the axis perpendicular to the surface plane. The SLD profiles depend on the interfacial volume fraction profiles $\Phi_i(z)$ of all chemical components i with known SLD ρ_i.

$$\rho(z) \; = \; \sum_i \; \Phi_i(z) \; \cdot \; \rho_i. \tag{3.7}$$

The profiles are described with parameter-based analytical functions[124,125], as specified in Chapter 6. To compute theoretical reflectivity curves for comparison with the experimental ones (Figure 3.10), the $\rho(z)$ profiles were discretized into hundreds of thin slabs of 2 Å thickness and constant SLD. The reflectivity curves were then calculated by application of Fresnel's reflection laws at each slab/slab interface and the phase-correct summation using the iterative procedure of Parratt[126]. In the last step, the model parameters describing the volume fraction profiles were varied until the best simultaneous agreement (characterized by the minimal chi-square deviation) was reached simultaneously with the experimental reflectivity curves measured in all water contrasts. Roughness parameters were restrained to values above 2 Å for all interfaces associated with the solid substrate and to values above 5 Å for all other interfaces. The fitting program was implemented in the IDL programming language (IDL 8.6, www.harrisgeospatial.com).

The huge advantage of the self-consistent model over the step-like fitting model is that it can fit all reflectivity data for various water contrasts simultaneously (here, 3 different water contrasts were used). That allows the determination of the spatial distribution of all components separately from each other and enables much more details about the internal structure.

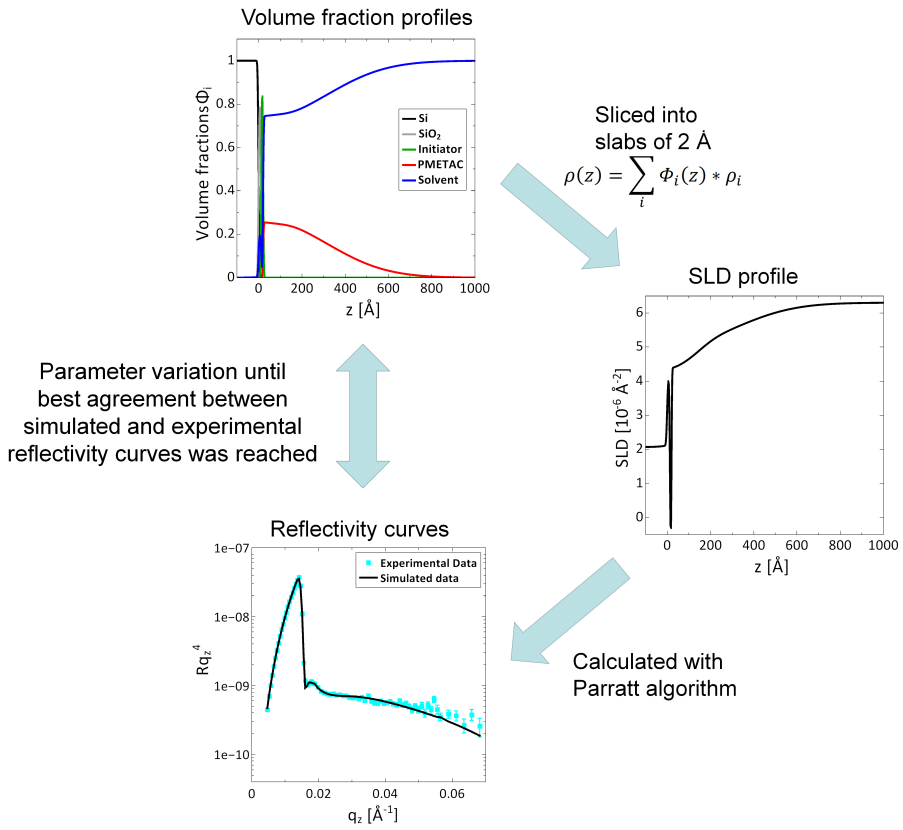

Figure 3.10: A theoretical reflectivity curve can be simulated by the volume fraction profiles of all components. The parameters, describing the volume fraction profiles, were varied until the theoretical reflectivity curve is in best agreement with the experimental obtained reflectivity curve.

Chapter 4

Uptake of pH-sensitive gold nanoparticles in strong polyelectrolyte brushes*

Abstract

The impact of electrostatic attraction on the uptake of AuNPs into PMETAC brushes was investigated. PMETAC/AuNP composite materials were prepared by incubation of the polymer brush coated samples into MPA-AuNP (5 nm in diameter) suspension. The electrostatic interactions were tuned by changing the surface charge of the AuNPs through variations in pH value, while the charge of the PMETAC brush was not affected. AFM, ellipsometry, UV/Vis spectroscopy, gravimetric analysis and TEM were employed to study the loading and penetration into the polymer brush. The results show that the number density of attached AuNPs depends on the pH value and increases with increasing pH value. There is also strong evidence that the particle assembly is dependent on the pH value of the AuNP suspension. Incubation of PMETAC brushes in AuNP suspension at pH 4 led to the formation of a surface layer on top of the brush (2D assembly) due to sterical hindrance of the aggregated AuNPs, while incubation in AuNP suspension at pH 8 led to deeper particle penetration into the brush (3D assembly). The straightforward control of particle uptake and assembly by tuning the charge density of the nanoparticle surface is a valuable tool for the development of materials for colorimetric sensor applications.

4.1 Introduction

In order to control the optical properties of brush/AuNP composites, it is important to understand how to control the uptake of the AuNPs within the brush. One important parameter is the charge of the AuNP, which is assumed to drive the adsorption and penetration of AuNPs into the brush[90,127].

In the present chapter, we addressed this aspect by studying the effect of charge of AuNPs, on their adsorption into a positively charged brush. The 5 nm AuNPs were coated with 3-mercaptopropionic acid (MPA) instead of citrate, since thiol-gold bonds are more stable than the physiosorbed citrate ions[128]. In addition, MPA carries a carboxylic acid group

*Similar content was presented in D. Kesal, S. Christau, P. Krause, T. Möller and R. von Klitzing, *Polymers*, **2016**, *8*, 134 (Uptake of pH-sensitive gold nanoparticles in strong polyelectrolyte brushes).

that can be protonated or deprotonated, which allows for charging or uncharging the surface of the AuNPs by changing the pH. For separating the effect of AuNP charge from brush properties, it is necessary that the brush charge remains constant. Therefore, PMETAC, a strong positively charged polyelectrolyte brush, was used. A combination of ellipsometry, AFM, UV/Vis spectroscopy, gravimetric analysis, and TEM allowed for obtaining a complete picture of particle loading and penetration of AuNPs inside the PMETAC brushes.

4.2 Results

4.2.1 PMETAC brush

Tuning of the brush thickness

The brush thickness was controlled by tuning polymerization time, ratio of CuCl/$CuCl_2$ and monomer concentration. The thickness was measured at ambient conditions by ellipsometry. Both for the CuCl/$CuCl_2$ ratio of 10:1 and 15:1 the brush thickness reaches a plateau after several hours (see Figure 11.1 in Appendix). Using a ratio of 15:1 (CuCl/$CuCl_2$) slightly thicker polymer brushes could be prepared compared to the ratio of 10:1, using the same polymerization time. The monomer concentration was adjusted to three values at a constant CuCl/$CuCl_2$ ratio of 15:1. The brush thickness increases with increasing polymerization time as well as the monomer concentration (Figure 4.1).

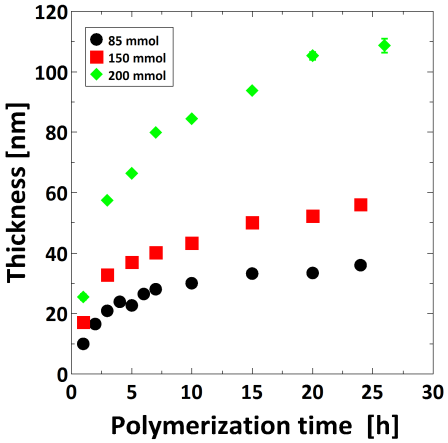

Figure 4.1: Thickness of PMETAC brush as a function of polymerization time and monomer concentration measured at ambient conditions by ellipsometry.

The surface roughness was determined using AFM topographical images with an area of 5 × 5 μm^2 measured at ambient conditions. Within the measured brush thickness range, the surface roughness is constant with a value of 0.7 ± 0.1 nm (Figure 4.2).

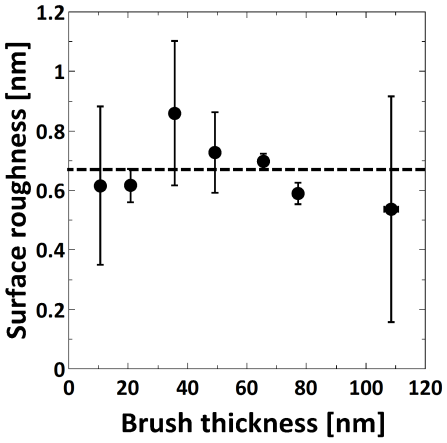

Figure 4.2: Surface roughness at ambient conditions determined from AFM micrographs as a function of ambient brush thickness (measured by ellipsometry).

Neat PMETAC brush in ambient conditions and water

In the present chapter, PMETAC brushes with a thickness of around 30 nm (ambient conditions) were used for the attachment of the particles. The samples were obtained from a monomer concentration of 85 mmol and a Cu(I)/Cu(II) ratio of 15:1. The thickness measured under ambient condition for different neat PMETAC brushes (sample 1-4) are listed in Table 4.1. All samples are from the same batch. They were synthesized simultaneously in the reactor under exact the same conditions.

Table 4.1: Thickness of neat PMETAC brushes measured by ellipsometry at ambient conditions.

Sample	**Thickness (nm)**
1	28.04 ± 0.57
2	29.24 ± 0.32
3	27.11 ± 0.80
4	27.84 ± 0.77

The samples 2-4 were used to prepare PMETAC/AuNP composite materials by incubating sample 2 into the AuNP suspension at pH 4, sample 3 into the AuNP suspension at pH 6, and sample 4 into the AuNP suspension at pH 8, while sample 1 was used as a reference

for a neat brush. The brush thickness in Milli-Q water was also measured for sample 1, both by ellipsometry and by full-indentation AFM (Table 4.2).

Table 4.2: Comparison of ellipsometry and the AFM full-indentation method for measuring the thickness in water for sample 1.

Method	**Thickness**
Ellipsometry	148.12 ± 6.42
AFM full-indentation	156.43 ± 9.44

As demonstrated in Table 4.2, the results obtained by the two independent methods are consistent within the experimental errors. This demonstrates that the full-indentation method can be also used to measure the thickness of polymer brushes. Beside thickness determination, AFM can be used in scanning mode to gain knowledge about the surface topography and material properties. Figure 4.3 shows the height (a) and phase (b) image for sample 1 recorded in Milli-Q water at room temperature. The height image reveals a homogeneous surface topology, while the phase image demonstrates a homogeneous composition for the PMETAC brush.

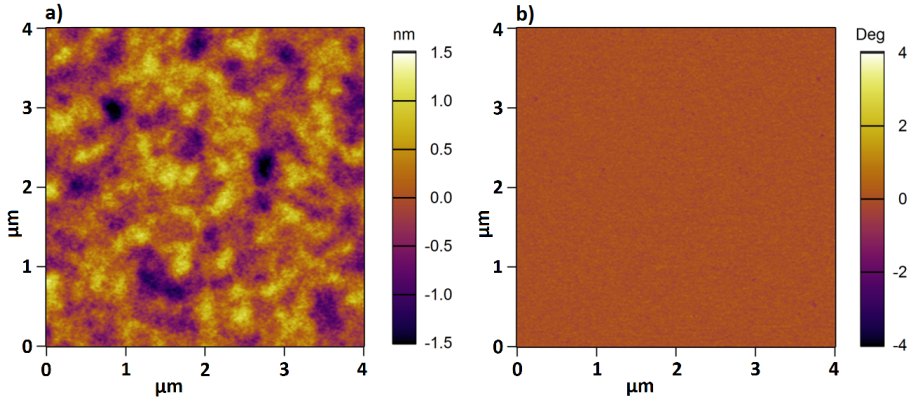

Figure 4.3: AFM height (a) and phase (b) image for sample 1 in Mili-Q water at room temperature.

4.2.2 Effect of pH on AuNP dispersion

Particle shape and size at different pH

The particle-particle interaction at different pH was investigated by mixing AuNP stock suspension with buffer solution with a pH ranging from 4 to 8. TEM measurements were performed to characterize the particle behavior and are shown in Figure 4.4. AuNPs at

pH 4 form compact aggregates. At pH 6, network-like aggregation occurs between AuNPs, while at pH 8 a stable suspension of individual AuNPs is observed. Clear differences in the AuNP bulk behavior can be observed, which likely has an effect also on the AuNP assembly in the PMETAC brush. Although an influence of the drying step on the particle distribution (see Chapter 3 section 3.3 instruments and measurement procedures) cannot be fully excluded, the strong impact of pH on the colloidal stability, as seen qualitatively in the TEM images, can be considered a robust result.

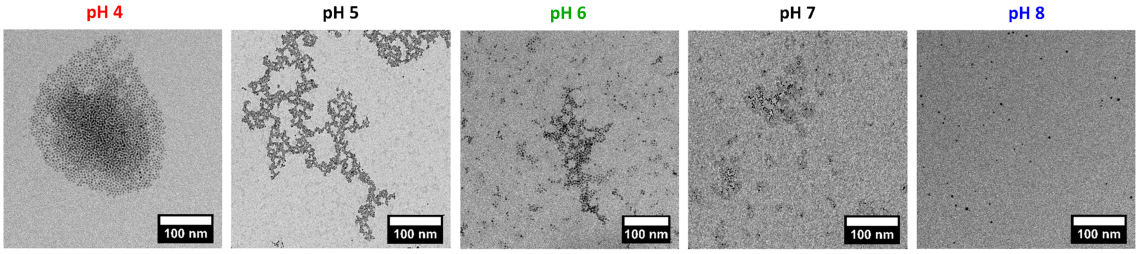

Figure 4.4: AuNPs dispersed in buffer solution with different pH ranging from 4 to 8 and measured by TEM.

UV/Vis spectroscopy characterization

AuNPs have the ability to interact with light through a collective oscillation of the conduction electrons on the metal surface, known as surface plasmon resonance (SPR). This phenomenon can be detected by UV/Vis spectroscopy[85]. AuNP suspensions at pH 4, at pH 6 and at pH 8 were measured at room temperature (Figure 4.5). Figure 4.5 shows that the surface plasmon peak shifts to longer wavelengths according to a decrease of pH.

Gravimetric analysis of AuNP concentration

The several synthesis steps necessary to produce MPA-capped AuNPs lead to some loss of product. This implies that the calculation of the AuNP concentration from the initial amount of $HAuCl_4$ would be too inaccurate. Therefore, the gold amount has been determined three times by gravimetric analysis of the MPA-capped AuNPs. The amount of gold (m_{gold}) in 1 mL AuNP suspension is $1.6 \pm 0.4 \cdot 10^{-3}$ g. From this, the concentration (c) of the incubation suspension at different pH can be calculated by estimating the total amount of AuNPs (n_{total}) in 1 mL of AuNP stock suspension (see Appendix for detailed calculations). The incubation suspensions were obtained by mixing 1 mL of AuNP

stock suspension ($n_{\text{total}} = 2.45$ nmol) with 9 mL of buffer solution. Therefore, c of the incubation suspension is 0.245 nmol/mL. According to Lambert-Beer law (Equation 3.2), the concentration c can be directly linked to the corresponding SPR absorbance peak measured by UV/Vis spectroscopy. Finally, the concentration within polymer brushes can be indirectly calculated by measuring the absorbance of the incubation medium before and after incubation. This procedure will be described more in detail in the next section.

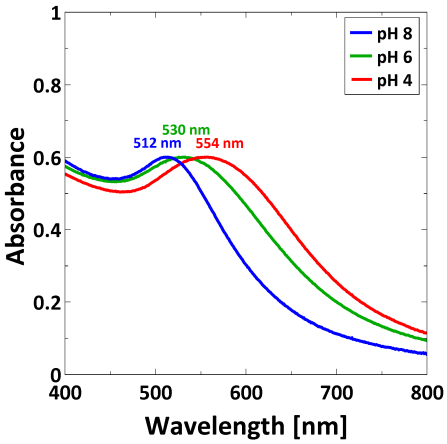

Figure 4.5: UV/Vis spectra recorded at room temperature for AuNP suspensions at pH 4, at pH 6 and at pH 8.

4.2.3 Composite material of PMETAC/AuNP

Characterization of PMETAC/AuNP composites by AFM

AFM was used to investigate both morphology (by scanning) and thickness (by full-indentation) of the composite brushes. Surface topography and phase images of composites at different pH are shown in Figure 4.6.

Two trends were observed in the height images a.1-c.1 shown in Figure 4.6. First, the amount of deposited AuNPs on top of the brush increases with increasing pH. Second, the tendency to aggregate decreases for increasing pH. Furthermore, the phase images reveal that two different materials are present, because the phase signal changes when the probe encounters regions with different composition.

After AuNP deposition, the thickness of the composites cannot be determined with monochromatic ellispometry, due to the dielectric function of the AuNPs as a new parameter. Therefore, the thickness was determined in water by the full-indentation method. The

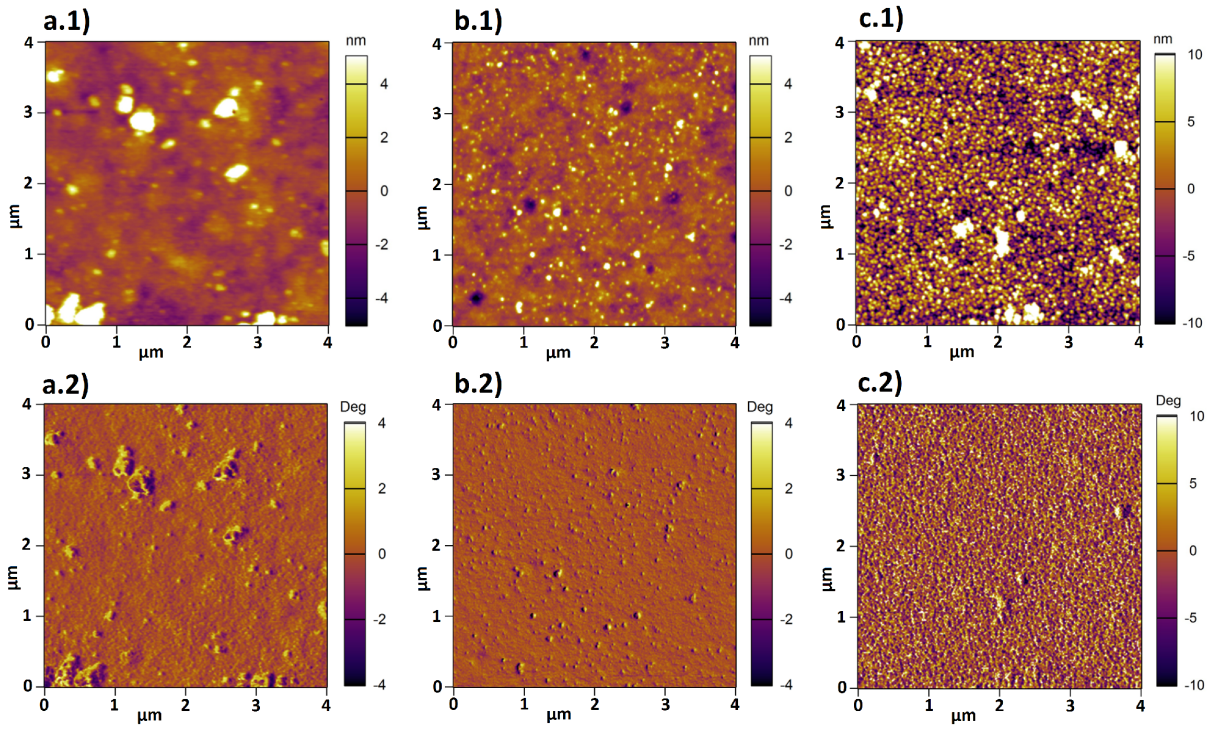

Figure 4.6: Height (a.1-c.1) and phase (a.2-c.2) images were recorded in water by AFM for composites (a.1/.2) at pH 4, (b.1/b.2) at pH 6, (c.1/.2) at pH 8.

values for the composites incubated at pH 8, at pH 6 and at pH 4 are listed in Table 4.3. The thickness of the neat brush is also reported for comparison.

Table 4.3: Measurements of the thickness in water of PMETAC/AuNP composites using the AFM full-indentation method. The thickness of the neat polymer brush was also listed for comparison reasons.

Neat PMETAC brush thickness (nm)	**Composite at pH 4 thickness (nm)**	**Composite at pH 6 thickness (nm)**	**Composite at pH 8 thickness (nm)**
156.43 ± 9.44	162.97 ± 6.03	170.68 ± 9.27	178.35 ± 11.77

The swollen thickness of the samples increases after loading with AuNPs. Furthermore, the values increases with increasing pH of the AuNP suspension.

UV/Vis characterization

After incubation in AuNP suspension, the PMETAC/AuNP composites were analyzed by UV/Vis spectroscopy. The plasmon band is analyzed as follows: the intensity is proportional to the amount of particle content, while the position of the plasmon peak

gives information about SPR coupling[129,130]. Here, PMETAC brushes incubated at different pH were measured in water, and the corresponding absorbance peaks are reported in Figure 4.7.

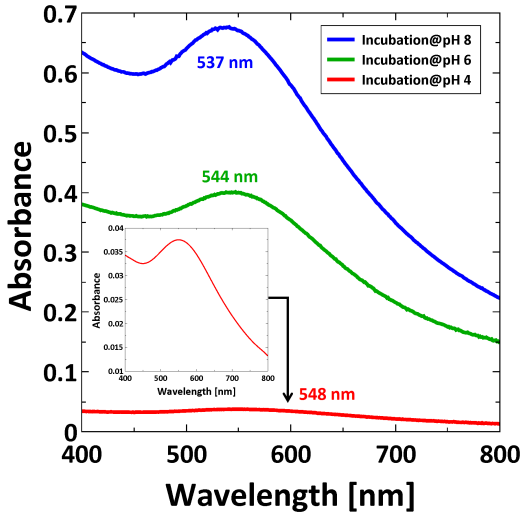

Figure 4.7: UV/Vis spectra recorded in water for PMETAC/AuNP composites incubated at pH 4, at pH 6, and at pH 8. Magnified representation of the SPR band for PMETAC/AuNP composite at pH 4 (inset).

Figure 4.7 reveals two trends. First, the intensity of the plasmon peak is decreasing for decreasing pH, which is a typical indication for lower particle uptake with decreasing pH. Second, the plasmon peak is shifted to a higher wavelength with decreasing pH, which indicates a decrease in the interparticle distance[131].

The amount of AuNPs within PMETAC brushes

The amount of AuNPs adsorbed in the PMETAC brushes was estimated from the difference of the AuNP concentration in suspension before and after brush incubation. In fact, from the measurement of the absorbance by UV/Vis spectroscopy of the AuNP suspensions before and after the incubation (see Appendix, Figure 11.2) a decrease of the absorbance after the incubation was found, which was explained by particle uptake. Since the amount of AuNP was measured by gravimetric analysis, c could be linked to the absorbance through Lambert–Beer's law (Equation 3.2). Therefore, the surface plasmon peak before and after incubation can be used to determine the particle number density (Equation 4.1) within PMETAC, since $A \propto c$. Using the calculated amount of AuNPs within the brush, it is possible to calculate the respective particle number densities. For this purpose, a box

model (Figure 4.8) was used. The calculated particle number densities are listed in Table 4.4.

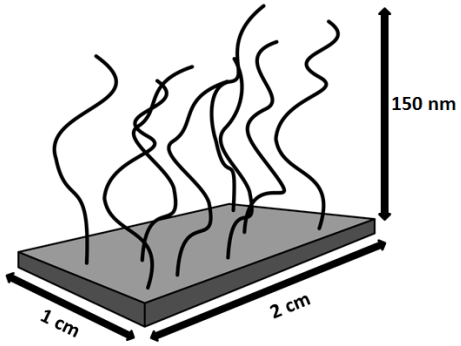

Figure 4.8: Determination of particle number densities using a box model.

Table 4.4: Particle number densities of AuNPs within PMETAC brushes obtained by UV/Vis of composites incubated at different pH.

Incubation medium	Absorbance before incubation	c before incubation (nmol/ml)	Absorbance after incubation	c after incubation (nmol/ml)	Δc (nmol/ml)	ΔN (Particles)	Particle number density (Particles/nm^3)
at pH 4			0.574 ± 0.018	0.234	0.011	$6.62 \cdot 10^{13}$	0.0011
at pH 6	0.602 ± 0.006	0.245	0.455 ± 0.019	0.185	0.059	$3.55 \cdot 10^{14}$	0.0059
at pH 8			0.399 ± 0.021	0.162	0.083	$4.98 \cdot 10^{14}$	0.0083

The difference between c after incubation and c before incubation is defined as Δc, which can be calculated back to ΔN_{total} with eq. 11.4 (see Appendix). Δc corresponds to the total amount of AuNPs within the PMETAC brush. Assuming that the brush is located on the whole glass slide (2×1 cm^2) and is 150 nm thick in swollen state (Figure 4.8), and assuming also a homogeneous AuNP distribution over the whole brush area, the volume of the incubated brush (V_{brush}) can be calculated. Therefore, the particle number density (Equation (4.1)) is 1.1×10^{-3} particles/nm^3 for the incubation of the brush at pH 4, 5.9×10^{-3} particles/nm^3 at pH 6 and 8.3×10^{-3} particles/nm^3 at pH 8. The particle number density of attached AuNPs increases with increasing pH of incubation suspension:

$$Particle\ number\ density = \frac{\Delta N_{total}}{V_{brush}}. \tag{4.1}$$

4.3 Discussion

In the present study, the thickness of the PMETAC brushes was tuned by means of CuCl/$CuCl_2$ ratio, polymerization time and monomer concentration. In particular, the

brush thickness increases with increasing $CuCl/CuCl_2$ ratio, polymerization time and monomer concentration, although changing the $CuCl/CuCl_2$ ratio did not result in significant changes (see Appendix, Figure 11.1). Similar growth behavior was observed for other polymers, like PDMAEMA for similar changes of $CuCl/CuCl_2$ and polymerization time[90] and poly(oligo(ethylene glycol)acrylamide) (PMEGAm) brushes for increasing monomer concentration[132]. The surface roughness of the prepared brushes was found to be independent of the brush thickness, with an average surface roughness of 0.7 ± 0.1 nm in ambient conditions (Figure 4.2).

PMETAC brushes with around 30 nm in ambient conditions (Table 4.1) were used to study the particle uptake by changing the pH of the incubation medium. The reasons for using thin polymer brushes were manifold. Christau *et al.* observed AuNP crowding on PDMAEMA brushes with increasing polymer brush thickness (beyond 40 nm thickness in ambient conditions)[90], which made it challenging to obtain single particles attached to the surface. In addition, recently published results have shown that there are instances that polymer brushes tend to degraft by exposing them to a good solvent. Those include brushes with a high degree of charges (e.g., polyelectrolyte brushes) or containing non-polymeric materials (e.g., NPs)[133–135]. To overcome the swelling-induced degrafting by reducing the tension on the brush, the molecular weight of the brushes was decreased.

MPA-capped AuNPs were synthesized by a ligand exchange reaction of citrate-covered AuNPs. They are characterized by pH-sensitivity (pK_A of MPA-capped AuNPs is 4.3[115]). TEM images (Figure 4.9) reveal that decreasing the pH decreases the interparticle distance due to the protonation of the carboxylic acid group on the surface, and therefore the reduction of electrostatic repulsions. AuNPs are still sterically stabilized through the capping, and can form aggregates via the formation of H-bond of the protonated carboxylic acid groups (Figure 4.9c)). Given that AuNPs exhibit SPR, which is dependent e.g., on the interparticle distance[81] through SPR coupling, UV/Vis measurements were carried out (Figure 4.5). The position of the SPR peak of MPA-capped AuNPs depends on the pH. The shift of the peak to a higher wavelength for decreasing pH was explained by the decrease in the interparticle distance. This is in agreement with previous results from Lim *et al.*[136], where decreasing of the interparticle distance leads to a red-shift of the SPR peak.

Since strong polyelectrolytes like PMETAC are insensitive to pH and have permanent positive charges, they present a suitable matrix to study pH effects on the distribution of AuNPs with a pH-sensitive capping. For all studied pH, AuNP uptake could be observed, which causes an increase in brush thickness. The increase is explained by an

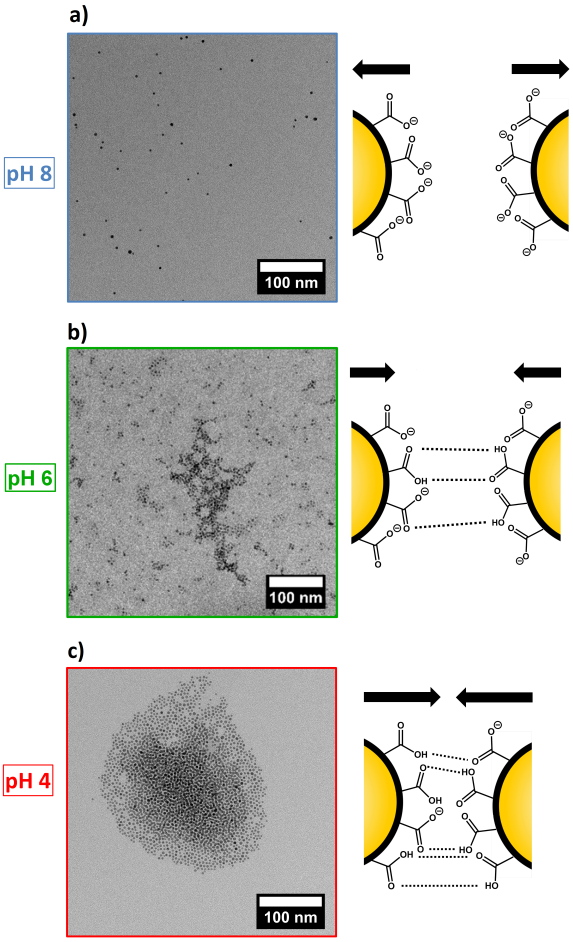

Figure 4.9: TEM images of AuNPs in different pH medium. a) Electrostatic stabilization of AuNPs leads to no attraction when exposed to pH 8. b) Formation of networks at pH 6 since negative charges decrease due to protonation of the carboxylic group. c) More than half of the carboxylic groups are protonated at pH 4, which leads to a lack of electrostatic stabiliziation. Hydrogen bond formation between neighboring AuNPs leading to attraction and aggregation.

increase in osmotic pressure due to an enhanced amount of counterions within the brush. The consequence is a stronger swelling in water (Table 4.3). Using gravimetric analysis and UV/Vis spectroscopy, the particle number density could be calculated. The results showed that the particle number density increases with increasing pH (Table 4.4), which is attributed to the more negatively charged AuNPs due to the deprotonation of the carboxylic acid groups of the MPA capping.

In fact, by comparing UV/Vis measurements of AuNP suspensions at different pH (Figure 4.5) with the measurements of PMETAC/AuNP composites (Figure 4.7), one can see that, except for the composite at pH 4, the absorption maxima appear at a higher wavelength

for the AuNPs in brush than in suspension. The reason is a change in refractive index from water ($n = 1.33$) to polymer brush ($n = 1.51$) which leads to a red-shift. At pH 4, the change of refractive index can be neglected because the AuNPs are aggregated in dispersion, and the plasmon coupling leads to a stronger red-shifted absorbance peak in the dispersion than in the brush.

By considering exclusively the composite materials, a higher particle uptake within the brush should lead to a red-shifting of the plasmon peak due to plasmon coupling, which is not the case (Figure 4.7). Here, a red-shift of the plasmon peak is observed for a lower particle uptake (at pH 4). This indicates a non-homogeneous distribution of AuNPs within the brushes after incubation at pH 4. A lower particle uptake and a simultaneous red-shift of the plasmon peak might indicate that the AuNPs are attached only on top of the brush surface (2D assembly). This would lead to a decreased interparticle distance, even though the averaged particle number density on the whole brush is lower. With respect to the results at pH 4, the higher particle uptake at pH 8 induces a plasmon peak at smaller wavelength. This indicates a more homogeneous distribution (3D assembly), which is related to deeper penetration in the brush. The interparticle distance is larger, due to the larger space available inside the brush than on the brush surface. Different assemblies at different pH can be therefore attributed to the AuNPs (Figure 4.9). AuNPs form aggregates from suspensions at pH 4, which cannot penetrate into the dense polymer brush and get stuck on top of the surface, while single particles are observed at pH 8, which can penetrate the brush easily and are embedded (Figure 4.10). In both, the attachment at pH 4 and at pH 8 is driven via electrostatic attraction between particle and brush. Nevertheless, at pH 4, more than half of the carboxylate groups of the MPA-capping is in a protonated state and the electrostatic attraction is less pronounced than at pH 8.

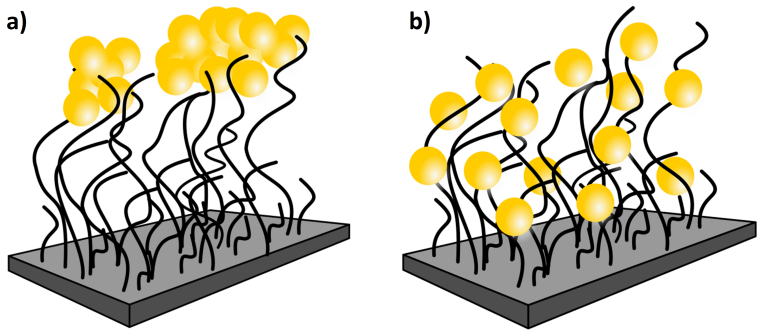

Figure 4.10: Two suggested assembly of brush/AuNP composites. Here, composites at pH 4 form more likely (**a**) a 2D assembly while composites at pH 8 form mainly (**b**) a 3D assembly.

In summary, sterical hindrance during incubation avoids a homogeneous distribution of AuNPs within the brush. In addition, increasing of the electrostatic interactions between AuNPs and polymer brush leads to a higher and deeper particle uptake.

4.4 Conclusion

The particle uptake of pH-dependent negatively charged AuNPs within strong positively charged PMETAC brushes was investigated at different pH. At low pH (pH 4), the AuNP form aggregates in the dispersion used for incubation due to protonation of the acid groups in the AuNP coating and reduced electrostatic repulsion. The formation of aggregates prevent the penetration of AuNP into the brush, which form aggregates at the brush surface. The AuNP aggregates have still negative charges and can bound to the brush via electrostatic attraction. This assembly structure leads to a low amount of attached AuNPs, but to strong plasmon coupling between the AuNP aggregates. At higher pH (pH 8), the acid groups are deprotonated, leading to highly charged AuNPs and a stabilized dispersion. The single AuNPs can penetrate into the brush and be physisorbed into the oppositely charged positive groups of the polyelectrolyte chains, leading to high uptake. In comparison to low pH, the plasmon coupling is reduced due to a more homogeneous distribution of the AuNPs.

To conclude, the study in this chapter remarks that two effects are important for the uptake of AuNPs by polymer brushes: (1) the stability of the AuNP dispersion that is used for incubation and (2) the interaction between AuNPs and the polymer chains of the brush. Furthermore, strong hints are given that the distribution of the AuNPs is dependent on the pH value during incubation, which will be addressed in the following two chapters.

Chapter 5

Internal structure of PMETAC brush/gold nanoparticle composites: a combined neutron and X-ray reflectometry study*

Abstract

This chapter addresses the pH-triggered distribution and relocation of MPA-coated AuNPs incorporated into PMETAC brushes. Brush/ particle composite materials were investigated against aqueous solutions and at different humidities using neutron and X-ray reflectometry, respectively. X-ray reflectometry measurements complement neutron reflectometry measurements and reveal results that could not be observed by neutron reflectometry measurements. Both methods allow scanning the particle density profile, but due to different contrasts, they are sensitive to different regions within the brush. The results show, that the particle number density as well as the particle distribution depend strongly on the pH value of the incubation medium: A rather non-homogeneous assembly (2D assembly) is found when the PMETAC brush is incubated in AuNP suspension at pH 4, while a more homogeneous assembly (3D assembly) is found when the PMETAC brush is incubated in AuNP suspension at pH 8. The main factor dominating the formation of 2D or 3D assembly is assigned to the particle-particle interaction and not to the particle-polymer interaction. No significant relocation of AuNPs within the brush can be found by changing the environmental conditions.

5.1 Introduction

The results of the last chapter give strong evidence that the particle assembly depends on the pH value of the AuNP suspension in which the polymer brush is dipped. AuNPs are rather uncharged at pH 4 and are not electrostatically stabilized. Thus leads to the formation of AuNP agglomerates in the suspension. Incubation of the brush in AuNP suspension at this pH avoids penetration of AuNP into the brush due to sterical hindrance of the agglomerated AuNPs. A layer of AuNPs is formed on top of the brush (2D assembly), which was detected with an AFM. On the contrary, AuNPs are rather charged at pH 8 and

*Similar content was presented in D. Kesal, S. Christau, M. Trapp, P. Krause and R. von Klitzing, *PCCP*, **2017**, *19*, 30636-30646 (The internal structure of PMETAC brush/gold nanoparticle composites: a neutron and X-ray reflectivity study).

are stabilized electrostatically in water. After incubation of the brush into a suspension at pH 8, no agglomerates could be detected with an AFM. Therefore it was speculated that the AuNP could penetrate deeper into the brush. So far, the distribution of the AuNP across the brush is unknown.

The present chapter elucidate the AuNP distribution perpendicular to the substrate surface based on X-ray and neutron reflectometry data. The internal distribution of pH-sensitive AuNPs in a PMETAC brush is studied as well as the reorganization of already embedded AuNPs in the brush. In particular, the same MPA-AuNPs with a diameter of 5 nm were embedded into PMETAC brushes with the exception that the incubation time is decreased to 6 h. NR is used to study the internal structure of AuNPs on brushes, which were incubated at different pH values in aqueous solution. XRR allows the detection of the particle distribution in the polymer matrix in dry and humid conditions. Further, UV/Vis combined with AFM and SEM scanning images as well as TEM measurements and ellipsometric measurements are carried out to obtain a complete picture of the particle loading, particle distribution, and particle reorganization inside the polymer brush.

5.2 Results

Prior to the reflectometry measurements, pre-characterization of the neat PMETAC brush as well as of the PMETAC/AuNP composites as shown in Chapter 4 is presented. This is done, because the incubation time was decreased from 24 h to 6 h, which has an impact on the amount of attached or incorporated AuNPs.

5.2.1 Ellipsometry

Ellipsometry was used to determine the neat brush thickness. The thickness of the dry brush (<2 %rh) for the reflectometry measurements was 20.1 ± 0.5 nm with a refractive index of 1.53 and the brush thickness in ambient conditions (≈ 30 %rh) was 21.2 ± 1.3 nm with a refractive index of 1.52. The thickness and refractive index were determined by ellipsometry in a home-built humidity cell as introduced earlier[116]. XXR and NR measurements were done on the same samples, while AFM, SEM and UV/Vis measurements were done with PMETAC brushes with a dry thickness (<2 %rh) of 32.35 ± 0.77 nm. Here, a thicker brush was used for better visualization of the particles in AFM and SEM images and a higher signal to noise ratio in UV/Vis measurements, since Christau et al. have showed that the amount of particles scales with the brush thickness[90].

5.2.2 AFM and SEM

AFM was used to display the loading and distribution of attached AuNPs on top of the polymer brush surface. Height images were recorded before and after attachment of the MPA-capped AuNPs at pH 4 and pH 8 (Figure 5.1). The images were recorded in ambient conditions. By comparing the composite brush with the neat brush, an attachment of the AuNPs is observed under both incubation conditions. Homogeneously distributed individual particles are detected in case of PMETAC incubated in AuNP suspension at pH 8. After incubation at pH 4, however, the AuNPs form bigger aggregates.

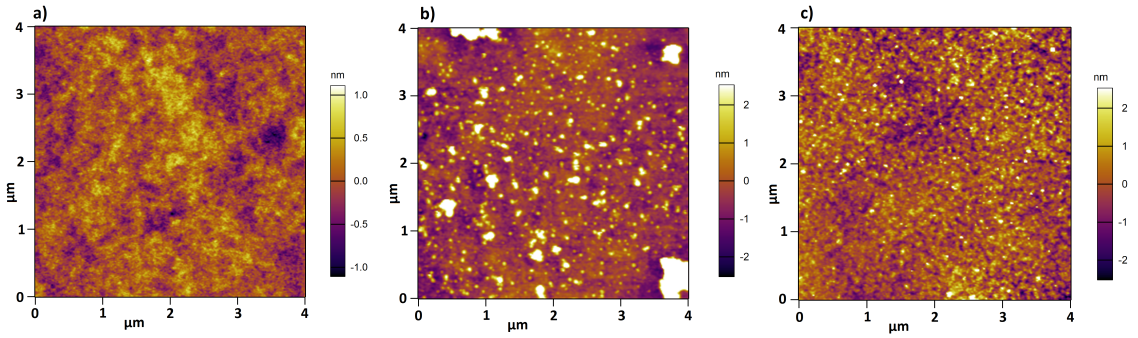

Figure 5.1: AFM height images of a) neat PMETAC brush, and after incubation b) at pH 4 and c) at pH 8. Images were recorded in ambient conditions.

SEM was used to image AuNPs assemblies at the brush, since AuNPs have a high contrast. However, SEM is recorded in dry state at high vacuum and the particle assembly might differ. Measurements were recorded after attachment of AuNPs in PMETAC brushes at pH 4 and pH 8, respectively. Aggregation of individual AuNPs into bigger aggregates is observed for PMETAC brushes after incubation in AuNP suspension at pH 4 (see Appendix, Figure 11.3). AuNP aggregates are attached to the brush surface. For PMETAC brushes incubated in AuNP suspension at pH 8, however, homogeneously distributed individual particles over the entire brush are observed (see Appendix, Figure 11.4).

5.2.3 UV/Vis Spectroscopy

A further proof for aggregation of AuNPs is plasmon coupling, which can be detected by UV/Vis spectroscopy[85]. UV/Vis spectroscopic measurements were carried out at room temperature in water for PMETAC/AuNP composites prepared at pH 4 and at pH 8. The wavelength as well as the intensity of the SPR peak for the different samples is listed in Table 5.1. The plasmon band (Figure 5.2) reveals two important information: the intensity

of the plasmon peak is assumed to be proportional to the amount of particle content, while the position of the plasmon peak gives information about SPR coupling[127,129]. The incubation of PMETAC brush in AuNP suspension at pH 8 has a roughly 7 times higher intensity peak of the plasmon band than the incubation of PMETAC brush in AuNP suspension at pH 4. This indicates a lower particle uptake for the PMETAC brush incubated in AuNP suspension at pH 4. Further, the plasmon peak is shifted to higher wavelength by 5 nm with decreasing pH (Figure 5.2 a)). This gives a strong hint for a non-homogeneous distribution of AuNPs in PMETAC brush, i.e. a layer of AuNPs at the top of the brush. Ellipsometry measurements showed that the thickness and the refractive index of the neat brush is pH independent (for more details see Chapter 7). That indicates that the aggregation is not induced by changes in brush conformation. The characterization of the neat PMETAC brush as well as the AuNPs itself were extensively characterized in previous articles[115,137] and in Chapter 4. The difference to Chapter 4 are that the incubation time was decreased, which has an impact on the amount of attached or incorporated AuNPs. A reduction of uptaken AuNPs is observed in a shift of the SPR absorption bands as well as in a decrease of the maximum intensity.

Table 5.1: UV/Vis measurements for two PMETAC brushes incubated at pH 4 and for two PMETAC brushes incubated at pH 8 were carried out in H_2O at room temperature. The maximum intensity of the plasmon band as well as the wavelength at maximum intensity λ_{max} for PMETAC/AuNP composites are shown here.

Sample	Absorption at λ_{max}	λ_{max} [nm]
Incubation@pH 4	0.030±0.003	530±2
Incubation@pH 8	0.202±0.033	525±1

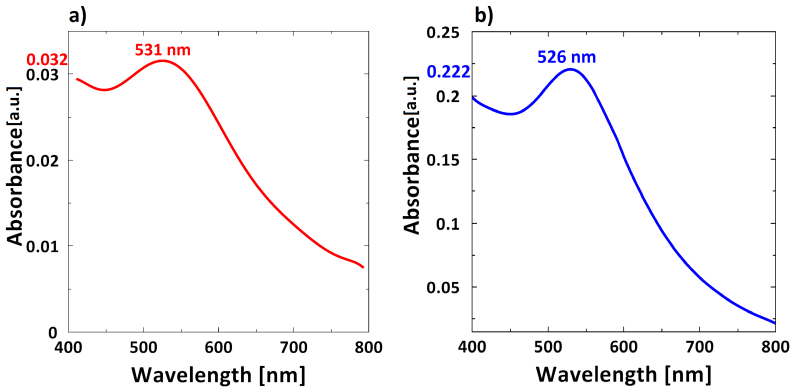

Figure 5.2: UV/Vis spectra of PMETAC/AuNP composites after incubation a) at pH 4 and b) at pH 8. The measurements were carried out in water at room temperature. The maximum intensity as well as the wavelength at maximum intensity is highlighted for each SPR band.

5.2.4 Neutron reflectometry (NR)

In the following, the distribution of AuNPs perpendicular to the surface is studied by NR. NR is a suitable method to study the present system, since the SLD is different for PMETAC, AuNPs and D_2O[138,139].

The internal structure of the PMETAC brushes before and after attachment of AuNPs was investigated by NR measurements. The NR measurements were carried out at 22 °C in D_2O, and the data were fitted using a multi-layer model (see Figure 3.9).

Neat PMETAC brush

The swollen structure of the neat PMETAC brush was investigated, which is shown in Figure 5.3. No Kiessig fringes appears, and the scattering length density (SLD) exhibits a more dense structure close to the substrate followed by a large dilute region where the SLD increases from the solid interface towards the liquid subphase (D_2O). The SLD has a steep increase, which indicates a pronounced swelling of the brush in D_2O. The water content in PMETAC brush is around 70 - 80 % measured by ellipsometry (see Chapter 8, Figure 8.1), which is in good agreement with other studies using NR as well as QCM-D[140,141].

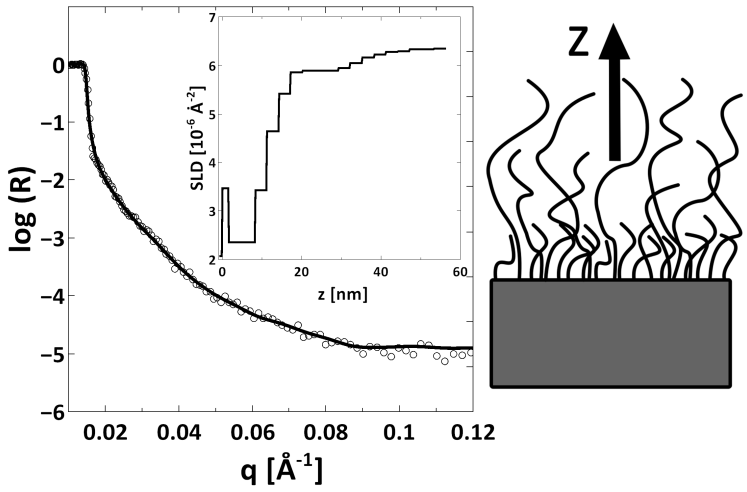

Figure 5.3: Neutron reflectometry (NR) data (symbols), fit (solid line) and SLD (inset) of a neat PMETAC brush measured in D_2O (swollen state) at 22 °C. z=0 corresponds to the surface position of the Si-substrate.

PMETAC/AuNP composites

After incubation at pH 4 In order to study the distribution of the AuNPs within the PMETAC brush, NR measurements were carried out for a PMETAC brush, which was incubated in AuNP suspension at pH 4 before. The reflectivity curve was recorded against D_2O and shows no Kiessig fringes as the reflectivity curve of the neat PMETAC brush (Figure 5.4). Also the SLD profiles of both, neat PMETAC brush and composite brush are quite similar.

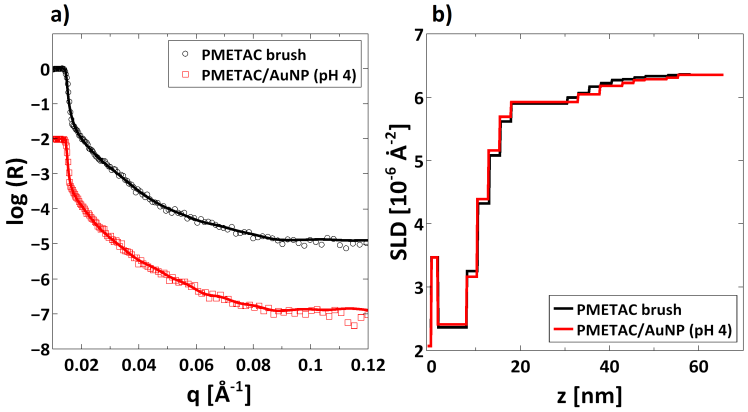

Figure 5.4: a) NR data (symbols), fit (solid line) of a neat PMETAC brush and PMETAC/AuNP composite prepared at pH 4 and measured in D_2O (swollen state) at 22 °C, and b) the corresponding SLDs. Reflectivity curves are shifted vertically for clarity.

After incubation at pH 8 By comparing the reflectivity curves of the neat PMETAC brush with a brush incubated in AuNP suspension at pH 8, changes in the reflectivity curve as well as in the SLD profile are obvious (Figure 5.5). Kiessig fringes are detected after the particle attachment at pH 8. The AuNP attachment causes a change in profile shape, SLD and thickness. The overall thickness increases after AuNP attachment. Compared to the neat PMETAC brush, the dense structure close to the substrate is decreased in thickness and has a higher SLD, while the SLD towards the subphase is lower for the PMETAC/AuNP composite. This effect will be interpreted in the discussion part based on the fact that the SLD of Gold is higher than for PMETAC but lower than D_2O ($SLD_{PMETAC} \approx 0.77 \times 10^{-6}$ Å^{-2} < $SLD_{AuNP} \approx 4.5 \times 10^{-6}$ Å^{-2} < $SLD_{D_2O} = 6.36 \times 10^{-6}$ Å^{-2} (Motofit database)).

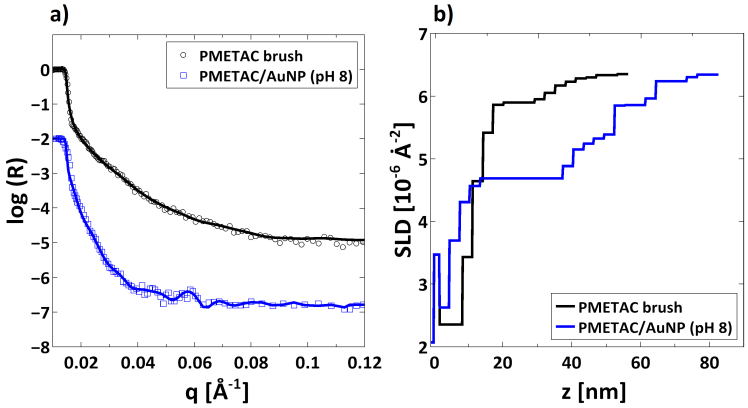

Figure 5.5: a) NR data (symbols), fit (solid line) of a pure PMETAC brush and PMETAC/AuNP composite prepared at pH 8 and measured in D_2O (swollen state) at 22 °C, and b) the corresponding SLDs. Reflectivity curves are shifted vertically for clarity.

5.2.5 X-ray reflectometry (XRR)

In the following the AuNP distribution in PMETAC brushes is studied with XRR. Using XRR should give a higher contrast due to the high electron density of the incorporated or attached AuNPs. XRR measurements were carried out against different relative humidities to check whether the water content has an effect on the reorganization of the AuNPs.

Neat PMETAC brush

The brush was measured in dry conditions (4-7 %rh), under ambient conditions (30 %rh) and humid conditions (≈92 %rh) (Figure 5.6). The reflectivity curve of the neat PMETAC brush was fitted with a one-layer model (Gaussian roughness). The fit results are summarized in Table 5.2.

Table 5.2: Data for the neat PMETAC brush at different r.h. obtained by X-ray reflectometry (XRR) measured at room temperature. As a comparison the polymer thickness at ambient conditions and dry conditions obtained by ellipsometric measurements are also shown.

		XRR Layer 1		
Humidity [%rh]	h_{elli} [nm]	h_{XRR} [nm]	ρ_e [Å^{-3}]	Roughness [nm]
4-7	20.1±0.5	20.3	0.516	0.5
30	21.2±1.3	22.2	0.479	0.9
92		36.3	0.371	0.9

The thickness determined by ellipsometry for dry conditions and 30 %rh is in very good agreement with the XRR data.

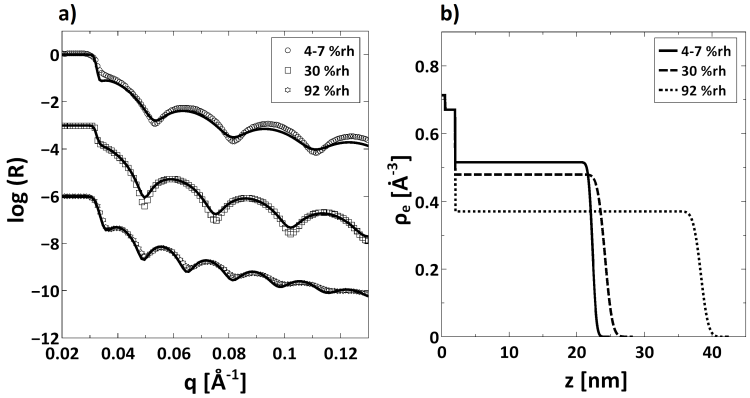

Figure 5.6: a) X-ray reflectometry (XRR) data (symbols) for neat PMETAC brush measured at different r.h. and fits (line). The data were fitted using a one-layer model. b) Corresponding electron density profiles in the z-direction for neat PMETAC brush measured at different humidity levels. z=0 corresponds to the surface position of the Si-substrate. Reflectivity curves are shifted vertically for clarity.

Increasing the humidity leads to an increase in thickness. Further, the electron density of the polymer brush decreases with increasing humidity while the roughness increases[142].

The volume percent of water (y) within the brush at different relative humidities can be determined as follows (Eq. 5.1)

$$\rho_{e,brush} = (1-y) \cdot \rho_{e,pure\ brush} + (y) \cdot \rho_{e,H_2O} \tag{5.1}$$

where $\rho_{\mathrm{e,brush}}$ is the electron density for the neat brush at different relative humidities. The assumption is that $\rho_{\mathrm{e,brush}}$ at a relative humidity of 4-7 %rh consists of pure polymer ($\rho_{\mathrm{e,pure\ brush}}$) and does not contain any water. The electron density for water is $\rho_{\mathrm{e,H_2O}} = 0.335$ Å^{-3}. The volume percent of water (y $\cdot$ 100 %) is summarized in Table 5.3.

Table 5.3: Volume percent of water in polymer brush at different relative humidties

Humidity [%rh]	H_2O [vol-%]
4-7	0
30	20.4
92	80.1

It shows that the volume percent of water inside the brush increase significantly with increased relative humidity.

PMETAC/AuNP composites

Since the electron densities of gold (AuNPs) and PMETAC (polymer) are completely different, XRR can be used to elaborate if the particles are trapped within the brush or if they form a mono- or multi-layer on top of the brushes. In previous work, Christau et al.[91] showed that citrate-coated AuNPs are more likely attached to the PDMAEMA brush surface and form a 2D assembly. Therefore a three-layer-model was needed for the fitting of XRR data of AuNPs in brushes. Layer 1 was assigned to the layer closest to the substrate, layer 2 consisted of a particle layer attached to the brush surface, and layer 3 refers to the particles protrusion out of the brush. For better illustration of the model see Figure 11.5 (see Appendix). For fitting the data for PMETAC/AuNP composites, also a three-layer-model was used. The composites were measured in the same way how the neat PMETAC brushes were measured and under the same conditions.

After incubation at pH 4 The XRR curves and the electron density profiles are shown in Figure 5.7 and Figure 5.8, respectively. And the results are summarized in Table 5.4. Furthermore, the reflectivity curve and fit at 99 %r.h. are plotted in a $R \cdot q^4$ representation for better visualization and are shown in Figure 11.6 (see Appendix).

Table 5.4: Data for PMETAC/AuNP composites after incubation at pH 4 at different %r.h. obtained by XRR measured at room temperature.

	XRR Layer 1		XRR Layer 2		XRR Layer 3	
Humidity [%rh]	h_1 [nm]	ρ_e [Å^{-3}]	h_2 [nm]	ρ_e [Å^{-3}]	h_3 [nm]	ρ_e [Å^{-3}]
4-7	20.5	0.516	4.9	0.680	0.7	0.116
30	22.1	0.481	5.0	0.673	0.7	0.337
92	36.4	0.375	4.9	0.673	0.7	0.158

The electron density profiles reveal that the particles have been attached to the brush surface leading to a sharply increasing electron density in the outermost region. The electron density of layer 1 has the same value and same thickness (within the error bar) as for the pure PMETAC brush at the same humidity level, which indicates no AuNP incorporation within layer 1 for the composite. Further, the thickness of layer 1 increases with increasing humidity. Layer 2 has the highest electron density and the electron density as well as the thickness do not change and are independent on humidity variation. The thicknesses and electron densities of layer 3 do not exhibit any systematic variation with humidity changes. The sum of the thicknesses of layers 2 and 3 is in the range of the particle diameter (≈5.6 nm), which could validate the existence of a particle monolayer. One has to keep in mind that previous AFM and TEM results showed that AuNPs form

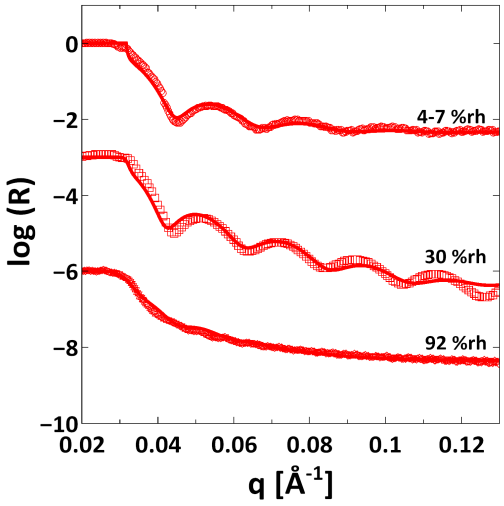

Figure 5.7: XRR data (symbols) and fits (line) for PMETAC/AuNP composite after incubation at pH 4 measured at different r.h.. The data were fitted using a three-layer model. Reflectivity curves are shifted vertically for clarity.

small aggregates at pH 4 and only a small amount of those aggregates is attached to the brush surface[137]. In order to minimize the parameters, we tried to fit the data with a two-layer-model. However, the fits are not satisfying, which are shown in Figure 11.7 (see Appendix).

In the next step the amount of attached AuNPs will be determined (Eq. 5.2). Due to the fact that ρ_e of layer 2 is independent of the relative humidity it is assumed that layer 2 consists only of air ($\rho_{e,air} = 0$ Å^{-3}) and AuNPs ($\rho_{e,Au} = 4.36$ Å^{-3})

$$\rho_{e,layer\ 2} = (1 - x) \cdot \rho_{e,air} + (x) \cdot \rho_{e,Au} \tag{5.2}$$

where x · 100 % is the volume percent of AuNPs in layer 2. Table 5.5 shows the volume percent for the AuNPs at different relative humidities.

Table 5.5: Volume percent of AuNPs at different relative humidties

Humidity [%rh]	AuNP [vol-%]
4-7	15.6
30	15.4
92	15.4

The volume percent of AuNPs is almost constant, which indicates that layer 2 does not swell by increasing the relative humidity . Assuming that only air and AuNPs are involved, the volume percent of AuNPs is 15.5 ± 0.1 vol-%.

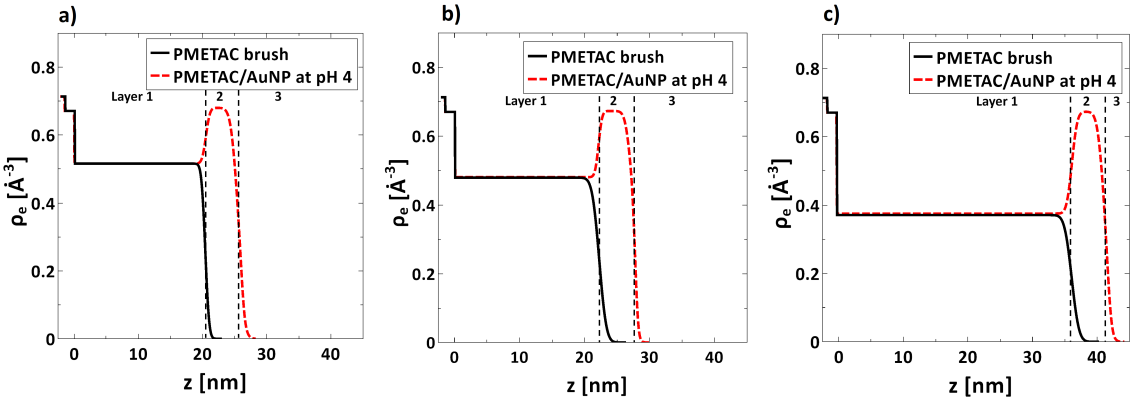

Figure 5.8: Electron density profiles in the z-direction from the substrate surface (z=0) for PMETAC/AuNP composite after incubation at pH 4 (red broken lines) and neat PMETAC brush (black solid lines) measured at different r.h. for a) 4-7 %rh, b) 30 %rh, and c) 92 %rh.

Combining all three layers together, the thickness of the brush after incubation is in general higher than the thickness of the pure PMETAC brush before incubation.

After incubation at pH 8 The XRR curves and the electron density profiles obtained by using a three-layer model to fit the reflectivity curves are shown in Figure 11.8 and Figure 11.9 (see Appendix), respectively. The results are summarized in Table 11.1 (see Appendix). The electron density profiles show clearly that the AuNPs are homogeneously distributed over the entire brush. Therefore, a one-layer model has been used and the XRR curves and the electron density profiles are shown in Figure 5.9 and Figure 5.10, respectively. The results are summarized in Table 5.6. In comparison, the one-layer model fits the data better than a three-layer-model.

Table 5.6: Data for PMETAC/AuNP composites after incubation at pH 8 at different r.h. obtained by XRR measured at room temperature.

	XRR Layer 1		
Humidity [%rh]	h [nm]	ρ_e [Å^{-3}]	Roughness [nm]
4-7	23.7	0.928	1.7
30	27.4	0.857	1.3
92	41.5	0.695	1.2

The electron-density profiles of PMETAC/AuNP composites after incubation at pH 8 show that the AuNPs are homogeneously distributed over the entire brush due to an increase in the electron density. The thickness is higher after the incubation of PMETAC brush in

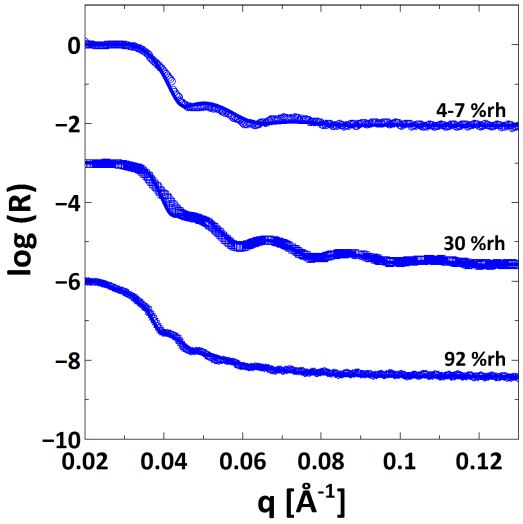

Figure 5.9: XRR data (symbols) and fits (line) for PMETAC/AuNP composite after incubation at pH 8 measured at different r.h.. The data were fitted using a one-layer model. Reflectivity curves are shifted vertically for clarity.

AuNP suspension at pH 8. Furthermore, the thickness increases with increasing relative humidity while the electron density decreases.

The volume percent of water (y · 100 %) within the PMETAC/AuNP composite material at different relative humidities can be determined as follows (Eq. 5.3)

$$\rho_{e,swollen\ PMETAC/AuNP} = (1-y)\ \cdot\ \rho_{e,PMETAC/AuNP} + (y)\ \cdot\ \rho_{e,H_2O} \tag{5.3}$$

where $\rho_{\mathrm{e,swollen\ PMETAC/AuNP}}$ is the electron density for the PMETAC/AuNP composite material at different relative humidities. The assumption is that $\rho_{\mathrm{e,PMETAC/AuNP}}$ at a relative humidity of 4-7 %rh consists of a mixture between AuNPs and PMETAC without water. The electron density for water is $\rho_{\mathrm{e,H_2O}}$=0.335 Å^{-3}. The volume percent of water is summarized in Table 5.7.

Table 5.7: Volume percent of water in PMETAC/AuNP composite material at different relative humidties

Humidity [%rh]	H_2O [vol-%]
4-7	0
30	11.9
92	39.3

It shows that the volume percent of water inside the brush increases with increasing relative humidity but not as much for a neat PMETAC brush (see Table 5.3).

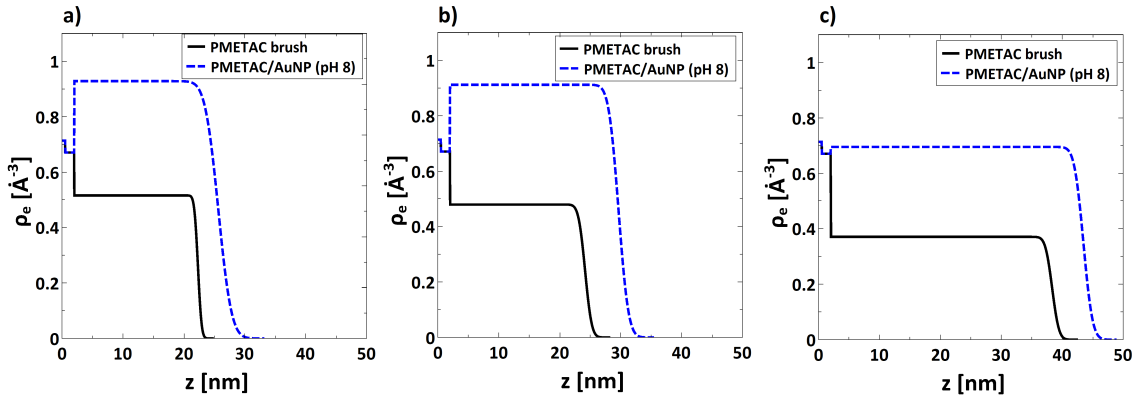

Figure 5.10: Electron density profiles in the z-direction from the substrate surface (z=0) for PMETAC/AuNP composite after incubation at pH 8 (blue broken lines) and neat PMETAC brush (black solid lines) measured at different r.h. for a) 4-7 %rh, b) 30 %rh, and c) 92 %rh.

5.3 Discussion

The chapter addresses the internal structure of PMETAC/AuNP composites in order to get an insight about the spatial distribution of AuNPs within the brush. Therefore NR and XRR measurements for the composite materials as well as for the neat brush were carried out against liquid water and vapor of different relative humidities.

5.3.1 Internal structure of PMETAC/AuNP composites against liquid water

After the incubation of PMETAC brush in AuNP suspension at pH 4 the SLD remains the same as of the neat brush. By considering exclusively the NR data, one would conclude that no AuNPs are penetrated or even attached to the brush. In contrast, AFM data and UV/Vis measurements give strong hints for an attachment of a small amount of aggregated AuNPs at the brush surface. Probably the amount of attached AuNPs is too small to be detected by NR measurements ($SLD_{PMETAC} \approx 0.77 \times 10^{-6}$ Å^{-2} < $SLD_{AuNP} \approx 4.5 \times 10^{-6}$ Å^{-2} < $SLD_{D_2O} = 6.36 \times 10^{-6}$ Å^{-2}). In Table 5.5 the volume percent of the AuNPs has been calculated. 15.5 ± 0.1 vol-% consists of AuNPs in layer 2. Assuming the outer layer consists of AuNPs and D_2O, the SLD of the composite material can be calculated as follows (Eq. 5.4):

$$SLD_{AuNP/D_2O} = (1 - x) \cdot SLD_{D_2O} + x \cdot SLD_{AuNP} \tag{5.4}$$

SLD_{AuNP/D_2O}=6.07 × 10^{-6} $Å^{-2}$, which shows that the contrast to D_2O (SLD_{D_2O}=6.36 × 10^{-6} $Å^{-2}$) is too low to detect the AuNPs by NR.

In contrast, after AuNP loading in pH 8 NR measurements indicate that AuNPs penetrate the brush. Compared to the pure PMETAC brush, the SLD close to the substrate increases while the SLD towards the subphase decreases because Au has a SLD between D_2O and the brush material. This suggests the formation of a 3D particle assembly where the AuNPs are located almost over the entire brush. AuNPs can penetrate the brush due to the fact that the chains are highly stretched in water and allow enough room for the electrostatically stabilized AuNPs to penetrate the brush. Further, an increase in thickness was observed after the particle attachment. Several effects might lead to the increase in brush thickness: 1) Volumetric or sterical effects, 2) it might be simply caused by an enhanced swelling due to the hydrophilicity of incorporated AuNPs which transfer water molecules into the brush, 3) or it might be explained by an increase in osmotic pressure due to enhanced amount of counterions within the brush.

5.3.2 AuNP distribution within PMETAC brushes at different relative humidities

XRR measurements were carried out to analyze the AuNP distribution. Due to their high electron density AuNPs give a good contrast within a polymer matrix. Even the 15.5 vol-% AuNPs in the outer layer after incubation in pH 4 is detectable. The thickness for the neat PMETAC brush increases with increasing humidity due to the water uptake within the brush. The water amount has been calculated in Table 5.3. At the same time, the electron density decreases with increasing humidity, since water has a lower electron density than the PMETAC brush. Furthermore, the roughness of the brush increases with increasing humidity. The polymer chains are more stretched away from the substrate with increasing humidity and the polydispersity of the polymer chains becomes more visible[143].

For PMETAC brushes after incubation in AuNP suspension at pH 4, XRR measurements reveal the presence of AuNPs on top of the brush. The contrast is high enough to detect AuNPs ($\rho_{e,PMETAC}$=0.52 $Å^{-3}$, ρ_{e,H_2O}=0.34 $Å^{-3}$, $\rho_{e,Au}$=4.37 $Å^{-3}$). The electron density profiles show that layer 1 has the same electron density and same thickness as the neat PMETAC brush and is the only layer for the brushes incubated in AuNP suspension at pH 4 that swells and shows a decrease in electron density with increasing humidity. It shows the same behavior and properties as the neat PMETAC brush, which indicates that no AuNPs have penetrated the brush during the incubation. However, layer 2 shows an increased electron density, which indicates that the AuNPs are attached to the brush

surface. Increasing the humidity has not a pronounced impact on the thickness and electron density; however a small amount of water is attached to the gold layer, which results in a slight increase of the thickness and decrease in electron density. Layer 3 does not exhibit any systematic change and counts for the roughness of the AuNP layer. It is a coincidence that the sum of thicknesses of layer 2 and layer 3 is in the range of the AuNP size, because exposing AuNP suspension to pH 4 leads to aggregation of those due to the loss of the negative charges on the gold surface. These aggregates are attached in small amounts to the surface of the brush, which are detected by AFM height images.

In contrast, the electron density profiles of PMETAC brushes incubated in AuNP suspension at pH 8 reveal a completely different behavior. Using the three-layer model reveals that layer 1 has a much higher electron density and thickness after the incubation. This indicates that AuNPs are incorporated within the brush after incubation. Furthermore, the three-layer model is designed to describe a AuNP monolayer on top of the brush surface, which matches with the assembly formation for PMETAC/AuNP composite after incubation at pH 4 but actually not for the assembly formation of PMETAC brush incubated in AuNP suspension at pH 8. Therefore, a one-layer model was used to fit the data, which shows that better fits can be obtained. The fact, that the reflectivity curves can be fitted by a one-layer model, indicates a uniform distribution of AuNPs inside the brush. With increasing humidity the thickness increases and the electron density decreases due to the water uptake. Table 5.7 shows, that embedding AuNPs into the polymer brush results in less swelling compared to the swelling behavior of a neat PMETAC brush (≈40 vol-% for PMETAC/AuNP vs. ≈80 vol-% for neat PMETAC brush). Furthermore, the roughness decreases with increasing humidity. The reason might be that swelling of the brush drags the AuNPs inside the brush, which results in a decrease in roughness.

The chapter shows clearly that the assembly of AuNPs in PMETAC brushes depends on the pH value. Considering the results obtained by AFM, UV/Vis spectroscopy, NR measurements, and XRR measurements, a model in swollen and dry state for both brush/AuNP composite types can be derived (see Figure 5.11). AFM height images, UV/Vis measurements, and NR measurements reveal a more non-homogeneous distribution (2D assembly) of AuNPs on PMETAC brush after incubation at pH 4 while a more homogeneous distribution (3D assembly) of AuNPs was found on PMETAC brushes after incubation at pH 8 in aqueous conditions. This is in agreement with our previous study[137], which is also pointed out in the previous chapter (Chapter 4). The reason for this behavior is that AuNPs tend to aggregate at pH 4 due to the loss of the negative charges and these aggregates of AuNPs are too bulky to penetrate the dense brush. While AuNPs at pH 8

are stabilized due to negative charges, which can easily penetrate the brush. In this work, PMETAC brushes are grown by the grafting from approach. A typical grafting density value of brushes grown by SI-ATRP is 0.5 chains/nm^2, which was determined by cleaving polymer brushes from the substrate[144]. It is assumed, that in this work the grafting density is lower than 0.5 chains/nm^2, since the initiator (BTPAm), which was used, has a smaller chain length than the initiator in the work of Patil *et al.*[144]. Yan *et al.* showed that higher grafting densities of polymer brushes can be achieved using initiators with a longer chain length[145]. Therefore, AuNPs at pH 8 can penetrate the brush. According to theoretical predictions[97,146], the penetration depth depends not only on particle size but also on the interaction between particle and brush (attractive vs. repulsive). Therefore, the penetration within deeper regions is also driven through the particle-brush attraction. Furthermore, the uptake of AuNPs in PMETAC brushes in pH 8 is higher than in pH 4 due to an increased electrostatic attraction. However, the electrostatic attraction at pH 4 is still high enough to fix the AuNPs onto the brush without detachment of AuNPs after incubation. The reason is that at pH 4 almost half of the carboxylate groups of the MPA-capped AuNPs are still charged (pK_a(MPA-AuNP)=4.3[115]).

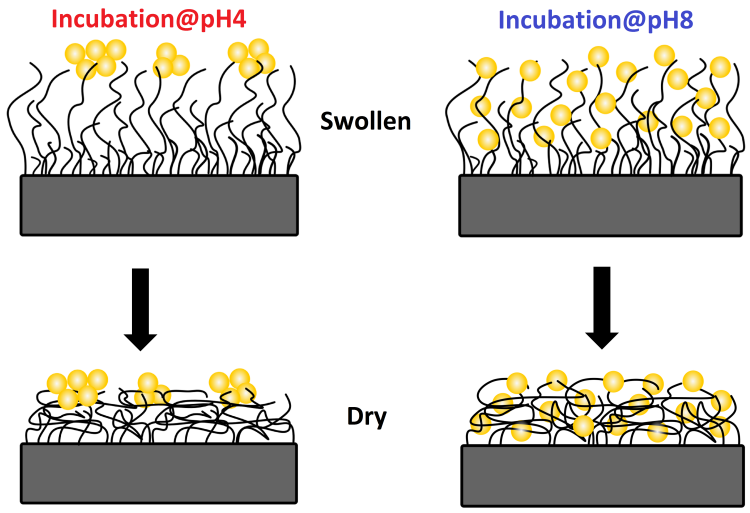

Figure 5.11: Suggested assembly of brush/AuNP composites in wet and dry conditions. PMETAC brushes incubated in AuNP suspension at pH 4 form more likely (a) a 2D assembly while PMETAC brushes incubated in AuNP suspension at pH 8 form mainly (b) a 3D assembly. Once the assembly is formed, the particles stay at their positions and will not get reorganized.

Going from aqueous conditions to vapor conditions with different relative humidities for both composite materials let them collapse. However, this collapse does not change the position of the attached AuNPs and no leakage of AuNPs has been noticed. A rather 2D assembly was still found for brush/AuNP composite materials after incubation at pH

4 and a rather 3D assembly was still found for brush/AuNP composite materials after incubation at pH 8.

5.4 Conclusion

In this chapter, the pH-triggered assembly of MPA-coated AuNPs incorporated into PMETAC brushes was studied by XRR and NR. XRR and NR are complementary methods due to different contrasts between the AuNPs and the brush. Both methods can be used to elaborate the particle distribution in polymer brushes. NR is suitable for measuring in liquid water while XRR can only be used in air or vapor, however it gives a better contrast between AuNP and polymer. XRR revealed a layer of AuNPs at the brush surface after incubation of PMETAC brush in AuNP suspension at pH 4 while NR could not show any attachment due to a lack of contrast.

The AuNP distribution can be controlled by the pH of the incubation medium thus leads to fabrication of colorimetric sensors with different optical properties. The attachment of AuNPs is driven by electrostatic attraction between PMETAC brush and AuNPs, while the AuNP distribution is dominated by the particle-particle interaction. Incubation in pH 4 leads to aggregate formation of AuNPs, which cannot penetrate the brush. Therefore a layer of AuNPs is formed at the brush surface. Incubation at pH 8 stabilized the AuNPs in suspension electrostatically, and they can penetrate the PMETAC brush.

Nevertheless, it was impossible so far to separate the components and examine the effects of AuNPs and brush on itself with the current fitting procedure that has been used for the NR measurements. However, in order to control the AuNP distribution, more detailed information about the composites internal structure is required. Therefore, the next chapter will deal with the question how the brush as well as the particles on its own behave after forming composites. This was elucidated by NR with contrast variation, and a self-consistent reflectivity analysis based on the analytical parametrization of the volume fraction profiles of all chemical components.

Chapter 6

Gold nanoparticle distribution in polyelectrolyte brushes loaded at different pH conditions*

Abstract

In this chapter, the distribution was further elucidated by neutron reflectometry (NR) with contrast variation, and a self-consistent reflectivity analysis based on the analytical parametrization of the volume fraction profiles of all chemical components. In contrast to former studies this analysis allows the determination of the spatial distribution of components separately from each other: polyelectrolyte, AuNP and water. PMETAC brushes were loaded with 5 nm AuNPs, which were coated with a pH-sensitive capping. The pH was varied during the incubation of the brush in the AuNP suspension. At lower pH, AuNPs form aggregates in suspension and are attached to the brush periphery. They adsorb into the brush but do not fully penetrate it due to their bulkiness. At higher pH, AuNP suspensions are electrostatically stabilized and the AuNPs penetrate the brush entirely. However, the AuNP distribution over the brush is not homogeneous but decreases gradually towards the substrate. Penetration of the AuNPs leads to a more extended conformation of the brush. According to the results of the detailed analysis of all components, increase in water content could be excluded as a reason for brush swelling but a replacement of water by the AuNP was observed.

6.1 Introduction

An effort has been made already in the previous chapter, using NR and XRR to elucidate the distribution of AuNPs. The AuNPs had a pH-sensitive capping with MPA and were embedded into PMETAC brushes at different pH. It was shown that the distribution of AuNPs can vary with pH from a rather 2D assembly at the brush surface to a more 3D distribution within the brush. However, in order to control the AuNP distribution, more detailed information about the composites internal structure is required. The incorporation of AuNPs changes not only the water content but also the brush conformation. So far, it was impossible to separate those two effects.

*Similar content was presented in D. Boyaciyan, L. Braun, O. Löhmann, L. Silvi, E. Schneck and R. von Klitzing, *JCP*, **2018**, *149*, 163322 (Gold nanoparticle distribution in polyelectrolyte brushes loaded at different pH conditions).

In the present chapter, the same composite of PMETAC brushes loaded with MPA capped AuNPs is investigated with a focus on the AuNP distribution within the brush. For this purpose, NR was carried out against several water contrasts and analyzed with the help of a self-consistent model based on the analytical parametrization of the volume fraction profiles of all chemical components. This approach yields much more detailed information on the internal structure of the composites than previous studies. AuNPs at pH 4 are attached to the brush periphery as aggregates without deeply penetrating the PMETAC brush. In contrast, at pH 8 AuNPs penetrate the brush completely. Under both pH conditions, the PMETAC brushes become more elongated upon AuNP distribution.

6.2 Results

To get a full understanding about AuNPs adsorption onto/into the PMETAC brush at different pH one needs information about the assembly of AuNP in suspension before the incubation of PMETAC brushes. However, AuNPs in suspension were already extensively characterized and the characterization is shown in Chapter 4 (Figure 4.9). Therefore, the next section addresses the internal structure of a PMETAC brush before and after the incubation in AuNP suspension to form PMETAC/AuNP composite materials. Neat PMETAC brush as well as PMETAC brushes after incubation at pH 4 and at pH 8 were measured by NR against different water contrasts.

6.2.1 NR measurements

NR is sensitive to the distribution of AuNPs within the brush, because the SLDs of PMETAC and AuNPs are very different[138,139]: $\rho_{PME} \approx 0.9 \times 10^{-6}$ Å^{-2} and $\rho_{AuNP} \approx 3.6 \times 10^{-6}$ Å^{-2}, respectively. ρ_{AuNP} can be estimated a priori by assuming a spherical shape, uniform face centered cubic (fcc) structure[129] of Au and a uniform coverage of MPA around the AuNP (see Figure 6.1).

A diameter of 4.8 nm for the AuNP core was obtained from TEM (see Chapter 3 section 3.2.3 AuNP synthesis). The length of MPA as a coating was estimated as 0.68 nm from theoretically calculations[147]. The SLD of the AuNPs, ρ_{AuNP}, was calculated by

$$\rho_{AuNP} = \frac{V_{Au} \cdot \rho_{Au} + V_{MPA} \cdot \rho_{MPA}}{V_{Au} + V_{MPA}} \tag{6.1}$$

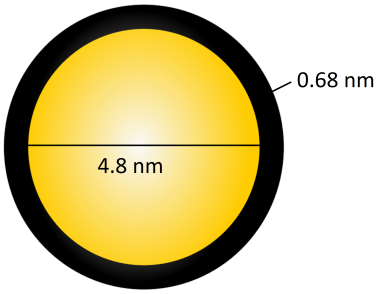

Figure 6.1: Schematic illustration of AuNPs coated with MPA.

with $\rho_{Au} = 4.66 \times 10^{-6}$ Å^{-2} and $\rho_{MPA} = 1.37 \times 10^{-6}$ Å^{-2} (calculation was done by dividing the sum of the scattering length contribution from all atoms within the molecule with its solvent-inaccessible molecular volume). V_{Au} and V_{MPA} denote to the volume of the gold and the MPA-capping, respectively. A SLD of $\rho_{AuNP} = 3.58 \times 10^{-6}$ Å^{-2} was obtained.

With the help of water contrast variation the interfacial distributions of PMETAC, $\Phi_{PME}(z)$, and of the AuNPs, $\Phi_{AuNP}(z)$ can be unambiguously disentangled (see Figure 6.2). Namely, the AuNPs are nearly invisible in the 4MW contrast, so that the corresponding reflectivity curve is dominated by the brush profile. In the H_2O contrast, on the other hand, the reflectivity curve is dominated by the AuNP distribution. Finally, in the D_2O contrast both components contribute. The neat brushes as well as the brushes after adsorption of AuNPs at pH 4 and at pH 8 were characterized against all three contrasts.

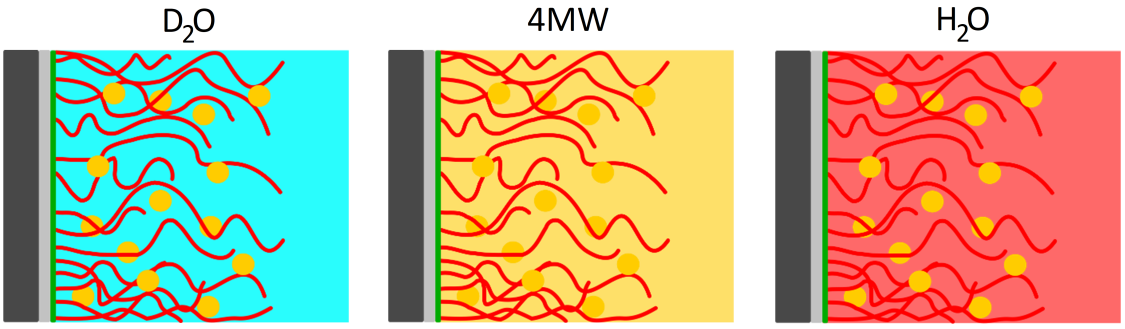

Figure 6.2: Schematic illustration of a PMETAC/AuNP composite in different water contrasts. Measuring the composite against D_2O (left) offers substantial contrast to both the PMETAC brush and the AuNPs. In 4MW (middle) the AuNP SLD is nearly matched out by the solvent, so that the measurement is mostly sensitive to the brush profile. In H_2O (right), the SLD contrast with the brush is weak and the measurement is mostly sensitive to the AuNP distribution.

Characterization of a neat PMETAC brush

Figure 6.3a shows the experimental reflectivity curves obtained with D_2O, 4MW, and H_2O contrasts. The solid lines represent the simulated reflectivity curves corresponding to the best-matching parameters in the common model (Figure 6.3b and c), which is based on the volume fraction profiles, $\Phi_i(z)$, of silicon ("Si"), silicon oxide ("SiO2"), initiator ("ini"), PMETAC ("PME"), and water ("W"). This roughness-free representation in Figure 6.3b merely serves for an illustration of the parametric mathematical model. The associated SLD profile $\rho(z)$ follows as

$$\begin{aligned}\rho(z) = \Phi_{Si}(z) \cdot \rho_{Si} + \Phi_{SiO2}(z) \cdot \rho_{SiO2} + \\ \Phi_{ini}(z) \cdot \rho_{ini} + \Phi_{PME}(z) \cdot \rho_{PME} + \\ \Phi_W(z) \cdot \rho_W\end{aligned} \tag{6.2}$$

where the position $z = 0$ is defined as the interface between the initiator layer and the aqueous region accommodating the PMETAC brush. $\Phi_{Si}(z)$ is modeled as a semi-infinite continuum with fixed SLD $\rho_{Si} = 2.07 \times 10^{-6}$ Å^{-2}, which is the literature value. $\Phi_{SiO2}(z)$ and $\Phi_{ini}(z)$ are represented as homogeneous slabs with adjustable thicknesses d_{SiO2} and d_{ini}, respectively, and adjustable roughnesses between the layers, characterized by roughness parameters $\delta_{Si/SiO2}$, $\delta_{SiO2/ini}$, and $\delta_{ini/PME}$. The SLD of SiO_2 is fixed at the literature value $\rho_{Si} = 3.47 \times 10^{-6}$ Å^{-2}. However, earlier studies showed that the SiO_2 can incorporate a finite amount of solvent, which is characterized by an adjustable parameter $\Phi_{solvent}^{SiO_2}$ [123–125,148]. The SLD of the initiator layer, ρ_{ini}, was set as a free parameter. For convenience and in lack of a reliable estimate, its solvent content was neglected. Initially, the SLD of PMETAC, ρ_{PME}, was a free parameter. According to the recent work of Micciulla et al.[123], the PMETAC volume fraction profile Φ_{PME} was modeled as a two-region distribution (Figure 6.3b),

$$\Phi_{PME}(z) = \Phi_{PME}^{in}(z) + \Phi_{PME}^{out}(z). \tag{6.3}$$

The inner region $\Phi_{PME}^{in}(z)$ corresponds to the dense brush region near the grafting surface, which is represented by a homogeneous slab characterized by its thickness d_{PME}^{in} and its maximal volume fraction Φ_{PME}^{0}. The outer region $\Phi_{PME}^{out}(z)$ describes the dilute brush periphery, represented by a stretched exponential function

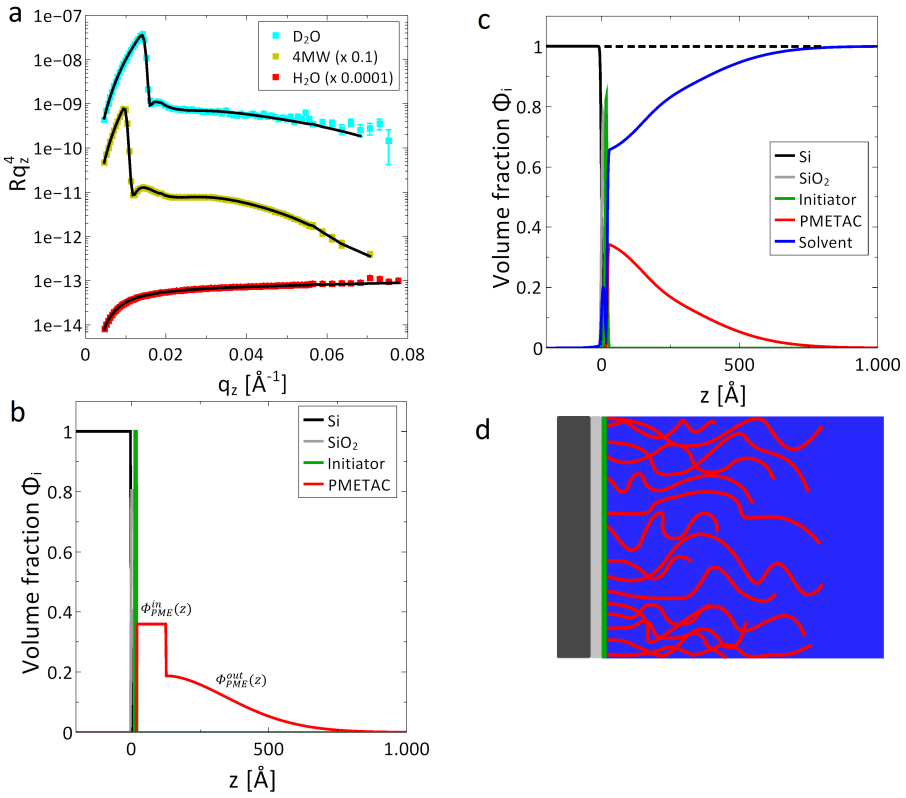

Figure 6.3: (a) Reflectivity curves and best fits for a neat brush. (b) Schematic illustration of the theoretical model used to interpret the experimental reflectivity curves. This roughness-free representation merely serves for an illustration of the parametric mathematical model. (c) Best-matching profiles obtained in the fits (solid lines in panel (a)) the reflectivity curves. The dashed line indicates that the sum of all volume fractions is one. (d) Schematic representation of a neat PMETAC brush in an aqueous solvent.

$$\Phi^{out}_{PME}(z) = I_{in/out}(z) \cdot \Phi^{0}_{PME} \cdot exp(-(\frac{z}{\Lambda})^{n}) \tag{6.4}$$

where $I_{in/out}(z)$ accounts for the gradual transition between the dense brush region and the dilute brush region in form of an error function characterized by the roughness parameter $\delta^{in/out}_{PMETAC}$. Λ and n denote the decay length of the brush volume fraction and the stretching exponent, respectively. Finally, the water volume fraction profile follows from the requirement that the sum of all volume fractions equals unity at each z-position

$$\sum_{i} \Phi_i(z) \equiv 1 \tag{6.5}$$

which is shown in Figure 6.3c, 6.4c, and 6.5c as dashed lines. Figure 6.3c shows the volume

fraction profile according to the best-matching model parameters, corresponding to the fits in Figure 6.3a. The two-region model is sufficient to describe the neat PMETAC brush. The volume fraction profiles also constitute the basis for the schematic illustration in Figure 6.3d. The inner region of the PMETAC brush, with thickness $d_{PME}^{in} = 110 \pm 10$ Å, comprises most of the total polymer amount. The outer region exhibits a characteristic decay length of $\Lambda = 330 \pm 20$ Å and a stretching exponent of $n = 1.8 \pm 0.2$.

The brush amount per surface area in terms of an equivalent thickness D_{PME} is conveniently obtained by integration

$$D_{PME} = \int_{-\infty}^{+\infty} \Phi_{PME}(z)dz. \tag{6.6}$$

D_{PME} corresponds to the thickness of a layer of 100 % PMETAC (without any water or free voids). $D_{PME} = 140$ Å $\pm$ 5 Å was obtained, which is thinner than the thickness $d_{elli} = 212 \pm 13$ Å measured by ellipsometry at ambient conditions ($\approx$ 30 %RH). The deviation can be attributed to the residual water content in the brush at ambient conditions and to differences between the volumes relevant for the calculation of SLD (partial molecular volume) and refractive index (inverse density). According to Löhmann et al.[149], a PMETAC brush prepared with the same protocol contains up to 20 vol% water in the range between 30 - 50 %RH.

The SLD of the initiator layer is obtained as $\rho_{ini} \approx 0.95 \times 10^{-6}$ Å^{-2} and that of PMETAC as $\rho_{PME} \approx 0.84 \times 10^{-6}$ Å^{-2}. The obtained SLDs agree well with the theoretical calculated value for $\rho_{ini} = 1.06 \times 10^{-6}$ Å^{-2} (calculated by dividing the sum of all atomic scattering lengths by the solvent-inaccessible volume) and the theoretical estimate of $\rho_{PME} = 0.88 \times 10^{-6}$ Å^{-2} based on a the METAC monomer volume of $V_{METAC} = 262$ Å^3,[150]. Furthermore, an experimental value of $\rho_{PME} = 0.82 \times 10^{-6}$ Å^{-2} was reported by Löhmann et al.[149] and is in line with our results. While several studies have reported that polymer and polyelectrolyte brushes tend to degraft when exposed to good solvents[133,151,152], no significant degrafting occurred in the present study. In fact, it would have been difficult to commonly model neutron reflectivity curves recorded sequentially in three water contrasts if significant degrafting had occurred on the time scale of the experiments. The reason why degrafting was not an issue in the present work may be that it is less pronounced for thin brushes formed by comparatively short chains, as was proposed earlier[153].

Characterization of a PMETAC brush after incubation in AuNP suspension at pH 4

Analysis of the reflectivity curves after AuNP adsorption requires the extension of the volume fraction model by the AuNP profile $\Phi_{AuNP}(z)$:

$$\begin{aligned}\rho(z) = \Phi_{Si}(z) \cdot \rho_{Si} + \Phi_{SiO2}(z) \cdot \rho_{SiO2} + \\ \Phi_{ini}(z) \cdot \rho_{ini} + \Phi_{PME}(z) \cdot \rho_{PME} \\ + \Phi_{AuNP}(z) \cdot \rho_{AuNP} + \Phi_{W}(z) \cdot \rho_{W}\end{aligned} \tag{6.7}$$

Here, ρ_{ini} and ρ_{PME} were fixed to the values obtained in the fits of the neat brush (see previous section), while ρ_{AuNP} was set as a free parameter. $\Phi_{AuNP}(z)$ is described as a unimodal distribution in the form of one rough slab, characterized by its respective center position (z^{AuNP}), thickness (d^{AuNP}), maximal volume fraction (Φ_0^{AuNP}), and roughness parameter on both sides of the slab (δ_{AuNP}^{left}, δ_{AuNP}^{right}). Concerning the PMETAC profile after AuNP adsorption, the two-region description according to Eq. 6.3 (see previous section) was no longer sufficient, reflecting that Φ_{PME} is significantly perturbed by the AuNP adsorption. Instead, a three-region description was employed (see Figure 6.4b), comprising two adjacent rough slabs and a stretched exponential function representing the dilute brush periphery in analogy to Eq. 6.4. This slightly more complex description was found to be versatile enough to capture the perturbation of the brush profile upon AuNP adsorption.

Figure 6.4a shows the experimental reflectivity curves against D_2O, 4MW, and H_2O obtained after adsorption of AuNP at pH 4. The solid lines in 6.4a again represent the simulated reflectivity curves corresponding to the best-matching parameters in the common model (Figure 6.4b and c).

The volume fraction profile shows that the PMETAC brush gets stretched after the incubation. The inner region of the PMETAC brush, with thickness $d_{PME}^{in} = 600 \pm 30$ Å, comprises most of the total polymer amount. The outer region exhibits a characteristic decay length of $\Lambda = 600 \pm 40$ Å and a stretching exponent of $n = 3 \pm 0.5$. It indicates, that the peripheral edge of the brush becomes somewhat sharper with respect to the neat PMETAC brush. The AuNPs are not homogeneously distributed over the brush. Instead, they are rather confined near the brush periphery and apparently unable to fully penetrate

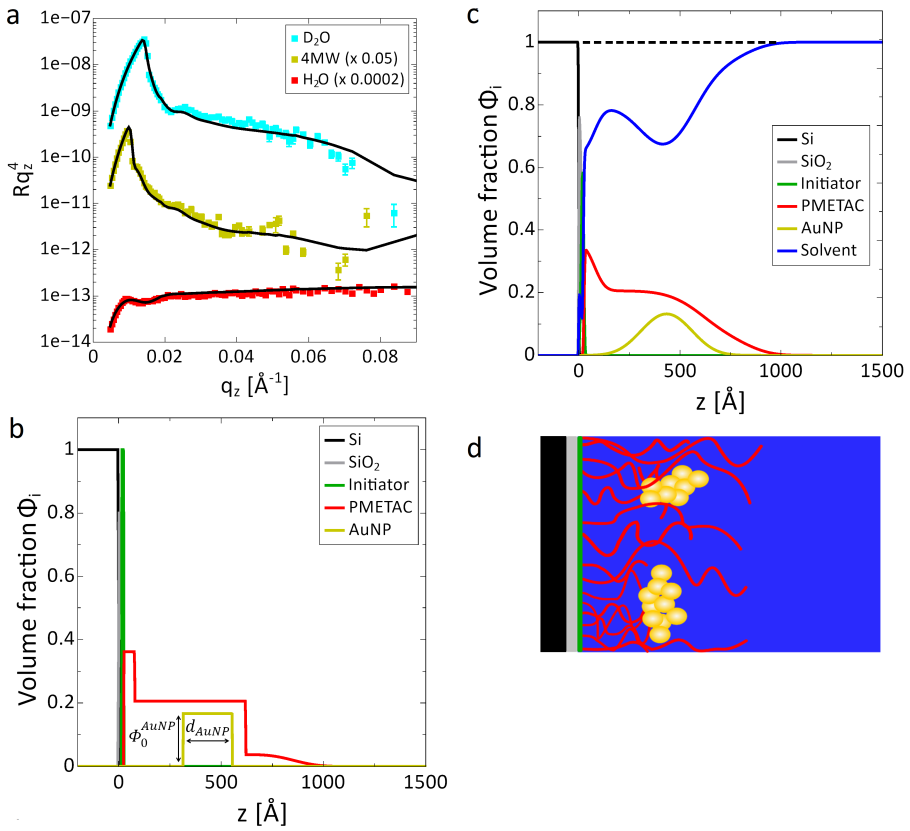

Figure 6.4: (a) Reflectivity curves and best fits for a PMETAC/AuNP composite at pH 4. (b) Schematic illustration of the theoretical model used to interpret the experimental reflectivity curves. This roughness-free representation merely serves for an illustration of the parametric mathematical model. (c) Best-matching profiles obtained in the fits (solid lines in panel (a)) the reflectivity curves. The dashed line indicates that the sum of all volume fractions is one. (d) Schematic representation of a PMETAC/AuNP composite at pH 4 in an aqueous solvent.

the brush. One can see this from $\Phi_W(z)$, that the AuNPs replace water at the position in which they are confined.

Previous chapters (Chapter 4 and 5) have demonstrated that the AuNPs are rather uncharged at pH 4 and therefore tend to aggregate. XRR measurements qualitatively suggested that these aggregates are preferably adsorbed to the brush periphery[137,154]. The aggregates were detected by AFM and TEM images. A schematic illustration of the AuNP distribution is drawn in Figure 6.4d.

The maximal volume fraction of AuNPs attached to the brush is around 18 vol%, which was also found by XRR measurements[154]. The number of adsorbed AuNPs per surface area can be extracted from the volume fraction profile according to

$$\sigma_{AuNP} = \frac{1}{V_{AuNP}} \int_{-\infty}^{+\infty} \Phi_{AuNP}(z) dz \tag{6.8}$$

where $V_{AuNP} \approx 58$ nm^3 is the average AuNP volume. With that, $\sigma_{AuNP} \approx 0.07$ nm^{-2} was obtained, corresponding to one AuNP per 14 nm^{-2}. The best-matching SLD of the AuNPs is obtained as $\rho_{AuNP} = 3.8 \times 10^{-6}$ Å^{-2}, which is in good agreement to our a-priori estimate of $\rho_{AuNP} = 3.58 \times 10^{-6}$ Å^{-2}.

Characterization of a PMETAC brush after incubation in AuNP suspension at pH 8

For the characterization of a PMETAC brush after incubation in AuNP suspension at pH 8, the same three-region description was used for the PMETAC brush in the PMETAC/AuNP composite, while for $\Phi_{AuNP}(z)$ a unimodal description was not sufficient. Instead, a bimodial distribution , represented by two rough slabs, was employed (see Figure 6.5b):

$$\Phi_{AuNP}(z) = \Phi_1^{AuNP}(z) + \Phi_2^{AuNP}(z). \tag{6.9}$$

The two rough slabs are characterized by their respective center positions (z_1^{AuNP} and z_2^{AuNP}), thicknesses (d_1^{AuNP} and d_2^{AuNP}), maximal volume fractions (Φ_0^{AuNP1} and Φ_0^{AuNP2}), and roughness parameters on both sides (δ_{AuNP1}^{left}, δ_{AuNP1}^{right} and δ_{AuNP2}^{left}, δ_{AuNP2}^{right}). Earlier results[137,154] showed qualitatively that at pH 8 the AuNPs are well dispersed in suspension because they are highly negatively charged and therefore electrostatically stabilized as individual particles. The reflectivity data and the description of the AuNP distribution are shown in Figure 6.5a. The solid lines show the best fits. The experimental data could be well described by the bimodial description. Figure 6.5c shows the volume fraction profiles according to the best-matching model parameters. Corresponding to the volume fraction profiles, a schematic illustration of the AuNP distribution is drawn in Figure 6.5d.

The SLD of AuNPs was found to be $\rho_{AuNP} = 3.9 \times 10^{-6}$ Å^{-2}, which is in good agreement with the value found for the AuNPs attached to the brush after the incubation at pH 4 and to our a-priori estimate. The good agreement concerning ρ_{AuNP} obtained for the two different data sets (PMETAC/AuNP composites at pH 4 and at pH 8) can be understood as an indication of the robustness of the analysis.

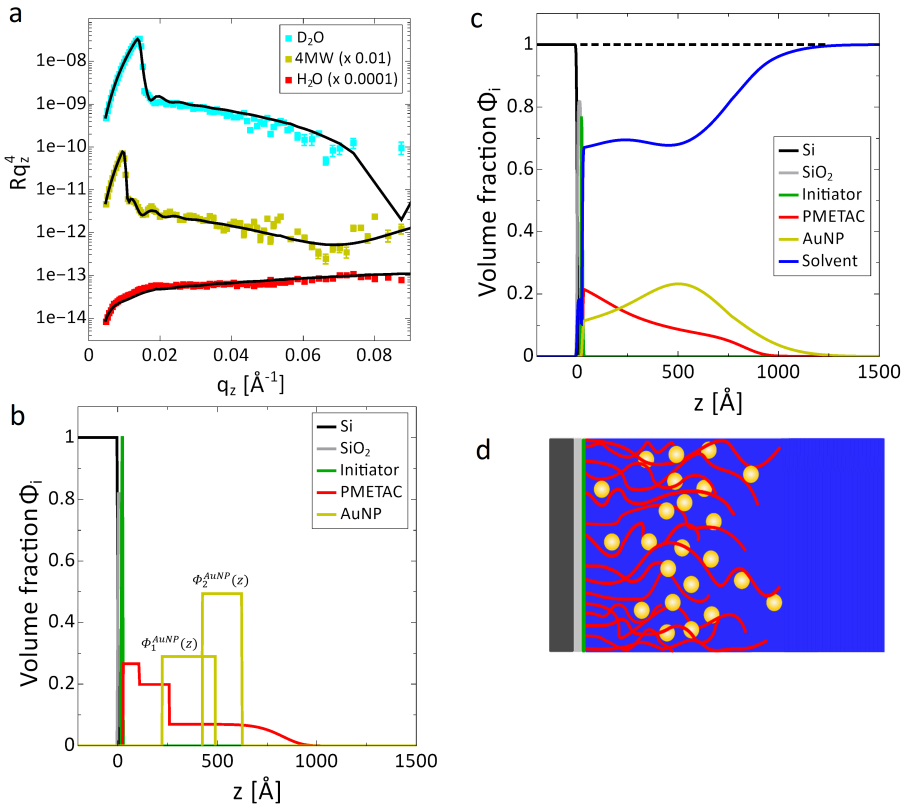

Figure 6.5: (a) Reflectivity curves and best fits for a PMETAC/AuNP composite at pH 8. (b) Schematic illustration of the theoretical model used to interpret the experimental reflectivity curves. This roughness-free representation merely serves for an illustration of the parametric mathematical model. (c) Best-matching profiles obtained in the fits (solid lines in panel (a)) the reflectivity curves. The dashed line indicates that the sum of all volume fractions is one. (d) Schematic representation of a PMETAC/AuNP composite at pH 8 in an aqueous solvent.

The volume fraction profiles show that the PMETAC brush swells up to ≈ 200 Å more in comparison to the neat PMETAC brush due to the AuNP incorporation, while water is replaced by the AuNPs. The inner region of the PMETAC brush, with thickness $d_{PME}^{in} = 230 \pm 20$ Å, comprises most of the total polymer amount. The outer region exhibits a characteristic decay length of $\Lambda = 600 \pm 30$ Å and a stretching exponent of $n = 7 \pm 2$, meaning that the brush periphery is nearly box-like with a low PMETAC fraction. AuNPs are distributed over the entire brush but not in a homogeneous manner. It was found that the relative amount of AuNPs in the dilute PMETAC region is higher with almost 25 vol% than in the dense PMETAC region towards the substrate with 15 vol%. The number of adsorbed AuNPs per surface area in total is obtained as $\sigma_{AuNP} \approx 0.18$ nm^{-2} (see Eq. 6.8), corresponding to one AuNP per 6 nm^{-2}.

6.2.2 Comparison of AuNP uptake in PMETAC brushes at different pH with different techniques (Chapter 4 - 6)

The amount of AuNP uptake determined with different techniques thorughout Chapter 4 to 6 are summarized in Table 6.1.

Table 6.1: Particle number densities of AuNPs within PMETAC brushes obtained by different techniques of composites incubated at different pH.

	UV/Vis		XRR	NR
pH	Inc. time of 24 h (Ch. 4) (Particles/nm^3)	Inc. time of 6 h (Ch. 5) (Particles/nm^3)	Inc. time of 6 h (Ch. 5) (Particles/nm^3)	Inc. time of 6 h (Ch. 6) (Particles/nm^3)
4	0.0011	0.0009	0.0005	0.0007
8	0.0083	0.0027	-	0.0018

Table 6.1 shows that different techniques lead to almost comparable particle number densities. However, the particle number density after the incubation at pH 4, which are obtained by UV/Vis (Chapter 5) is almost 2 times higher than the particle number densities, which are obtained by XRR (Chapter 5) and NR (Chapter 6). The discrepancy could come from that XRR as well as NR is more sensitive for detecting AuNPs. Further, more assumptions were made for calculating the particle number density by UV/Vis. In general, the uptake of AuNPs at pH 4 is a slower process than at pH 8. Further, a saturation of uptaken AuNPs is already reached for an incubation time of 6 h for pH 4 but not for pH 8. Both effects can be contributed to the lower electrostatic attraction between particle and the brush, since AuNPs are less negatively charged at lower pH.

6.3 Discussion

Earlier NR experiments[154] with one single water contrast (D_2O) and a standard box-model description of the SLD profile already yielded qualitative insights into the PMETAC brush and composite structures. However, it had not been possible to extract the amounts and SLDs of the individual components. In the present work, the combination of multiple water contrasts with a self-consistent analysis based on continuous volume fraction profiles make it possible to extract the amounts, SLDs, and distributions of all chemical components and, with that, provides comprehensive information on the composites internal structure.

The volume fraction profile of a neat PMETAC brush (Figure 6.3c) shows that the brush is highly hydrated. The observed high water content can be attributed to the osmotic

pressure of the counterions inside the brush[99]. A stretching exponent of $n = 1.8 \pm 0.2$ reflects a moderate polydispersity, compared to $n = 0.9 \pm 0.2$ found in the work of Micciulla et al.[123]. The lower polydispersity in the present chapter can be attributed to a slow polymerization during PMETAC synthesis[155,156].

AuNPs do not fully penetrate the brush after incubation of a PMETAC brush in AuNP suspension at pH 4, since they are aggregated and too bulky to penetrate the brush. Instead, they mostly adsorb at the brush periphery. As already pointed out further above, AuNPs at pH 4 still have deprotonated carboxylic acid groups and thus the tendency to interact with the positively charged PMETAC brush. The associated release of counterions is normally expected to result in a reduction of the osmotic pressure inside the brush and, in turn, in a more compact brush conformation. For similar reasons, polyelectrolyte brushes assume more compact conformations in the presence of salt[111,157]. In contrast to this expectation, the adsorption of AuNPs leads to a more extended brush conformation (see Figure 6.4c). This finding is robust and must be attributed to volumetric effects of the AuNPs themselves: They occupy up to almost 20 vol% (see Figure 6.4c) and therefore replace the PMETAC further away from the solid surface. The obtained volume fraction profiles further exclude an alternative swelling mechanism based on the enhanced water incorporation or an increase in osmotic pressure along with the particles.

At pH 8, AuNP adsorption occurs into the entire brush, as evidenced from the broad AuNP volume fraction profile in Figure 6.5c. The overall AuNP amount per unit area ($\sigma_{AuNP} \approx 0.18\ nm^{-2}$) is 2.6 times larger than at pH 4 ($\sigma_{AuNP} \approx 0.07\ nm^{-2}$). The associated much stronger volumetric effect is manifested also in the even more extended brush conformation observed at pH 8 (see Figure 6.5c). It cannot be excluded, however, that a part of the effect results also from the mutual repulsion between brush-adsorbed AuNPs. When comparing the different AuNP distributions at pH 4 and pH 8, it is rewarding to consider the osmotic penalty, $F_{osm} = N \cdot V_{AuNP} \cdot \Pi_{osm}$, associated with the insertion into the brush of an aggregate of N particles versus that of an individual AuNP ($N = 1$). Here, Π_{osm} denotes to the osmotic pressure inside the brush, which scales approximately linearly with the PMETAC volume fraction. It is seen that this penalty is much larger for the aggregates than for the individual particles, which rationalizes the impermeability of the dense brush region for the aggregates (at pH 4) but not for the individual AuNPs (at pH 8). In this context it should be noted that the distribution of AuNPs is not homogeneous. PMETAC brushes posses two regions, a dense inner region and a dilute outer region, which is characteristic for polyelectrolyte brushes created via the grafting from approach[158,159]. More AuNPs are attached to the dilute brush region

while less AuNPs can penetrate the dense brush region. This trend can also be interpreted as a manifestation of this osmotic penalty. The exact distribution of particles within the brush as well as the exact overall adsorbed particle amount depends on a subtle interplay of various physical mechanisms promoting and suppressing particle adsorption into polyelectrolyte brushes. These mechanisms have been discussed in the literature, are partially antagonistic, and include (i) favorable interactions between polymers and particles[98], which at pH 8 are at least partially of electrostatic nature, (ii) release of counterions upon particle insertion, (iii) the electrostatic self-energy of charged particles which reduces upon adsorption due to the high ion concentration inside the brush[160], and (iv) the osmotic penalty mentioned above, which consists of a contribution from the polymers[95,98] and for polyelectrolyte brushes additionally of the counter-ion contribution[99]. In view of this complexity and without reliable estimates for the individual contributions at hand, the obtained brush and AuNP distributions were refrained from a quantitative theoretical interpretation.

6.4 Conclusion

The internal structure of solid-grafted PMETAC polyelectrolyte brushes in an aqueous environment before and after the adsorption of surface-modified AuNPs at two different pH conditions was investiagted. In order to determine the interfacial distributions of the brush and the adsorbed particles, NR in multiple water contrasts was carried out to systematically hide one of the components in each measurement, so that the distribution of the other one is obtained unambiguously. The reflectivity data were analyzed with a self-consistent model based on analytically parametrized volume fraction profiles. This procedure did not only enable the determination of the SLDs of brush and particles but also provided structural information of much greater detail than what had been obtained in previous reflectivity studies using standard approaches[154].

The measurements revealed that AuNPs adsorbing at pH 4 in the form of aggregates and are unable to fully penetrate the brush, despite significantly favorable electrostatic interactions. Adsorption instead occurs mostly at the brush periphery and is accompanied by a significant stretching of the brush due to the particles volumetric effect. At pH 8, AuNPs are highly charged, adsorb as individual particles into the entire brush at very high overall numbers, and induce an even more pronounced brush extension. The insights gained in the present work provide valuable information for the future design of PMETAC/AuNP composites for stimuli-responsive colorimetric sensors.

Continuing work showed that there is strong evidence that exposing PMETAC/AuNP composites to aqueous solution with different pH values changes the interaction between the attached AuNPs and the polymer chains of the brush. Thus has an impact on the conformational structure and the optical properties. The effect of different pH values on PMETAC/AuNP composites after incubation will be subject of the next chapter.

Chapter 7

Making strong polyelectrolyte brushes pH-sensitive by incorporation of gold nanoparticles*

Abstract

The present chapter addresses the effect of electrostatic particle-particle and particle-brush interaction after incubation. Although the neat PMETAC brush is not pH-sensitive, after embedding pH-sensitive AuNPs the PMETAC/AuNP composite becomes pH-sensitive in a reversible manner. This is detectable by the reversible shift of the plasmon band and reversible thickness change of the composites by exposing them to different pH. Furthermore, PMETAC/AuNP composites were tested with respect to its stability against pH variations. The anionic AuNPs adhere well to cationic PMETAC brushes even after post-treatment at low pH where the charge density of the AuNPs is strongly reduced.

7.1 Introduction

In previous studies, NR and XRR was used to show that the AuNP amount and distribution can be easily controlled by pH during the incubation of PMETAC brush in AuNP suspension since the AuNPs are pH-sensitive[154]. Incubation at pH 4 leads to aggregation of AuNPs, due to the lack of electrostatic stabilization. Those aggregates are attached to the brush surface forming a 2D assembly. Incubation at pH 8 stabilized the AuNPs in suspension electrostatically, and they can penetrate the brush, which results in a 3D assembly. The attachment of AuNPs in both cases is driven by electrostatic attraction between the brush and the particles and leads to the fabrication of colorimetric sensors with different optical properties (depending on the assembly formation)[137].

In terms of the use as colorimetric sensors, this work is devoted to understand as to which factor dominates the interaction to trigger SPR band shifts: particle-particle interaction or particle-brush interaction. Furthermore, no study was made in terms of the stability of brush/AuNP composite materials as colorimetric sensors for long-term use.

In the first part, the colorimetric properties of PMETAC/AuNPs composite materials are varied with the variation in pH as a post-treatment. There is strong evidence that

*Similar content was presented in D. Boyaciyan, P. Krause and R. von Klitzing, *Soft Matter*, **2018**, *14*, 4029-4039 (Making strong polyelectrolyte brushes pH-sensitive by incorporation of gold nanoparticles).

exposing PMETAC/AuNPs composite materials to different pH values changes the interaction between particle and brush. Changing the interaction has an influence on the conformational structure, which triggers SPR band shifts. Here, UV/Vis and the AFM nanoindentation method are elaborated to measure the optical response of the composite materials by changing the pH value after the incorporation of AuNPs into the polymer matrix.

As a second part, stability tests of PMETAC/AuNP composites are performed for the development of long lasting colorimetric sensors. The results show that PMETAC is a suitable choice for the immobilization of AuNPs with regard for the use as nanosensors.

7.2 Results

The AuNP interaction at different pH in suspension is extensively described in Chapter 4 (Figure 4.9) and the assembly of AuNPs in PMETAC brushes at different pH is characterized in Chapter 5 and 6. The first section shows the optical and conformational response of PMETAC/AuNP composites at different pH as a post-treatment. The second section deals with the stability of PMETAC/AuNP composites.

7.2.1 pH-induced color and thickness change of PMETAC/AuNP composites: post-treatment

pH-induced color change

AuNPs can interact with light through SPR. Incorporating them into a brush matrix induces optical properties to an optically transparent polymer brush. UV/Vis spectroscopic measurements were carried out to monitor the plasmon band shifts of the incorporated AuNPs by exposing the composite materials to different pH as a post-treatment. The plasmon band was measured for each composite material at room temperature for several pH 4/pH 8 cycles (Figure 7.1) . The cycle starts for each composite material with the pH in which the PMETAC brush was incubated.

As known from former studies[137,154] and Figure 5.2 the UV/Vis spectrum after incubation in AuNP suspension at pH 4 is red-shifted in comparison to the one obtained after incubation in AuNP suspension at pH 8. This was explained by the adsorption of AuNP aggregates after incubation in AuNP suspension at pH 4. Irrespective of the pH during

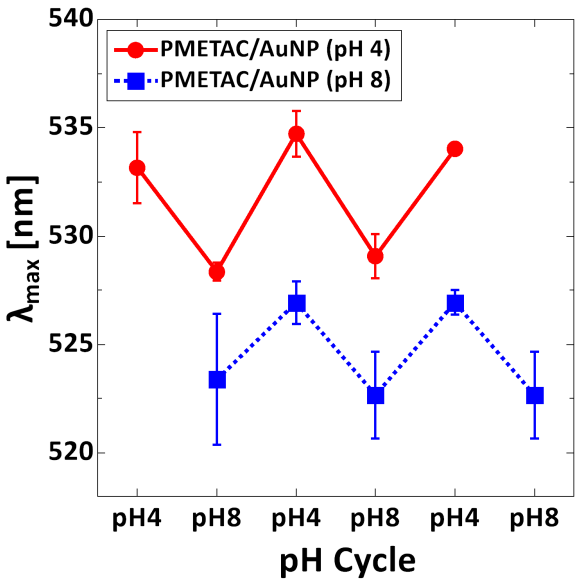

Figure 7.1: Wavelength at maximum intensity λ_{max} of PMETAC brush after incubation in AuNP suspension at pH 4 (red solid line) and after incubation in AuNP suspension at pH 8 (blue dotted line) for repeating pH 4/pH 8 cycles.

incubation in AuNP suspension the spectrum is always red-shifted when the composite was dipped into water of pH 4. The plasmon band shifts by 5.8 ± 0.7 nm for PMETAC brush after incubation in AuNP suspension at pH 4. For PMETAC brush after incubation in AuNP suspension at pH 8, the plasmon band shifts to 4.1 ± 0.4 nm. The color change is reversible without hysteresis, which indicates no aggregation of AuNPs after changing the pH value.

pH-induced thickness change

The conformational change of the neat PMETAC brush and both composite materials were characterized by exposing them to different pH and measuring the thickness. Ellipsometry and full-indentation AFM were used to characterize the thickness change for the neat PMETAC brush at room temperature for several pH 4/pH 8 cycles (Figure 7.2).

The results for the neat PMETAC brush indicates a high ability to swell in liquid environment up to 80 %[140,141]. No conformational changes with respect to the pH change are observed. Furthermore, the results obtained by the two independent methods are consistent within the experimental errors. This demonstrates that the full-indentation method can be also used to measure the thickness of polymer brushes[161].

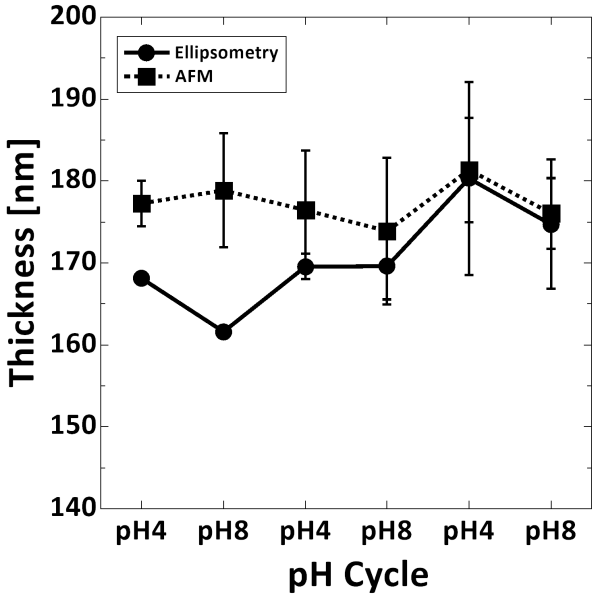

Figure 7.2: Thickness characterization for the neat PMETAC brush at room temperature by ellipsometry and full-indentation AFM for repeating pH 4/pH 8 cycles.

After AuNP deposition, the thickness of the composites cannot be determined with monochromatic ellispometry, due to the dielectric function of the AuNPs as a new parameter. Therefore, the thickness was determined for several pH 4/pH 8 cycles by the full-indentation method (Figure 7.3).

Allthough the thickness of the neat brush is not affected by the pH, incorporating AuNPs to the brush leads to a response of the composites in conformation with respect to pH changes. This response is reversible, leading to zigzag curves. No hysteresis is found for several pH cycles. Irrespective of the pH during incubation, both composite materials are in a more swollen state when exposed to pH 4 (thickness has the highest value). Increasing the pH from 4 to 8 leads to a conformational change to a more collapsed state (thickness is lower than for the neat PMETAC brush). Further, the thickness change is more pronounced for the PMETAC brush after incubation in AuNP suspension at pH 8 due to a higher amount of attached AuNPs and a stronger interaction between the AuNPs and the brush. A thickness change of 27 nm occurs upon increasing the pH from 4 to 8 for PMETAC brush after incubation in AuNP suspension at pH 4. In case of PMETAC brush after incubation in AuNP suspension at pH 8, the thickness changes of around 60 nm upon increasing the pH from 4 to 8.

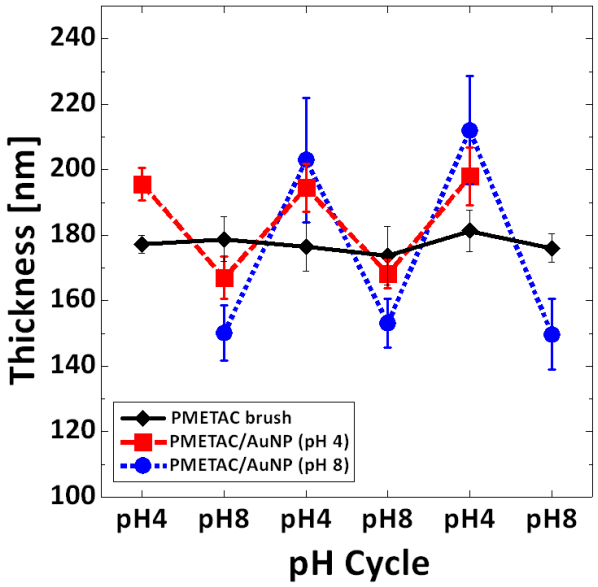

Figure 7.3: Thickness characterization for the composite materials at room temperature by full-indentation AFM for repeating pH 4/pH 8 cycles. The AuNPs were embedded either at pH 4 (squares) or at pH 8 (circles). For comparison, the thickness of the neat PMETAC brush is added.

Characterization of pH-induced thickness change by NR

The conformational change of PMETAC/AuNP composites was also tried to characterize by NR. Here, the conventional buffer systems (see Chapter 3 section 3.2.4) were used for NR measurements. Since the buffer systems are not deuterated the contrast was too low to see conformational changes in the reflectivity curves. To obtain a high contrast and see changes in the reflectivity curves, deuterated buffer systems have to be used but especially deuterated TRIS as well as citric acid are very costly.

7.2.2 Stability of PMETAC/AuNP composites

In order to check whether detachment of AuNPs occurs, the absorbance of both composites were measured in H_2O by UV/Vis after exposing them to pH 4/pH 8 in combination with sonication for 60 s. After each sonication step, the composite material was measured in H_2O by UV/Vis. That has been done for four times as a cycle. Prior to the stability check the composite material was measured in H_2O by UV/Vis (Figure 7.4).

The absorbance after each sonication step in pH 4/pH 8 was measured for the composites in order to check whether leakage of AuNPs occurs (Figure 7.5).

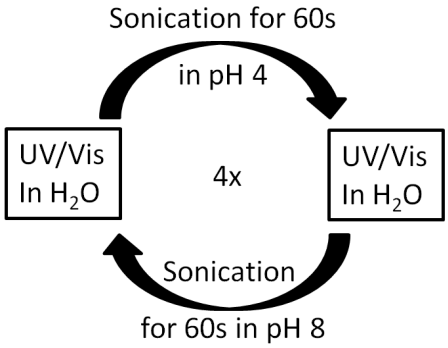

Figure 7.4: Plan of the stability check of composite materials after incubation PMETAC brush in pH 4 and pH 8.

The absorbance fluctuations are all within the error. Therefore, no significant absorbance changes is observed. Nevertheless, to determine if neat PMETAC brushes get affected by exposing to pH 4/pH 8 in combination with sonication, the thickness after each step was measured by ellipsometry in H_2O (Figure 7.6).

Figure 7.6 shows that PMETAC brushes are inert against pH changes in combination with sonication and do not tend to degraft from the substrate. The fluctuation in thickness comes due to its not uniform layer thickness on the substrate. Due to its stability this material is a promising candidate for a colorimetric sensor.

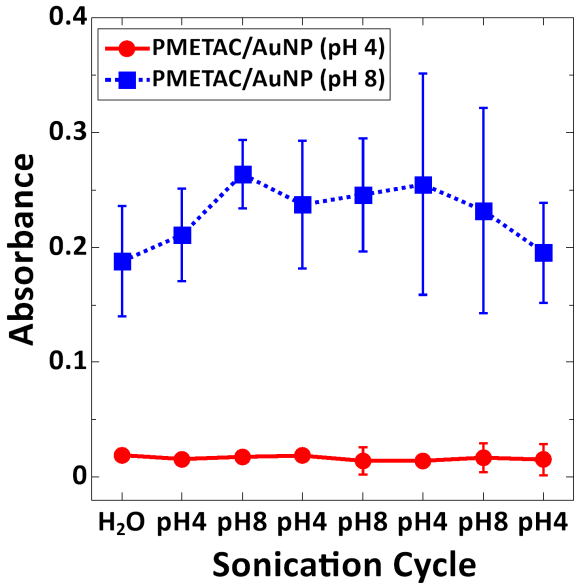

Figure 7.5: Maximum intensity of the SPR absorption band after each sonication step is shown for a composite material after incubation of PMETAC brush in AuNP suspension at pH 4 and at pH 8.

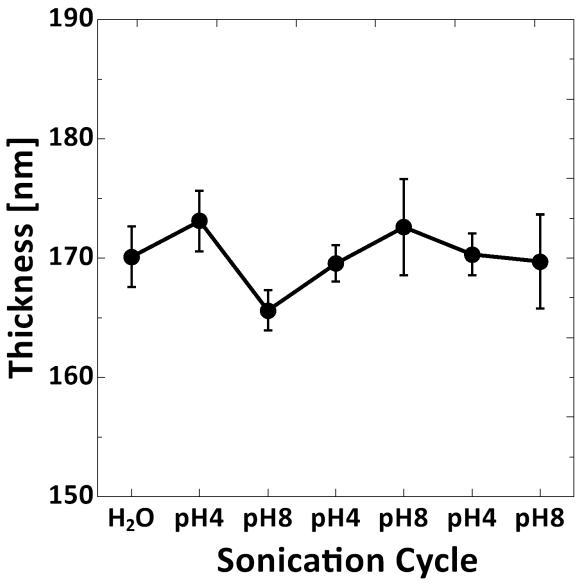

Figure 7.6: Thickness of a neat swollen PMETAC brush after each sonication step determined by ellipsometry.

7.3 Discussion

7.3.1 Response of AuNPs in PMETAC brushes by pH changes

Combining the results of UV/Vis measurements with the thickness measurements by full-indentation AFM shows that incorporation of AuNPs to an inert polymer brush triggers pH-sensitive response.

UV/Vis measurements show clearly the optical sensitivity of an inert brush after the uptake of AuNPs. The Mie-theory is in general used to describe the SPR band shifts of nanoparticles[84,87]. It is the exact solution of Maxwell's equations for the description of the scattering of an electromagnetic wave by a homogeneous sphere. In general a red-shift occurs when the interparticle distance is decreasing[162,163]. Furthermore, increase in refractive index of the environment leads also to a red-shift[82].

Decrease of the pH leads to protonation of the carboxylate groups of the AuNP capping within the brush. Those AuNPs can interact with neighboring AuNPs within the brush through hydrogen bonding. Attraction occurs leading to a decrease of interparticle distance which results in a red-shift. The results show that decreasing the pH leads to a red-shift. The SPR bands for PMETAC brush after incubation in AuNP suspension at pH 4 shifted more than for PMETAC brush after incubation in AuNP suspension at pH 8 while the

amount of AuNP uptake was smaller. AuNPs are not hindered by the brush after incubation of PMETAC brush in AuNP suspension at pH 4 (2D assembly) and a decrease of the interparticle distance (stronger plasmon coupling) is much easier leading to a stronger shift.

Looking at the results of full-indentation AFM exclusively, composites placed into pH 4 leads to a higher swelling than placed into pH 8 leading to less swelling compared to the neat PMETAC brush. The swelling change is stronger for PMETAC brush after incubation in AuNP suspension at pH 8 due to a stronger interaction between incorporated AuNPs with the polymer matrix. Furthermore, it is a reversible process, which shows no aggregation of AuNPs within the brush.

Combining the results of UV/Vis with full-indentation AFM, a blue-shift for the composites going from pH 4 to pH 8 was noticed while the composites are in a collapsed state (thickness is less than for the neat brush). Actually the expectation would be that a red-shift occurs when the thickness is decreasing since the distance between particles becomes shorter and the refractive index of the surrounding increases. Mie-theory is not able to adequately explain the observed changes. It can only be explained by the plasmon resonance for single particles. Once the particles are assembled into the brush, plasmon coupling is involved and the Mie-theory cannot be used anymore. In order to describe the effect one has to use classical electrodynamics. That means placing a dielectric medium between two neighboring electric point charges reduces the dipole-dipole interaction of those which causes a blue-shift[164–166].

This argument would be consistent with the obtained result. Placing the composite materials in pH 4 leads to a swollen composite (Figure 7.7 a)). AuNPs are less negatively charged and can interact with the surrounding polymer and with each other. By placing the composite materials in pH 8 that causes a collapse of the composites due to the reason that the AuNPs are stronger negatively charged and form a strong complex with the surrounding PMETAC through electrostatic interactions which leads to a decreased thickness as well as an interruption of plasmon coupling between neighboring nanoparticles due to more polymer material between the AuNPs through polymer wrapping. Similar effects were studied by Per Linse and Coworkers for polyelectrolytes and oppositely charged macroions using Monte Carlo simulations[167–169].

The SPR shifts for PMETAC brush after incubation in AuNP suspension at pH 4 are on average ΔSPR-shift = 5.8 $\pm$ 0.7 nm while the SPR shifts for PMETAC brush after incubation in AuNP suspension at pH 8 are on average ΔSPR-shift = 4.1 $\pm$ 0.4 nm. SPR

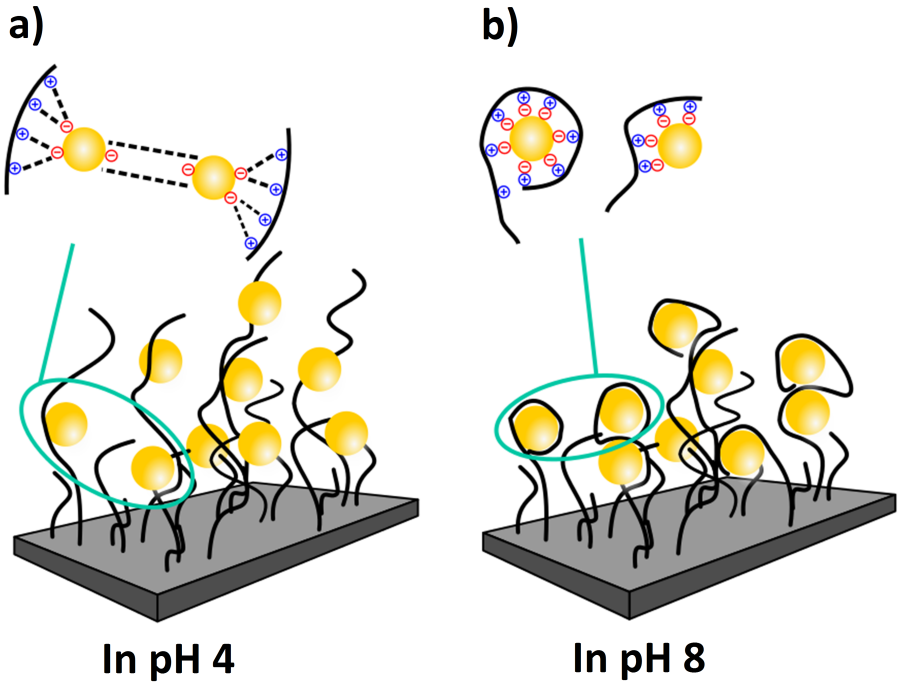

Figure 7.7: Particle-particle and particle-brush interaction in different pH. Placing the composite materials to pH 4 (a)) leads to an uncharging of the AuNPs. Particle-particle as well as particle-brush interaction occurs which leads to a swollen brush and plasmon coupling. In contrast, placing the composite materials to pH 8 (b)) causes charges on the AuNP surface. Particle-brush interaction is preferred and formation of a strong complex between AuNPs with the surrounding PMETAC brush takes place. The result is a collapsed brush and an interruption of plasmon coupling between neighboring AuNPs due to more polymer material between AuNPs.

shifts in AuNP suspension are 42 nm, which are reported in previous results[137]. The SPR shifts in the composite materials are caused via the involvement or disruption of plasmon coupling as well as refractive index changes in the surrounding medium of the AuNPs[170,171]. Both effects are influenced by a stronger or weaker particle-brush interaction. In contrast, SPR shifts in AuNP suspension are just caused through surface plasmon coupling. The shifts of the composite materials are small compared to the shifts in AuNP suspension because of a much smaller amount of AuNPs.

7.3.2 Durability of PMETAC/AuNP composites

Stability tests of the composite reveals that once AuNPs are assembled into the brush, AuNPs do not tend to detach from the brush showing a highly stable composite material due to electrostatic interaction. Further, AuNPs do not rearrange after sonication at

different pH, which would otherwise manifest in a shift of the SPR band. Therefore PMETAC is highly suitable for the use as a brush matrix to form colorimetric sensors.

7.4 Conclusion

The results revealed that cationic PMETAC is suitable as a matrix for the incorporation of negatively charged AuNPs for building long lasting colorimetric sensors. Once AuNPs are attached or incorporated to the PMETAC brush, they do not tend to leak out, due to the involvement of electrostatic attraction, which is beneficial for the attraction and fixation of AuNPs.

Moreover, a pH-response of an pH-insensitive PMETAC brush can be induced by the incorporation of pH-sensitive AuNPs. The strength of the response as well as the optical properties of those composite materials was varied during the incubation of PMETAC brushes in AuNP suspension, changing the pH of the incubation medium resulting in different assembly formation (2D or 3D assembly).

After attachment of the AuNP, the optical response of the brush can be altered through changing the pH of the medium in which the composite materials are exposed to. It has been shown that a 2D assembly has a more red-shifted SPR band and shows a larger change in the SPR shift than a 3D assembly due to stronger plasmon coupling.

The particle-particle as well as particle-brush interaction can be greatly changed through pH changes, which is the dominant factor for the colorimetric changes of the composite materials.

The next chapter will deal with the question what impact has a change in the nature of the polymer brush on the assembly formation of MPA-capped AuNPs. There, a non-ionic PNIPAM brush was used.

Chapter 8

Uptake and stability of pH-sensitive gold nanoparticles in non-ionic polymer brushes*

Abstract

This chapter discusses how changing the nature of the polymer brush, by using a non-ionic PNIPAM brush instead of a polyelectrolyte brush, can have an effect on the assembly formation of AuNPs due to the change in the particle-brush interaction. A systematic study is carried out by varying the pH value of the AuNP suspension during incubation between pH 4 and pH 8. By using AFM, SEM, TEM, UV/Vis and ellipsometry, it was found out that the AuNP uptake is increasing after the incubation of PNIPAM brushes in AuNP suspensions from pH 4 to pH 6 and is highest at pH 6. While further increase in pH leads to a decrease in particle amount. Almost no AuNP uptake was observed after incubation at pH 8. The ability to change the particle-brush interaction is rather restricted to the pH-sensitive AuNPs, in which the capping can be protonated and deprotonoted with respect to the pH value. The interplay between the right amount of protonated and deprotonated carboxylate groups is important to be electrostatically stabilizied and furthermore interact via hydrogen bondings with the amide moiety in PNIPAM and this was found at pH 6.

8.1 Introduction

In the previous chapters, the control of electrostatic interaction on the uptake and distribution of pH-sensitive AuNPs into positively charged PMETAC brushes and the resulting composite materials as its use for colorimetric sensors were studied. The electrostatic interaction between brush and AuNP was controlled by varying the pH value during incubation. It was found out that the particle-particle interaction and not the particle-polymer interaction is the main factor dominating the formation of a 2D or 3D assembly. Furthermore, it was found out that the resulting PMETAC/AuNP composite materials have a great potential for the use as colorimetric sensors.

This chapter deals with the question as to which factor dictates the particle-particle interaction the assembly formation. In order to address this question, the nature of

*Similar content was presented in D. Boyaciyan, P. Krause and R. von Klitzing, *Soft Matter*, **2018**, *14*, 4029-4039 (Making strong polyelectrolyte brushes pH-sensitive by incorporation of gold nanoparticles).

the polymer brush is changed by using a non-ionic PNIPAM brush. The uptake and distribution of AuNPs in PNIPAM brushes is elaborated. The pH during the incubation is varied between pH 4 to pH 8. Additionally, stability tests of brush/AuNP composites are performed to prove their use as colorimetric sensors. The highest AuNP uptake is found at intermediate pH value, while at higher pH almost no AuNP uptake is observed. The results also clearly show, that PMETAC is more suitable than PNIPAM as a matrix for the incorporation of AuNPs in terms of creating colorimetric sensors for a long-term prospective.

8.2 Results

8.2.1 Swelling behavior of a non-ionic PNIPAM brush in comparison to a cationic PMETAC brush

Since the brush will be swollen during particle attachment, it is of interest to study the swelling behavior of the neat polymer brushes. In previous chapters PMETAC brushes were used for the incorporation of AuNPs while in this chapter PNIPAM brushes for the incorporation of AuNPs were used. PMETAC and PNIPAM brushes with thicknesses of 30 nm, 60 nm, and 90 nm (dry thickness, measured at <2 %rh) were synthesized to characterize the uptake of water into the brush matrix with regards to the thickness and nature of the polymer brush. The water content inside the brush in vapor conditions or under water can be calculated by using Eq. 8.1

$$Water\ content\ (in\ \%) = \frac{h_{sw} - h_{dry}}{h_{sw}}\ x\ 100\ \% \tag{8.1}$$

where h_{sw} is the swollen thickness in vapor or water and h_{dry} is the dry thickness measured at <2 %rh. The data show that there is almost no dependency between the water uptake and the different brush thickness, neither for swelling in vapor (see Figure 8.1 a)), nor for swelling in water (see Figure 8.1 b)). By comparing PMETAC brushes with PNIPAM brushes, it is obvious that PMETAC brushes swell stronger in water than PNIPAM brushes, since water is a better solvent for PMETAC. The average water uptake is 53 ± 4 % for PNIPAM brushes and 81 ± 8 % for PMETAC brushes.

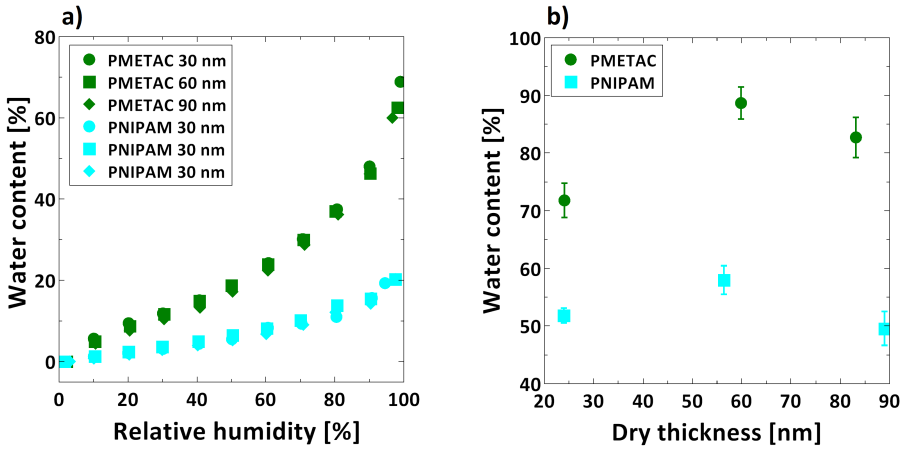

Figure 8.1: Water uptake of PMETAC and PNIPAM brushes with different brush thickness in a) vapor and b) water.

8.2.2 PNIPAM/AuNP composites

Characterization of AuNP uptake and distribution in PNIPAM brushes

The same pH-sensitive AuNPs were used as in previous chapters. In analogy to Chapter 4 the AuNP uptake after incubation of the brush in AuNP suspension can easily be proved either by detecting SPR absorption bands with UV/Vis spectroscopy, or by scanning the surface of the composite material by AFM. Also SEM can be used to visualize the AuNP assembly within the brush due to a high contrast of AuNPs in SEM images.

The pH during incubation was varied systematically between pH 4 and pH 8 and the composites were afterwards measured in H_2O at room temperature by UV/Vis. Figure 8.2 a) shows the SPR absorption bands for PNIPAM brushes after the incubation in AuNP suspension at pH 4, 6, and 8. It is obvious that AuNPs are attached to the PNIPAM brush after the incubation in AuNP suspension at pH 4 and pH 6 but no SPR absorption band was observed at pH 8, which is in contrast to the particle uptake in PMETAC brushes. The SPR absorption bands were measured also for PNIPAM brushes after the incubation in AuNP suspension at pH 5 and pH 7. The maximum intensity of the plasmon band as well as the wavelength at maximum intensity λ_{max} were plotted against the pH of the incubation medium, which is shown in figure 8.2 b). Two trends can be noticed. The absorbance is increasing for the composite materials after incubation from pH 4 to pH 6, which shows that the particle uptake increases. And for composite materials after incubation from pH 6 to pH 8 the absorbance is decreasing, which shows that the particle uptake decreases. By looking at the position of λ_{max}, the wavelength shifts to shorter

wavelength with increasing the pH value of the incubation medium, which is an indication for an increase in the particle distance.

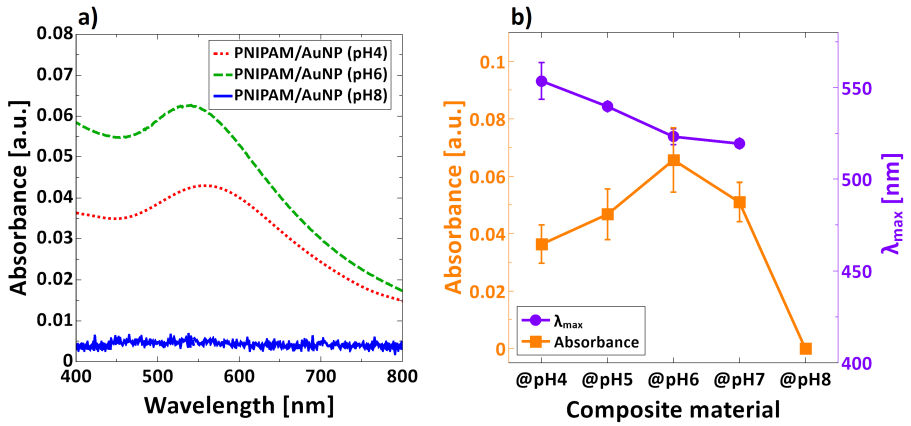

Figure 8.2: a) UV/Vis spectra of PNIPAM/AuNP composites after incubation at pH 4, pH 6, and pH 8. b) The maximum intensity of the plasmon band as well as the wavelength at maximum intensity λ_{max} in dependency of the incubation pH. Measurements were carried out at room temperature and in H_2O.

AFM height imaging and SEM imaging are used to display the attachment of AuNPs to the brush surface after incubation in AuNP suspension at different pH (see Figure 8.3). Only images after the incubation at pH 4, pH 6, and pH 8 are shown. The additional images at pH 5 and pH 7 are shown in Figure 11.10 (see Appendix). AFM and SEM images confirm the different assemblies of AuNPs onto the PNIPAM brush. AFM scans were performed under water. The particle aggregation decreases with increasing pH. Composite material generated by incubating PNIPAM brushes in AuNP suspension at pH 6 shows a homogeneous distribution of AuNPs with particles attached to the brush surface. PNIPAM brush incubated in AuNP suspension at pH 8 shows almost no attachment of AuNPs onto the brush surface. SEM cross-section of the brush after incubation in AuNP suspension at pH 4 shows the attachment of AuNP aggregates on top of the brush surface. Furthermore, incubation of the brush in AuNP suspension at pH 6 displays a homogeneous distribution of AuNPs at the brush surface while some particles tend to penetrate the brush. In contrast, incubation of the brush in AuNP suspension at pH 8 leads to almost no particle attachment. SEM images show clearly the different particle assembly with regard to the pH value of the incubation medium. However, SEM is recorded in dry state at high vacuum and therefore the particle assembly is probably different compared to the swollen state.

The thickness of a neat PNIPAM brush and the composite materials was determined in water by the full-indentation method shown in Figure 8.4. For comparison, the thickness of a neat brush is also measured by ellipsometry. By just looking at the thickness of a

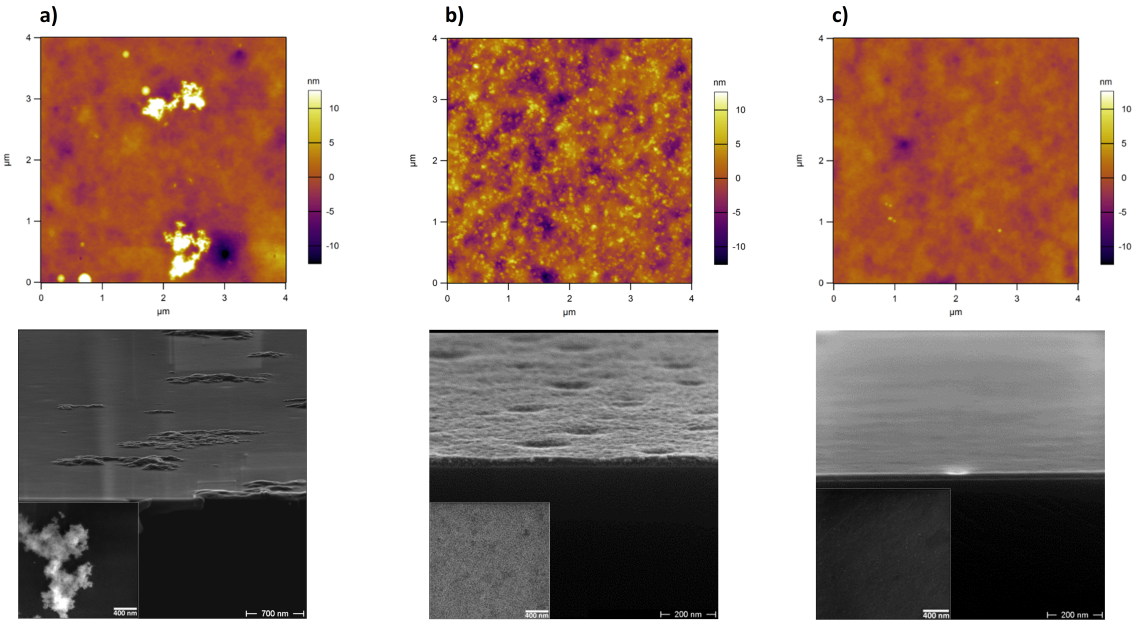

Figure 8.3: AFM height images (upper images) and SEM cross-sections (lower images) of composite materials after incubation of PNIPAM brush in AuNP suspension at a) pH 4, b) pH 6, and c) pH 8. The inset of each cross-section shows a top-view of the composite materials. AFM height images were performed under water and at room temperature while SEM images were recorded in dry state at high vacuum.

neat PNIPAM brush obtained by ellispometry and the full-indentation method, it shows, that the results are consistent within the experimental error. It was already confirmed for PMETAC brushes in Chapter 4 and demonstrates again that the full-indentation method can be used to measure the thickness of the composite materials. By comparing the thickness of a neat PNIPAM brush with the composite materials, the thickness increases after loading the PNIPAM brush with AuNPs regardless of the pH. Since the increased thickness provides information about the particle uptake, the same trend (compared to Figure 8.2 b)) is observed. The thickness increases for the composite materials with increase of the pH from 4 to 6. While the swelling thickness decreases with further increase of the pH from 6 to 8. The maximum of the increase in thickness and therefore of the particle uptake is at pH 6.

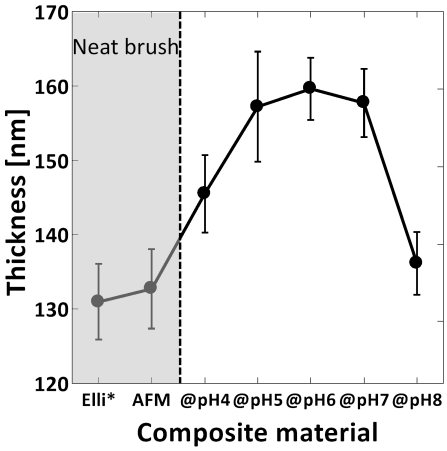

Figure 8.4: The thickness of a neat PNIPAM brush and the composite materials after the incubation in AuNP suspension from pH 4 to pH 8 are measured by the full-indentation method in H_2O. For comparison reasons, the thickness of a neat PNIPAM brush, which was measured by ellipsometry, is added to the figure.

Stability of PNIPAM/AuNP composites

The stability of those composite materials is essential for the potential use as colorimetric sensors. Therefore, stability tests were carried out for PNIPAM brushes after incubation in AuNP suspension at pH 6 and at pH 4 by exposing the composite materials to pH 4 and pH 8 and applying sonication for 15 s to check whether AuNP leakage or degrafting of the brush occurs. After each sonication step, the composite material was measured in H_2O by UV/Vis. That has been done for four times as a cycle. Prior to the stability check the composite material was measured in H_2O by UV/Vis. The stability procedure is shown in Figure 8.5.

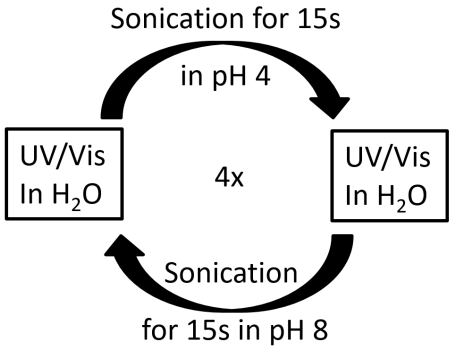

Figure 8.5: Stability procedure for a neat PNIAPM brush and the composite materials.

A simple way to check whether leakage of AuNPs occurs, is to measure the intensity of the SPR absorption band by UV/Vis. Figure 8.6 shows the maximum intensity of the

SPR absorption band after each sonication step.

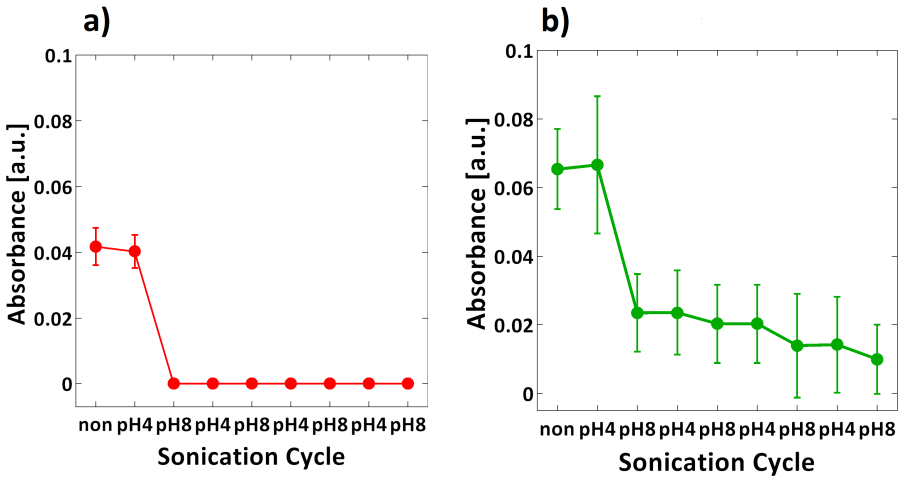

Figure 8.6: Maximum intensity of the SPR absorption band after each sonication step is shown for a composite material after incubation of PNIPAM brush in AuNP suspension at a) pH 4 and b) pH 6.

After sonication in pH 4 no change in absorbance could be detected, while a strong decrease in absorbance can be observed after sonication in pH 8. After the first sonication cycle the highest decrease in the intensity is noticed for both composite materials while the magnitude in decrease levels off with further sonication cycle for PNIPAM brush after incubation in AuNP suspension at pH 6. For PNIPAM/AuNP composites after incubation at pH 4, all AuNPs were detached after the first sonication cycle. To check, whether the PNIPAM brush gets affected by the exposure to pH 4/pH 8 in combination with sonication, the thickness of a neat PNIPAM brush after each sonication step was measured by ellipsometry in H_2O (Figure 8.7). The same stability test was applied and no degrafting of the PNIPAM brush occurred.

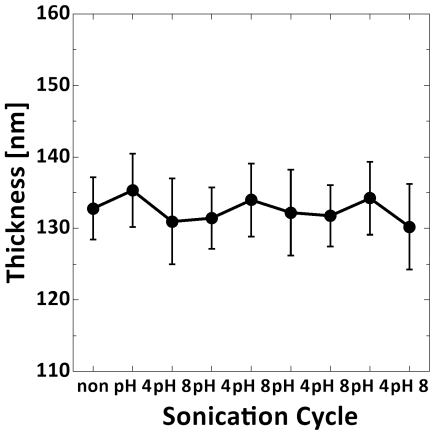

Figure 8.7: Thickness of a neat swollen PNIPAM brush after each sonication step determined by ellipsometry.

8.3 Discussion

8.3.1 Swelling ability of PNIPAM and PMETAC brushes

The nature of the polymer brush has a high impact on how much water is absorbed. Here, PMETAC brushes were compared against PNIPAM brushes regarding the swelling ability in water and vapor. The results show that thickness variation of the polymer brushes has no effect on the swelling properties. Comparing both polymer brushes, water is a better solvent for PMETAC than for PNIPAM. One major role for the better swelling ability of PMETAC brushes is that they are polyelectrolytes. Water interacts stronger with the charged groups of PMETAC than with the polar amide and carbonyl groups of PNIPAM. In addition, the PMETAC brushes are highly stretched away from the surface due to charge repulsion with neighboring chains[172].

8.3.2 Distribution of AuNPs in PNIPAM brushes

The assembly formation was characterized by measuring the SPR absorption band with UV/Vis in water. By just looking at the position of λ_{max}, the value decreases with increased pH. The increase in λ_{max} is a result of an increase in interparticle distance and a lower SPR coupling. On the other hand, the absorbance reaches a maximum at pH 6. The absorbance is proportional linked to the amount of uptaken AuNPs. At pH 8 the AuNP uptake is so low that no SPR absorption band can be detected. Figure 8.8 shows the particle assembly in PNIPAM brushes.

The characterization by using the full-indentation method shows that for all studied pH values, the brush thickness increases after the incubation in AuNP suspension, which was also observed for PMETAC brushes. Here, the same trend as for the absorbance can be seen. The highest swelling thickness is achieved after the incubation of PNIPAM brush in AuNP suspension at pH 6.

For characterizing the the distribution of AuNPs, imaging techniques were also used. SEM imaging shows the cross-section and gives more insight into the assembly formation. However, it is in a dry state and under high vacuum, which probably leads to a different assembly of AuNPs than under water. Incubation of PNIPAM brushes in AuNP suspension at pH 4 leads to a 2D assembly, since AuNPs tend to aggregate and those aggregates are too bulky to penetrate the brush. Conversely, the AuNPs can interact strongly with the PNIPAM brush via hydrogen bonding. At pH 6, AuNPs just form networks, since enough charges are available to prevent full aggregate formation and a rather 3D assembly is formed. SEM reveals a monolayer formation on top of the brush, while some single AuNPs penetrate the brush. At pH 8, almost no AuNPs are attached or within the brush. The majority of the carboxylate groups of the AuNPs capping are deprotonated and therefore barely interact with the PNIPAM brush.

AFM measurements in water were used to characterize the surface topography of PNIPAM brushes after the incubation in AuNP suspension. The images of PNIPAM brushes after incubation in AuNP suspension at pH 4 to pH 6 show an increase in particle attachment and a rather homogeneous distribution at pH 6. In contrast, further increase to pH 8 reveals a rapid decrease of particle attachment. For PMETAC brushes (Chapter 4), the AuNP amount uptaken in PMETAC brushes was the highest at pH 8 and decreases gradually to lower pH. The uptake of AuNP is driven by electrostatic interactions, while the uptake in PNIPAM brushes is driven by hydrogen bonding. Increase in pH of the AuNP suspension, increases the charge density of AuNPs surface. The charges are necessary to electrostatically stabilize single AuNPs. However, the negative charges do not interact with the non-ionic PNIPAM brush. Whereas a decrease in pH of the AuNP suspension decreases the charge density of AuNPs surface (carboxylate groups of the AuNPs MPA-coating gets protonated). Protonated carboxylate groups can interact with the amide moiety in PNIPAM by forming hydrogen bonds. However, the protonation leads to a lack of electrostatic stabilization of AuNPs resulting in aggregate formation. It is an interplay between the exact amount of protonated and deprotonated carboxylate groups of the AuNP capping to have a sufficient amount of AuNPs attached or incorporated into the brush.

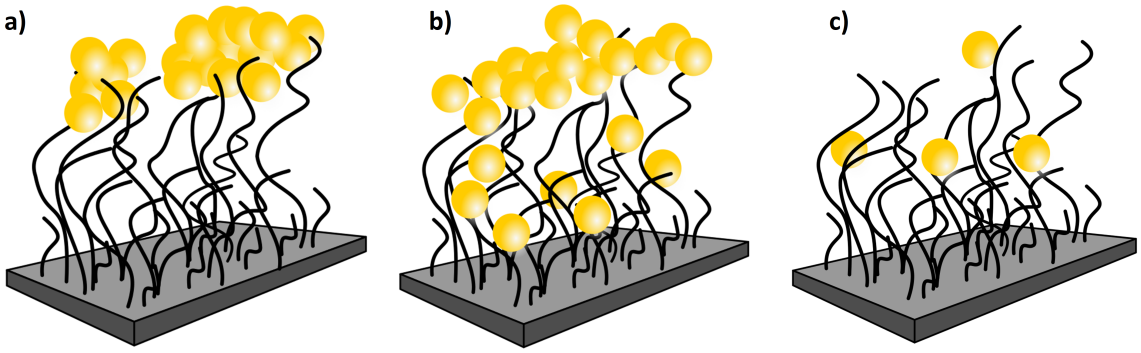

Figure 8.8: Suggested assembly formation for PNIPAM brushes incubated in AuNP suspension at a) pH 4, b) pH 6, and c) pH 8.

For the development of brush/AuNP composite materials for colorimetric sensor applications, the stability of those composite materials is of a high interest. Therefore, the composite materials (after incubation at pH 4 and pH 6) were exposed to pH 4 and pH 8 in combination with sonication for 15 sec and were characterized by UV/Vis. No leakage occurs at pH 4 in combination with sonication since the capping of the AuNPs are protonated and interact with the PNIPAM brush via hydrogen bonding (see Figure 8.9 a)). While at pH 8 leakage of AuNPs occurs after sonication. AuNPs cannot interact with the PNIPAM brush since the capping of the AuNPs in pH 8 are more likely deprotonated. Furthermore, two populations of AuNPs attached to the brush are assumed. One is strongly bound AuNPs inside the brush and the other populations of AuNPs are loosely bound at the brush surface ((see Figure 8.9 b)). Therefore, after the first sonication cycle the strongest detachment of AuNPs occurs since the loosely bounded AuNPs can easily be shaken out of the brush. Due to the leakage of AuNPs, PNIPAM cannot be used as a matrix for the incorporation of AuNPs with regard as a application of colorimetric sensors.

8.4 Conclusion

The present chapter shows, that the AuNP uptake and distribution can be tuned by changing the particle-particle as well as particle-brush interaction through the pH value of incubation medium. It shows that incubating PNIPAM brush in AuNP suspension at pH 6 leads to the highest particle uptake in which a layer of AuNPs on top of the brush is formed while some of them penetrated the brush. No brush/AuNP composite materials could be formed by incubating PNIPAM brush in AuNP suspension at pH 8. Previous studies revealed a different uptake and distribution of AuNPs in which PMETAC instead

of PNIPAM was used as polymer matrix for the incorporation of AuNPs. We could show, that the nature of polymer brush has a crucial impact on how many AuNPs are uptaken and how they assemble into the brush.

Stability test of PNIPAM/AuNP composite materials shows by exposing them to different pH media in combination with sonication that leakage occurs due to alteration of brush-particle interaction with respect to the pH value. For the use of brush/AuNP composite materials as long lasting colorimetric sensors, it would be better to use PMETAC instead of PNIPAM as a polymer matrix. Hydrogen bonding is not sufficient for the fixation of AuNPs inside PNIPAM brushes. However one could think of using PNIPAM brush as a drug delivery system by capture and release[66,173]. One could use pH-sensitive drugs and let them attach/detach with respect to the pH value.

Since no particle uptake was found after incubation of PNIPAM brush in AuNP suspension at pH 8, the last chapter will deal with the question whether applying an electric field during incubation in AuNP suspension at pH 8 can help to force the AuNPs inside the brush matrix by charging the substrate positively.

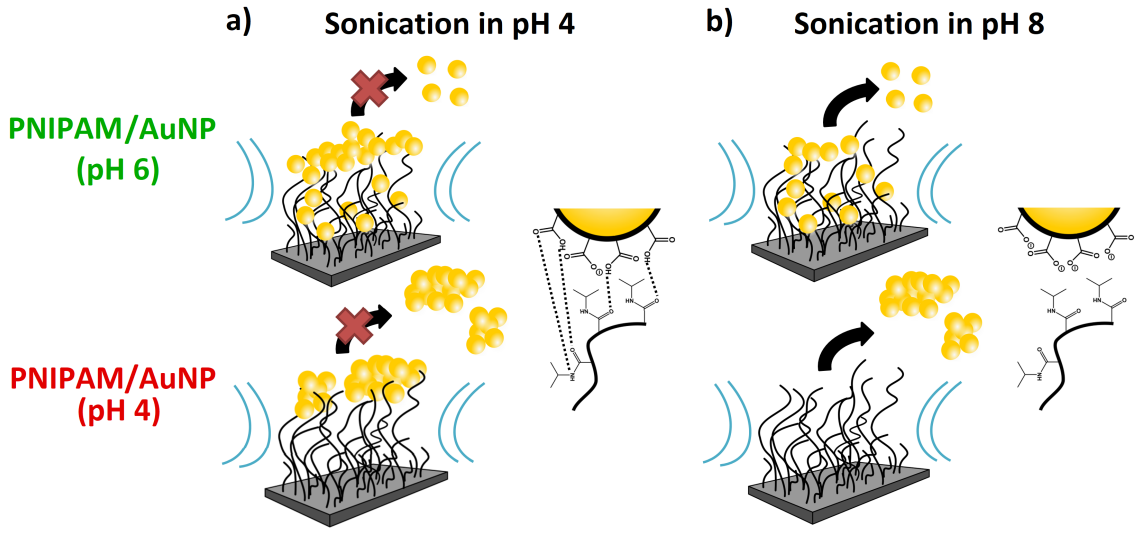

Figure 8.9: Suggested effect of sonication on PNIPAM brush after incubation in AuNP suspension at pH 6 (upper picture) and at pH 4 (lower picture). a) No leakage of AuNPs occurs in pH 4 with sonciation since the capping of the AuNPs are rather protonated and can form hydrogen bonds with the PNIPAM brush. b) leakage of AuNPs occurs in pH 8 with sonication since the capping of the AuNPs are rather deprotonated and cannot interact with the PNIPAM brush and therefore are shaken out of the brush through the sonication.

Chapter 9

Impact of an applied electric field on non-ionic poylmer brushes and the uptake of pH-sensitive gold nanoparticles*

Abstract

This chapter reports on the behavior of neat PNIPAM brushes as well as on the uptake of AuNPs under an applied electric field. In particular, PNIPAM brushes were incubated in AuNP suspension at pH 8 and an electric field was applied to force AuNPs to attach at/in the PNIPAM brush, since they are negatively charged and do not interact with the non-ionic PNIPAM brushes. UV/Vis, AFM, X-ray reflectometry and ellipsometry were used to characterize the neat PNIPAM brush as well as the uptake of AuNPs under an electric field. By generating positive charges at the silicon surface, AuNPs could successfully be attached to the brush. However, degrafting of polymer brushes was observed due to the applied electric field. Beside the attraction of negatively charged AuNPs, also hydroxid ions were dragged into the brush and promotes degrafting. The hydroxid ions stem from the autoprotolyse of water and they are reacting preferential with the ester backbone of the initiator.

9.1 Introduction

The last chapter showed that incubation of a PNIPAM brush in AuNP suspension at pH 8 does not lead to an attachment of AuNPs, since the capping of the AuNPs is deprotonated and negatively charged and therefore does not interact with the non-ionic PNIPAM brush. Decrease of the pH value leads to protonation of the AuNPs capping and allows to interact with the PNIPAM brush through hydrogen bonding. However, protonation of the capping correlates with less negative charges around the AuNP and therefore a lack of electrostatically stabilized AuNPs. Hydrogen bonds can also be formed between neighboring AuNPs, which leads to agglomeration. In order to avoid agglomeration and still be able to interact with the PNIPAM brush, AuNPs are forced into the brush by applying an external electric field at pH 8.

*The results shown in this chapter were mainly obtained in the research lab of Prof. Jan Genzer, NCSU, Raleigh, USA

Heine et al. showed theoretically by using numerical self-consistent field that polymer bushes stretches away from the substrate or are retracted to the charged surface upon control of an applied voltage[174].

Alteration in conformation by an electric field was shown experimentally by Weir et al.[175]. In this study, high grafting density PDMAEMA brushes are grown on silicon substrates and the change in thickness of the brushes is measured in response to the applied voltage between the brush substrate and a parallel electrode in a liquid surrounding by ellipsometry and NR. Applying a voltage (negative voltage) in which the brush-bearing substrate is negatively charged causes deswelling of the brush due to electrostatic attraction between the positive charged PMETAC and the negative charges at the Si-wafer. Using a positive voltage in which the Si-wafer is negatively charged causes swelling due to the repulsion between the PMETAC brush and the substrate. At very high positive voltages, the brush chain is shown to be physically removed from the substrate caused by too much stress due to the induced swelling. Nevertheless, Cantini and co-workers showed that applying an electric field can be used to modulate the interactions of surfaces with proteins, mammalian and bacterial cells[176]. Here, self-assembled monolayers (SAMs) that respond to electrical potentials is used. The molecular conformation is altered by switching the voltage to promote or inhibit the interaction with biological entities.

In this chapter, DC voltages are applied during the incubation of PNIPAM brushes in AuNP suspension at pH 8 to force AuNPs inside the brush and form composite materials with homogeneously distributed AuNPs. Our findings suggest that AuNPs are successfully attached with the help of an externally applied electric field. The use of an electric field allows a well-defined, versatile, and highly reproducible method to offer the possibility of controlling the interaction between particle and brush during incubation.

9.2 Results

9.2.1 Behavior of neat polymer brushes under an applied electric field

The behavior of neat polymer brushes in an applied electric field was studied. It should be noted that as an initiator e-BMPUS was used instead of BTPAm, which might influence the grafting density. Here, polymer brushes made of PNIPAM or PMMA with different molecular weights were placed in the petri dish and ultrapure water was added. Using a pristine sample each time, voltages of 0, 1, 3, 4, 5, and 7 V were applied for 24 h between

the brush and the counter-electrode in both directions of bias voltage. Before the voltage was applied, each sample was equilibrated in the liquid for at least 10 min. The thickness of the brush was measured before and after applying an electric field with different voltages by ellipsometry at ambient conditions to determine the polymer loss. The relative polymer loss can be determined with Eq. 9.1

$$Rel.\ polymer\ loss\ =\ \frac{h_{el}\ -\ h_{amb}}{h_{amb}} \times\ 100\ \% \tag{9.1}$$

where h_{el} is the thickness of the polymer brush after applying an electric field and h_{amb} is the thickness before applying an electric field.

PNIPAM brushes with different molecular weights under an applied electric field

PNIPAM brushes with thicknesses of 35 nm, 65 nm, and 95 nm were synthesized and each of them was immersed in ultrapure water and the electric field was applied. After each time a freshly prepared sample was used. Figure 9.1 shows the relative loss of PNIPAM brush for different molecular weight with different voltages in both direction of bias.

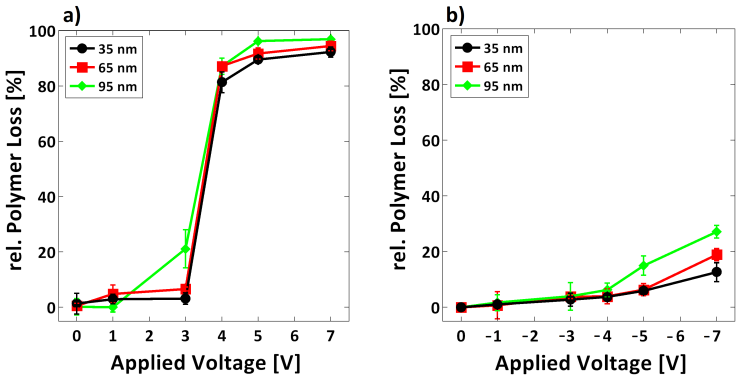

Figure 9.1: Relative polymer loss for PNIPAM brushes with different molecular weight under an applied electric field for a) in positive bias and b) negative bias. The thickness refers to the brush thickness under ambient conditions (≈ 30 %rh).

Figure 9.1 a) shows an applied voltage with positive bias. With increase in voltage the loss of polymer increases. Loss of polymer starts after 3 V. Furthermore, a small difference in polymer loss is observed for different molecular weight. Increase in molecular weight leads to an increase in polymer loss for an applied electric field. In contrast, on figure 9.1 b) the relative loss of polymer is shown for an applied electric field with negative bias. The relative loss is less pronounced. Significant loss of polymer starts from 4 V on.

Same dependence can be observed for loss of polymer with different molecular weight. An increase in molecular weight leads to an increase in polymer loss.

PMMA brushes with different molecular weights under an applied electric field

In order to understand the mechanism of detachment, PMMA as a polymer materials was used instead of PNIPAM. PMMA is more hydrophobic and is collapsed when immersed to water, which could prevent degrafting. Here, thicknesses of 25 nm, 75 nm, and 85 nm for PMMA brushes were used to check the impact of an applied electric field on the polymer loss. Figure 9.2 shows the relative loss of PMMA brush for different molecular weight under an applied voltage.

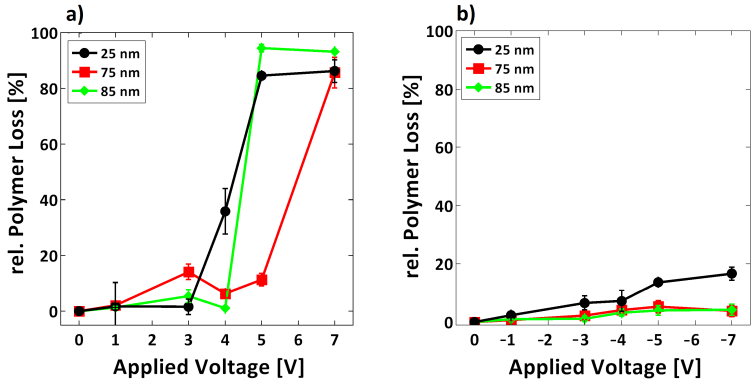

Figure 9.2: Relative polymer loss for PMMA brushes with different molecular weight under an applied electric field for a) in positive bias and b) negative bias. The thickness refers to the brush thickness under ambient conditions ($\approx$ 30 %rh).

Looking at the loss of polymer in positive bias, a loss is observed from 4 V on. No systematic behavior for different molecular weight was observed. For negative bias, the loss of polymer starts from 5 V on. Here, a small difference is seen by using different molecular weight. Increase in molecular weight causes an decrease in polymer loss.

Comparing PNIPAM with PMMA brushes, one can see a retention of polymer loss of $\approx$ 1 V by using PMMA brushes.

9.2.2 AuNP uptake in PNIPAM brushes by an applied electric field

The comparison between PNIPAM and PMMA on the brush stability shows that PMMA is more stable than PNIPAM. However, PNIPAM brushes were used for the incorporation

of AuNPs during an applied electric field, since water is a better solvent for PNIPAM than for PMMA. PMMA would be collapsed during the incubation and that hinders the incorporation of AuNPs.

For the AuNP uptake, PNIPAM brushes were placed in the petri dish and AuNP suspension was added. Different voltages were applied and the incubation time was set to 6 h. The incubation time for PNIPAM brushes in AuNP suspension during an applied electric field has been set not higher than 6 h in order to minimize the damage on the PNIPAM brush. Afterwards, the samples were removed, sonicated for 1 min in ultrapure water and dried under a stream of nitrogen. XRR measurements are an easy way to check whether AuNPs are attached on the brush, since gold has a good contrast. The samples were measured against air in ambient conditions. The reflectivity curves were fitted with an one-box model unless the fitting model is indicated otherwise.

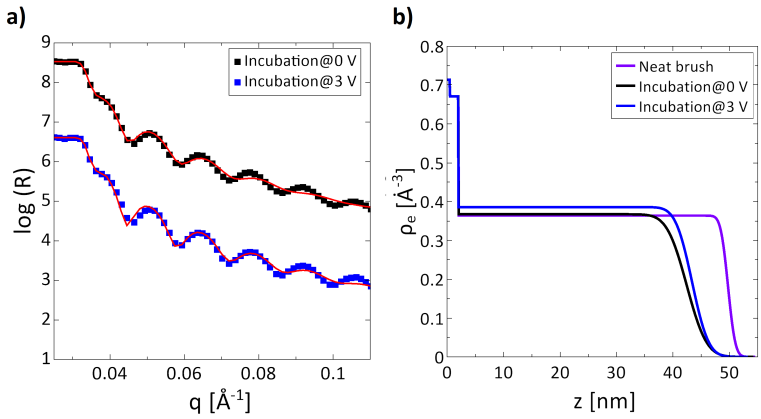

Figure 9.3: a) Reflectivity curves of PNIPAM brushes before and after applying an electric field during incubation and b) corresponding electron density profiles. To compare, the SLD of a neat brush was added. Measurements were done in ambient conditions.

As a first approach, PNIPAM brushes were incubated in AuNP suspension at pH 8 with applying a positive bias of 3 V. To compare the uptake of AuNPs, the brush was also incubated in AuNP suspension at pH 8 without an electric field. After incubation both samples were measured by XRR and the reflectivity curves as well as the electron density profiles can be seen in Figure 9.3. In addition, the SLD of a neat brush was added. The neat brush refers to a PNIPAM brush, which did not come in contact to a AuNP suspension.

The electron density profiles reveal that no significant change in the electron density between both is observed. Further the surface topography was measured by AFM (Figure 9.4). It shows that the surface has been not affected during the incubation compared to

a neat PNIPAM brush. Only a thickness decrease after incubation of around 5 nm was observed compared to the thickness of a neat brush.

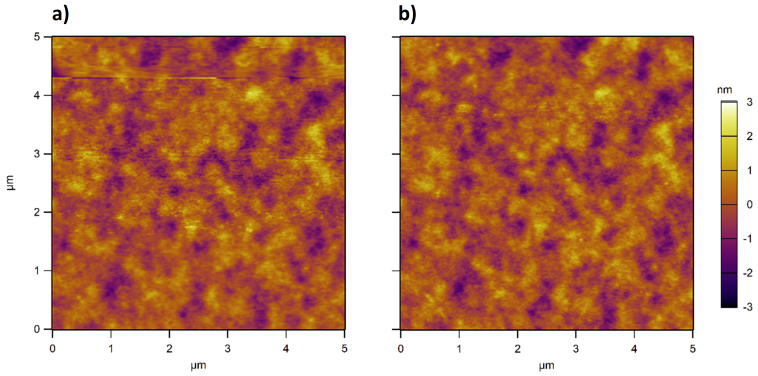

Figure 9.4: AFM topographical images after a) PNIPAM brush just incubated in AuNP suspension at pH 8 and b) with an applied electric field of 3 V during incubation. AFM images were carried out in ambient conditions.

Another approach was to increase the voltage during incubation. Nevertheless, that would have a tremendous impact on the stability of the brush. Therefore, the counter-electrode (gold wire) was put outside the medium. No actual current would flow but just the potential is applied and could drag the AuNPs inside. A Voltage of 3 V and 6 V was choosen and XRR measurements were carried out (Figure 9.5).

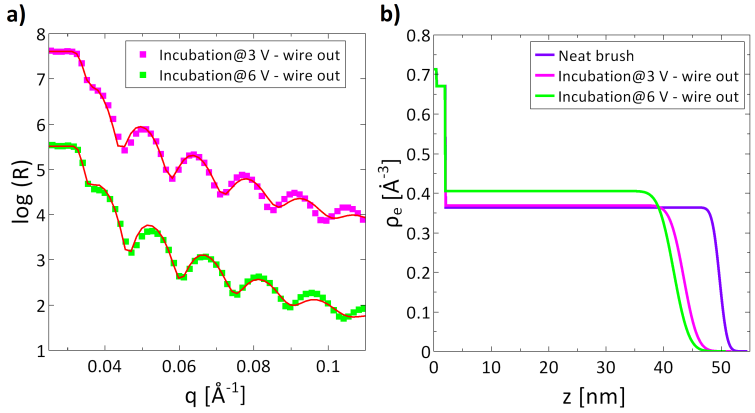

Figure 9.5: a) Reflectivity curves of PNIPAM brushes after applying an electric field of 3 V and 6 V during incubation and b) the corresponding electron density profiles. To compare, the SLD of a neat brush was added. Measurements were done in ambient conditions.

Again no significant differences are observed in the electron density. Compared to the neat brush, again a slight thickness decrease was observed. The surface topography was measured by AFM in ambient conditions (Figure 9.6).

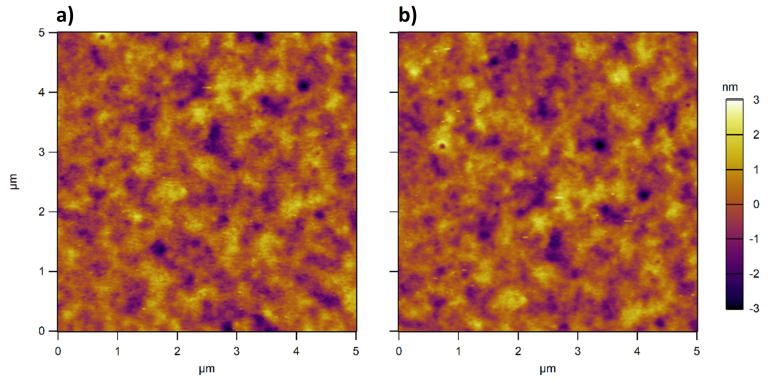

Figure 9.6: AFM topographical images after a) PNIPAM brush in an electric field of 3 V during incubation and b) with an applied electric field of 6 V during incubation. In both, the counter-electrode was outside of the medium during applying an electric field. AFM images were carried in ambient conditions.

Both images show that no AuNP attachment can be detected.

In all scenarios no increase in AuNP uptake was observed. The issue with applying an electric field during incubation is that once the electric field is switched off, the force to drag them inside the brush is gone and the particles do not interact with the brush and can move freely without any fixation to the brush. The particles have to be fixed after applying an electric field. Here, a decrease in pH can help to form hydrogen bondings between the particles and the brush, which was taken advantage of (Figure 9.7).

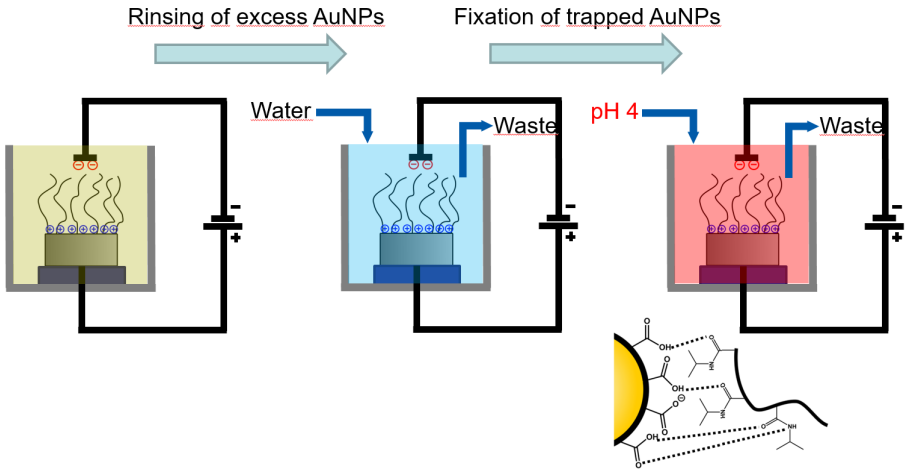

Figure 9.7: In the first step, an electric field of 3 V was applied for 6 h during incubation of PNIPAM brush in AuNP suspension at pH 8. As a second step, the excess AuNP suspension was rinsed with ultrapure water. As a last step, the trapped AuNPs were fixed by decreasing the pH from 8 to 4. All steps were done in the presence of an electric field.

The PNIPAM brush was incubated in AuNP suspension at pH 8 and an electric field of

3 V was applied for 6 h. As a second step, the excess AuNPs were rinsed with ultrapure water and the AuNPs who were dragged inside the brush were fixed by decreasing the pH from 8 to 4 as a last step in presence of an electric field. XRR measurements were carried out in ambient conditions and compared to the neat PNIPAM brush (Figure 9.8).

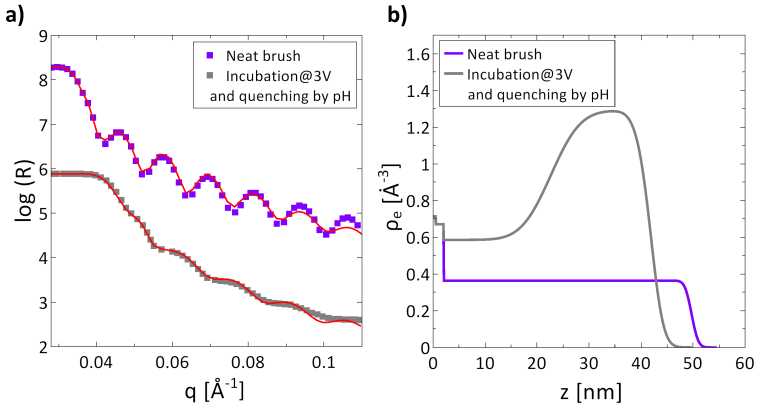

Figure 9.8: a) Reflectivity curves of PNIPAM brushes before and after applying an electric field of 3 V and quenching by pH. b) The corresponding electron density profiles. Measurements were done in ambient conditions.

The XRR curve of the sample after the rinsing and quenching step was fitted with a three-layer model. The electron density profiles clearly show an increase of the electron density in layer 1 and a thick layer on top of the brush. The overall increase in electron density suggest an uptake of AuNPs.

AFM measurements were also carried out (Figure 9.9).

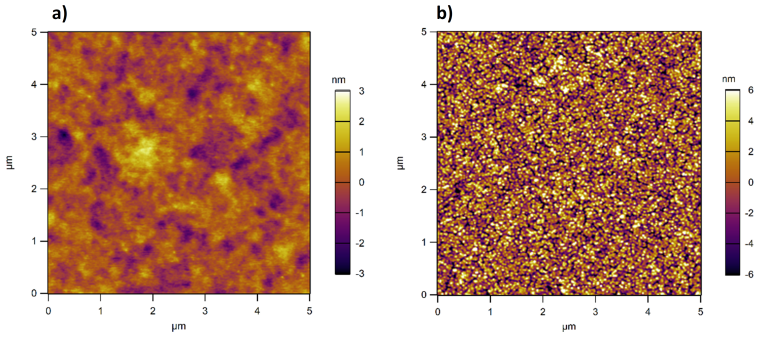

Figure 9.9: AFM topographical images for a) neat PNIPAM brush and b) after applying an electric field during incubation and rinsing with ultrapure water and fix the trapped AuNPs by decreasing the pH. AFM images were carried in ambient conditions.

It clearly shows that AuNPs are attached on top of the brush. No agglomeration is noticed but particle crowding can be found. Table 9.1 summarize the thickness, electron

density, and roughness for each layer, obtained by the three-layer model. In comparison, the thickness, electron density, and roughness for all other samples were added. For comparison purposes, nanoindentation measurements by AFM were carried out for all samples to measure the overall thickness and the results were added to the table.

Table 9.1: XRR Data and nanoindentation measurements summarized for all samples. Both measurement technqiues has been done in ambient conditions at room tepmerature.

	AFM	XRR layer 1		XRR layer 2		XRR layer 3	
Sample	h [nm]	h_1 [nm]	ρ_{e1} [Å^{-3}]	h_2 [nm]	ρ_{e2} [Å^{-3}]	h_3 [nm]	ρ_{e3} [Å^{-3}]
Neat Brush	49±5	49.9	0.36	-	-	-	-
Incubation@pH 8 0V	45±3	42.3	0.37	-	-	-	-
Incubation@pH 8 3V	44±3	43.1	0.39	-	-	-	-
Incubation@pH 8 0V-wire out	46±4	43.5	0.37	-	-	-	-
Incubation@pH 8 3V-wire out	42±3	42.1	0.40	-	-	-	-
Incubation@pH 8 3V and quenching by pH	43±4	22.5	0.59	18.4	1.35	1.3	0.58

The thickness determined by the fullindentation method with AFM is in very good agreement with the XRR data.

9.3 Discussion

9.3.1 Polymer brushes under an applied electric field

Several papers showed that polymer brushes can be either further stretched away from the substrate or collapsed under an applied electric field[177,178]. Further, Weir et al.[175] observed in their experiments a polymer brush loss for high voltages of positive bias. They conclude, that the pH value in the vicinity of the electrode is increased by the attraction of OH^- counterions, and this high pH value could lead to cleavage of the ester group within the ATRP initiator molecule (Figure 9.10) via hydrolysis.

Here, degrafting of polymer material was also observed (see Figure 9.1 and 9.2). The polymer loss for a positive bias voltage was more pronounced than for a negative bias voltage. It shows, that cleavage is also promoted for a negative bias when H_3O^+ are dragged into the brush leading to a low pH at the substrate. In both, positive and negative bias voltage, the loss of PNIPAM brush occurred at lower voltages compared to PMMA brushes. The reason is that PMMA is more hydrophobic than PNIPAM and therefore retention of OH^- or H_3O^+ counterions inside the brush occurs due to sterical hindrance.

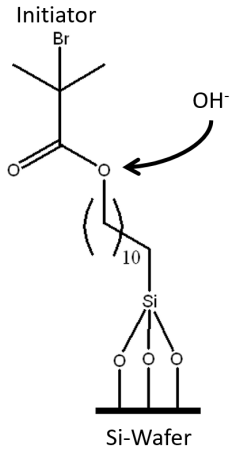

Figure 9.10: Mechanism of the cleavage of the ester group within the initiator molecule by the attraction of OH^- counterions.

For PNIPAM brushes, the loss of polymer depends on the molecular weight. PNIPAM swells in water and due to their swelling a force onto the initiator is applied. The force gets stronger with higher molecular weight[179]. In contrast, PMMA brushes did not show any systematic change with regards to the molecular weight. It should also be mentioned that the standard potential of the dioxygen half reaction in water is $E^{\circ}_{O_2/H_2O} = 1.23\ V$[180] and therefore electrolysis of water occurs during an applied electric field, which could also have an impact on the instability of the brush.

Nevertheless, PNIPAM brushes were still used for the incorporation of AuNPs in an electric field during incubation, since PNIPAM swells better than PMMA in water. In order to increase the stability for future measurements, one could think of using a copolymer brush of PMMA-b-PNIPAM[152]. PMMA would hinder the hydrolysis of the ester moiety at the initiator while the PNIPAM is used as the matrix for the incorporation of AuNPs. Another approach would be to use a different initiator without any moieties that can be hydrolyzed. Bain et al.[133] synthesized a novel initiator, which is non-ester based. By using the so called "BAIN-initiator" instead of e-BMPUS the hydrolysis could be inhibited and the stability would increase.

9.3.2 AuNP uptake in PNIPAM brush under an electric field

In order to minimize the damage of the PNIPAM brush during the incubation, the incubation was taken place at 3 V for 6 h. A positive bias voltage was chosen, which creates positive charges along the substrate to drag the negatively charged AuNPs into the polymer matrix to form a 3D assembly.

Several approaches has been made in order to drag the AuNPs inside the brush. As a first approach, the counter-electrode was put inside the incubation medium and a voltage of 3 V was applied for 6 h. No increase in the electron density by XRR was observed compared to the neat brush as well as the brush incubated in AuNP suspension at pH 8 without an electric field (see Table 9.1). As a second approach, the counter-electrode was placed outside the incubation medium and voltages of 3 V and 6 V were applied. Also here, no increase in the electron density was observed after incubation. Further, AFM measurements also revealed no attachment of AuNPs. In all approaches, a decrease in the brush thickness was observed after applying an electric field, due to the instability of the initiator. In Chapter 8 it was shown that AuNPs can bind to PNIPAM at lower pH, since the carboxylate group of the MPA-capping is protonated and can form hydrogen bondings with the amide moiety of the PNIPAM backbone[181]. This finding was taken advantage of by lowering the pH in the presence of an applied electric field to fix the AuNPs to the PNIPAM brush. After applying an electric field for 6 h, excess AuNPs were rinsed with water and the trapped AuNPs inside or attached to the brush were quenched by lowering the pH value. The excess AuNPs were rinsed in order to avoid agglomeration during the quenching process. With the combination of using an electric field and quenching by lowering the pH could successfully incorporate AuNPs into the PNIPAM matrix. However, XRR measurements revealed that most of the AuNPs are attached to the brush surface. The XRR reflectivity curve was fitted with a three-layer model, since previous experiences with attached AuNPs at the brush surface (see Chapter 5) showed the success of this fitting model. AFM measurement shows that the AuNPs attached to the brush surface are well distributed without agglomeration. It can be concluded, that on top of the brush a multi-layer film of AuNPs is created without agglomeration while some AuNPs could penetrate the brush.

The amount of attached AuNPs can be determined with Eq. 5.2. Assuming that only air and AuNPs are involved, the volume percent of AuNPs in layer 2 is $\approx$ 30 $vol-\%$. Combining all three layers together, the thickness of the brush after applying an electric field during incubation in combination with quenching is lower than the thickness of the neat PNIPAM brush, which is referred to the instability of the initiator in an electric field.

9.4 Conclusion

This chapter showed an active approach to force AuNPs inside PNIPAM brushes by applying an electric field. Since almost no AuNP uptake was noticed after the conventional incubation of PNIPAM brushes in AuNP suspension at pH 8, the AuNPs were absorbed in PNIPAM brushes by using a positive bias voltage in combination with a pH change during incubation. An increase of the AuNP amount was noticed by XRR and AFM measurements after the incubation.

On the flip side, damage on the brush itself was noticed due to dragging either OH^- for positive bias voltage or H_3O^+ for negative bias voltage into the polymer brush, which leads to cleavage at the ester moiety of the initiator. Retention of polymer loss was observed by using more hydrophobic polymer brushes. Copolymerization of PMMA-b-PNIPAM brushes could decrease the degree of loss during an applied electric field. However, little is known so far about the brush stability during the applied electric field. Further, the cleavage could be used for the determination of molecular weight.

For future studies improvements has to be made of in terms of preventing detachment of polymer brush during the applied voltage. Also the pH value inside the brush has to be measured in order to get more information about the mechanism of cleavage during an applied electric field. Furthermore, more characterization techniques would be helpful to get a better insight in the distribution of AuNPs. NR with contrast variation would help to get information about the spatial distribution.

Chapter 10

Conclusion and future perspectives

10.1 Summary and conclusion

In this thesis the impact of electrostatic interaction between particles as well as between particle and brush are discussed with respect to the uptake and distribution of AuNPs in cationic and non-ionic polymer brushes. The overall goal is to achieve brush/AuNP composite materials with tailored optical properties. For the perspective to be used as colorimetric sensors, it is crucial to know how the assembly of AuNPs in polymer brushes can be controlled.

In all studies MPA-coated AuNPs with a diameter of around 5 nm are used for the incorporation into the polymer matrix. Variation in pH value triggers a change in AuNP surface charge caused by the pH-sensitivity of the MPA capping. First, the particle-particle interaction at different pH is investigated by mixing AuNP stock suspension with different buffer solutions with pH values ranging from 4 to 8. MPA-capped AuNPs are pH-sensitive, since the capping bears a carboxylic group with a pK_a of 4.3. TEM measurements reveal that AuNPs form aggregates at pH 4. At pH 6, network-like aggregation occurs between AuNPs, while at pH 8 a stable suspension of individual AuNPs is observed. Decreasing the pH value decreases the interparticle distance due to protonation of the carboxylic acid group at the AuNP surface, resulting in a reduction of electrostatic repulsion.

As a polymer matrix strong cationic PMETAC and non-ionic PNIPAM brushes are used. Both brushes are not affected by pH variations. Therefore any pH effect on the brush/AuNP composite is caused by the pH-sensitivity of AuNPs. The thesis is divided into three main parts with respect to the polymer brush material and stability of brush/AuNP composites. The first part (Chapter 4, 5, 6, and 7) discusses the assembly of AuNPs into strong cationic PMETAC brushes while the second part (Chapter 8 and 9) is devoted to use non-ionic PNIPAM brushes as a polymer matrix for the incorporation of AuNPs. The third part deals with the stability of brush/AuNP composites as a post-treatment and the results are shown at the end of Chapter 7 for PMETAC/AuNP composites and at the end of Chapter 8 for PNIPAM/AuNP composites.

In the first part (Chapter 4 - 7) of this thesis, strong positively charged PMETAC brushes are incubated in AuNP suspension at different pH. Since PMETAC brushes are insensitive to pH due to permanent positive charges, they present a suitable matrix to study pH effects on the uptake and distribution of AuNPs with a pH-sensitive capping. The first study

(Chapter 4) is dedicated to the investigation of the amount of AuNPs within PMETAC brushes after the incubation at different pH value. For all studied pH, AuNP uptake is observed, which causes an increase in brush thickness due to the particles volumetric and osmotic effects. Using gravimetric analysis and UV/Vis spectroscopy, it is found that the particle number density within the PMETAC brush increases with increasing pH. This finding is attributed to the increase of negative charges of the AuNPs due to the deprotonation of the carboxylic acid groups of the MPA-capping at higher pH, which can interact strongly with the cationic PMETAC brush.

The second chapter (Chapter 5) describes the AuNP distribution perpendicular to the substrate surface by analyzing the composites via XRR and NR. The results show, that incubation of PMETAC brushes in AuNP suspension at pH 4 leads to the formation of a surface layer of AuNPs (2D assembly), while incubation in AuNP suspension at pH 8 leads to deeper particle penetration into the brush and a rather homogeneously distribution (3D assembly). The main factor dominating the different assembly formation is assigned to the interaction between particles. At low pH the AuNPs tend to aggregate in suspension due to a lack of electrostatic stabilization. The aggregated AuNPs are still able to interact with the PMETAC brush but to a less distinct. The aggregates are attached to the brush surface because they are too bulky to penetrate the brush. At higher pH, the carboxylate groups of the AuNPs coating are deprotonated, leading to highly charged AuNPs and a stabilized dispersion. Single AuNPs can penetrate into the brush, leading to a high uptake and a more homogeneous distribution within the brush. Furthermore, no rearrangement of the AuNPs after incubation is noticed when a change in the environment (aqueous solution to ambient conditions) induces a collapse or swelling of the composite materials. Comparing the results of NR and XRR with UV/Vis in Chapter 4 shows that the different assembly formation of AuNPs in PMETAC brushes are in good agreement to their SPR absorption bands. However, XRR revealed a layer of AuNPs at the brush surface after incubation of PMETAC brush in AuNP suspension at pH 4 with a volume percent of around 16 vol-%, while NR could not show any attachment due to a lack of contrast. Further, it had not been possible to extract the amounts and SLDs of the individual components by NR. Also, it was so far impossible to separate the components from each other and examine the effects of AuNPs and brush on itself with the current fitting procedure.

Therefore, Chapter 6 deals with the question, how the individual components (AuNPs and PMETAC brush) are distributed after incubation. This is elucidated by NR with contrast variation, and a self-consistent reflectivity analysis based on the analytical parametrization of the volume fraction profiles of all tested chemical components. This procedure provides

structural information of much more detail than using standard approaches, since the new analysis allows the determination of the spatial distribution of components separately from each other and it can fit all reflectivity data for various water contrasts simultaneously. With the more advanced procedure it is found out that AuNPs do not fully penetrate the brush after incubation of a PMETAC brush in AuNP suspension at pH 4, since they are aggregated and too bulky to penetrate the brush. Instead, they mostly adsorb to the brush periphery. The associated release of counterions due to the attachment is normally expected to result in a reduction of the osmotic pressure inside the brush, and, in turn, in a more compact brush conformation. In contrast to this expectation, the adsorption of AuNPs leads to a more extended brush conformation, which is attributed to volumetric effects of the AuNPs themselves. They occupy up to almost 20 vol-%, which is in good agreement to the XRR studies. At pH 8, AuNP absorption occurs inside the entire brush. The overall AuNP amount per unit area is found to be $\sigma_{AuNP} \approx 0.18$ nm^{-2}. The associated much stronger volumetric effect is manifested also in the even more extended brush conformation. However, the AuNP distribution is not homogeneous. PMETAC brushes posses two regions, a dense inner region and a dilute outer region. More AuNPs are attached to the dilute region while less AuNPs can penetrate the dense brush region, which is contributed to the osmotic penalty. This advanced procedure enables not only more information about the internal structure but also provides the SLDs of PMETAC and the MPA-AuNPs, which are 0.84×10^{-6} Å^{-2} and 3.8×10^{-6} Å^{-2}, respectively. This is in good agreement to the theoretical values with 0.88×10^{-6} Å^{-2} and 3.6×10^{-6} Å^{-2}, respectively.

The first three Chapters have reported on the assembly formation of PMETAC/AuNP composites. The uptake and distribution of AuNPs is controlled by the pH value of the AuNP suspension in which the PMETAC brush is immersed during incubation. With that, UV/Vis measurements could show that the different assembly formations posses different SPR absorption bands, which can be used to develop colorimetric sensors with different optical properties. Therefore, Chapter 7 presents the capability of PMETAC/AuNP composites for its use as colorimetric sensors. The study focuses on, which interaction dominates more to trigger SPR band shifts: the interaction between particles or the interaction between particle and brush. The colorimetric properties of PMETAC/AuNPs composite materials are varied with the variation in pH as a post-treatment. It is shown that incorporation of pH-sensitive AuNPs to the inert PMETAC brush triggers pH-sensitive response. pH variation can induce SPR absorption band shifts in PMETAC/AuNP composites of up to 6 nm in a reversible manner. The shifts of the composite materials are small compared to the shifts in AuNP suspension (around 42 nm) because of a much smaller

amount of AuNPs, which are involved. The pH variation also induces conformational changes of the composites and in a reversible manner. Summarizing the results of SPR band shift and conformational change, a blue-shift for the composites is noticed when the pH is changed from pH 4 to pH 8 while the composites are in a collapsed state at pH 8. Those findings are in contradiction with the expectation. A red-shift should occur when the thickness is decreasing, since the distance between particles becomes shorter and the refractive index of the surroundings increases due to compression of polymer material in a confined space. The observed effect can be explained with classical electrodynamics. Placing a dielectric medium between two neighboring electric point charges reduces the dipole-dipole interaction of them which causes a blue-shift. At pH 4, AuNPs are less negatively charged and can interact electrostatically with the surrounding PMETAC as well as with each other via hydrogen binding, which leads to a swollen composite. Increasing the pH to 8 causes a collapse of the composites due to the reason that the AuNPs are stronger negatively charged and form a strong complex with the surrounding PMETAC through electrostatic interactions. That leads to a decrease in thickness as well as an interruption of plasmon coupling between neighboring AuNPs due to an enrichment of polymer material between the AuNPs through polymer wrapping. It clearly shows, that the particle-brush interaction dictates the optical response. With respect to the composite's stability, it was also shown that the AuNPs adhere well to cationic PMETAC brushes even at low pH where the charge density of the AuNPs is strongly reduced.

In the last two chapters (Chapter 8 and 9) the nature of the polymer brush is changed by using a non-ionic PNIPAM brush. Chapter 8 describes the influence of a non-ionic PNIPAM brush on the assembly formation of MPA-capped AuNPs. Here, the pH during incubation is varied systematically between pH 4 to pH 8. The highest particle uptake and penetration is observed after the incubation at pH 6 in which a layer of AuNPs on top of the brush is formed while some of them penetrated the brush. At pH 4, AuNPs can strongly interact with the PNIPAM brush via hydrogen binding. However, the AuNPs are not electrostatically stabilized and tend to aggregate and are just attached to the brush surface. No PNIPAM/AuNPs composite materials could be formed after the incubation at pH 8. The carboxylate groups are deprotonated and the ability to bind to the PNIPAM via hydrogen formation is not given. The interplay between the exact amount of protonated and deprotonated carboxylate groups of the MPA-capping is important to be electrostatically stabilized and also have the ability to interact via hydrogen bonding with the amide moiety of the PNIPAM backbone, which is found at intermediate pH value. Stability tests of PNIPAM/AuNP composites are also performed to prove their use as colorimetric sensors. Leakage is found for composites when exposed to higher pH, since the AuNPs capping is

deprotonated and therefore the negatively charged AuNPs loose their ability to interact with the PNIPAM brush via hydrogen bonding. It clearly shows, that the nature of the polymer material has a crucial impact on the uptake of pH-sensitive AuNPs and that PMETAC is more suitable as a matrix for the incorporation of MPA-capped AuNPs in terms of creating colorimetric sensors as a long-term prerspective.

The last Chapter (Chapter 9) discusses the incorporation of negatively charged AuNPs at pH 8 into the non-ionic PNIPAM brush by using an electric field. Since almost no AuNP uptake is detected after the conventional incubation of PNIPAM brush in AuNP suspension at pH 8, the AuNPs are successfully absorbed in PNIPAM brushes by using a positive bias voltage in combination with a pH value decrease during incubation (quenching). However, damage on the brush itself is detected beforehand when an electric field is applied. The reason is that water undergoes autoprotolysis to OH^- and H_3O^+ and those are also dragged inside the brush, depending on the bias voltage which is applied. They can cleave the ester moiety of the initiator by hydrolysis resulting in degrafting of the brush. However, retention of polymer loss is achieved by using PMMA as a more hydrophobic polymer brush.

The ability of the composites to act as a platform for optical sensing has been discussed. The attachment of AuNPs is driven either by electrostatic attraction for PMETAC brushes or hydrogen bonding for PNIPAM brushes, while the AuNP distribution in general is dominated by the particle-particle interaction. The perspective for its use as colorimetric sensors depends on the polymer's nature. Here, cationic PMETAC brushes are more favorable than non-ionic PNIPAM brushes. The sensing mechanism of the composites arises from variation of the interparticle distance in the polymer matrix, which can be achieved by tuning the interaction between particle and brush via variation in the pH value.

10.2 Future perspectives

For the investigation of polymer brush/AuNPs composite materials light is shed onto creating colorimetric sensors with tailored optical properties by changing the interaction strength between polymer and particle as well as between particle and particle during incubation. The stability of brush/AuNPs composites is a crucial point for application purposes. So far, just the leakage of AuNPs in composites was analyzed. But one of the biggest challenges in terms of the daily usage of these composite materials is also the

mechanical stability. Gaining information about elastic properties would provide a good understanding of the response to external stresses and give also a fundamental insight into the nature of those composite materials. Here, force-distance curves by AFM could provide information about the local mechanical responses of polymer brush/AuNP composite materials. Knowledge of the elasticity would be a step forward using these composite materials for daily life.

Also, little is known about the distribution of AuNPs in PNIPAM brushes after an applied electric field and after post-treatment at different pH. NR measurements with contrast variation would help to get more information about the AuNP distribution within the PNIPAM brush. For future studies, improvements has to be made first in order to prevent detachment of polymer material during an applied electric field. In order to prevent degrafting, a copolymer in which the first polymer block attached to the initiator is hydrophobic could be used to hinder degrafting. With that regard, so far no experimental studies are available about the mechanism of the cleavage during an applied electric field.

A complete different approach would be to use the SPR of the incorporated AuNPs to generate heat which dissipates into the environment and induces a collapse of a thermo-responsive polymer matrix (e.g. PNIPAM) in contrary to the use of AuNPs as sensing platform. By using a laser with a wavelength close to the absorption maximum of the SPR of the AuNPs, the radiation energy will be absorbed from the AuNPs and will be transferred to mechanical energy into the environment. By using a thermo-responsive polymer matrix, the emitted heat induces a collapse of the polymer brush and a shrinking of the composite. The control of swelling and collapsing via photothermal heating enables a new field in nanotechnological oriented engineering. Size changes have been already accomplished with PNIPAM based microgels loaded with AuNPs via photothermal heating[182]. In contrast, Backes et al.[183] loaded magnetic particles into PNIPAM based microgels. The uptake of magnetic nanoparticles into the microgels triggered a small response to an external magnetic field. That could also be adapted to polymer brushes. Incorporation of magnetic nanoparticles should induce magnetic properties into the polymer brush systems and could provide a higher response to an external magnetic field.

Although impressive progress has been achieved in the preparation of responsive coatings with unique properties in the last decade, new possibilities are still waiting for further exploration in this field of material science. One important consequence is the technology transfer. With simple fabrication strategies, detection platforms produced in the lab can be more conveniently translated into prototypes and then eventually into working devices suitable for consumer use.

Chapter 11

Appendix

Appendix to chapter 4

Calculations of AuNP amount:

The mass of AuNP (m_{gold}) in 1 mL AuNP suspension is $1.6 \pm 0.4 \cdot 10^{-3}$ g, as derived by gravimetric analysis. In order to calculate the total amount of substance (n_{total}) of AuNPs in 1 mL suspension, the total number of particles (N_{total}) in 1 mL AuNP suspension has to be calculated. This was done by estimating the mass of a single AuNP. Assuming a spherical shape and an uniform face centered cubic (fcc) structure [47] with a AuNP radius (r) of 2.4 nm, the mass of a single AuNP m_{AuNP} was calculated:

$$V_{AuNP} = \frac{4}{3}\pi r^3 \tag{11.1}$$

$$m_{AuNP} = V_{AuNP} \cdot \rho_{fcc\ bulk} \tag{11.2}$$

where V_{AuNP} is the volume of one single AuNP with r = 2.4 nm and $\rho_{fcc\ bulk}$ is the density for fcc gold (19.3 g/cm^3). The mass is $m_{AuNP} = 1.18 \cdot 10^{-18}$ g. The toal number of particles N_{total} were calculated using:

$$N_{total} = \frac{m_{gold}}{m_{AuNP}} \tag{11.3}$$

Thus, the number of particles N_{total} in 1 mL AuNP stock suspension is $1.48 \cdot 10^{15}$. The amount of substance n_{total} in 1 mL AuNP stock suspension is 2.45 nmol and was calculated using the Avogadro constant $N_A = 6.022 \cdot 10^{23}$ mol^{-1}:

$$n_{total} = \frac{N_{total}}{N_A} \tag{11.4}$$

Variation in rate of polymeriaztion by changing the $CuCl/CuCl_2$ ratio:

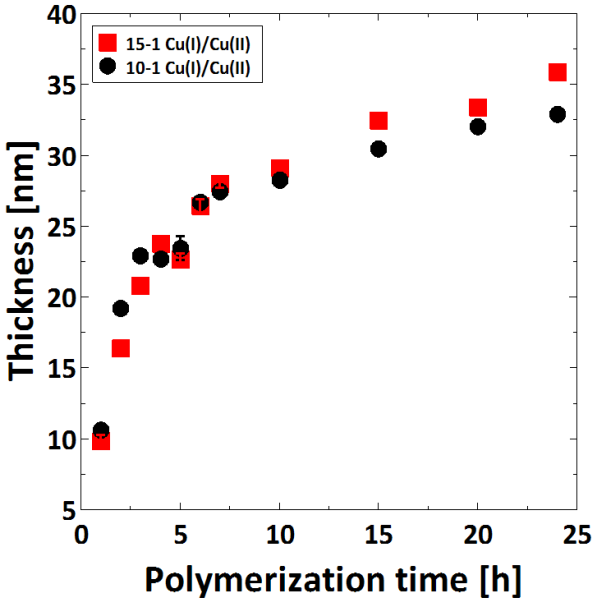

Figure 11.1: Tuning the PMETAC brush thickness by varying the $CuCl/CuCl_2$ ratio. The data are measured at ambient conditions using ellipsometry. The polymer thickness is increasing with polymerization time. Changing the Cu(I)/Cu(II) ratio gave no significant change.

UV/vis spectra before and after incubation in AuNP suspension:

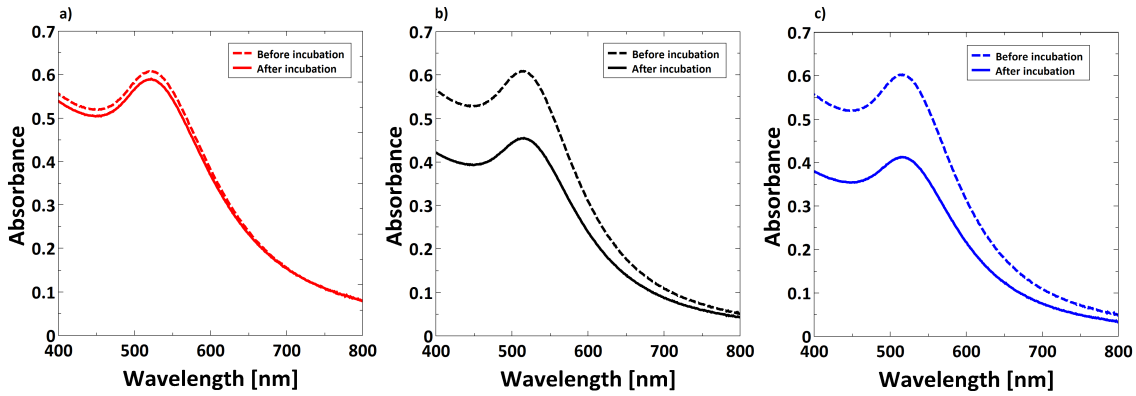

Figure 11.2: UV/Vis spectra before (dashed lines) and after (solid line) incubation of PMETAC brush in AuNP suspension. Shown for composites (**a**) at pH 4; (**b**) at pH 6; and (**c**) at pH 8. A decrease of the UV/Vis absorbance after the incubation was found which increases with increasing pH of the AuNP incubation suspension. The difference before and after the incubation is equal to the amount of AuNPs within the brush since the UV/Vis absorbance is proportional to the concentration of the AuNP suspension.

Appendix to chapter 5

SEM images of PMETAC/AuNP composite materials at pH 4

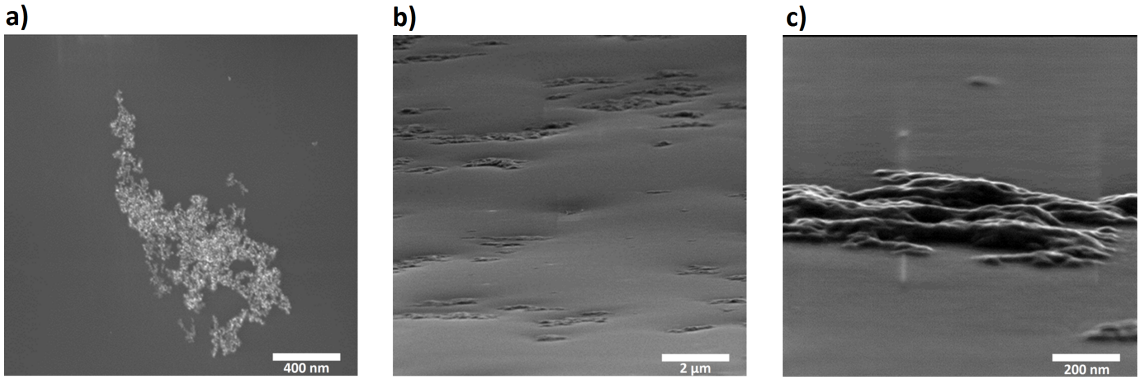

Figure 11.3: SEM images of PMETAC brushes after incubation in AuNP suspension at pH 4. Images as the top-view a) and the side-vied b) and c).

SEM images of PMETAC/AuNP composite materials at pH 8

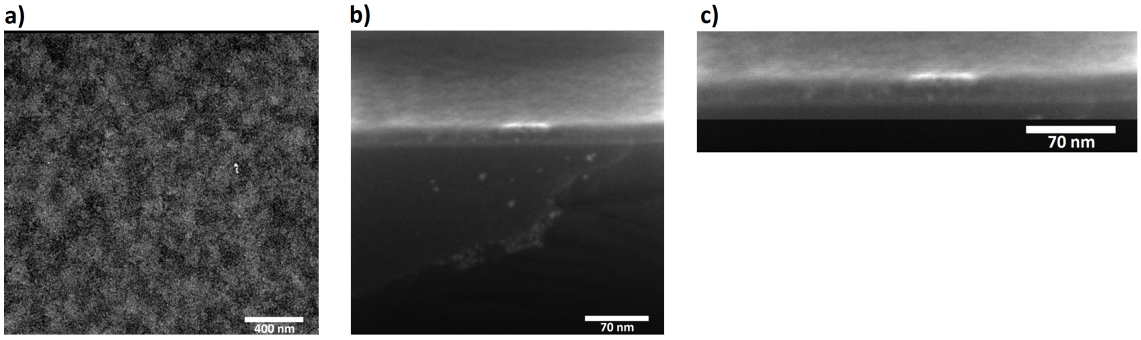

Figure 11.4: SEM images of PMETAC brushes after incubation in AuNP suspension at pH 8. Images as the top-view a) and the side-vied b) and c).

Three-layer-model for XRR

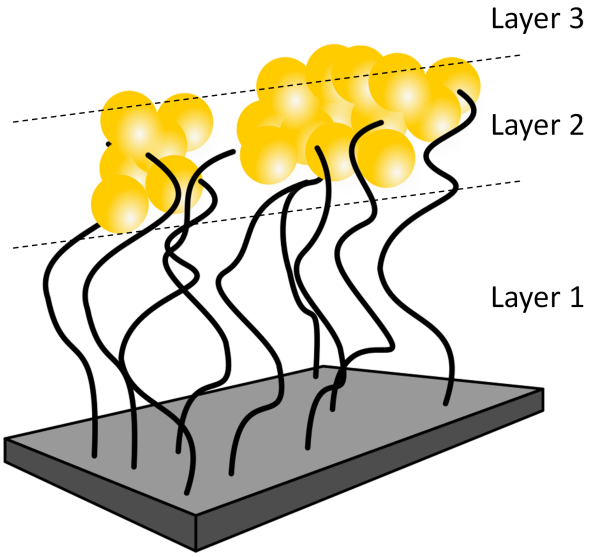

Figure 11.5: Three-layer model for fitting the XRR data after attachment of AuNPs.

XRR data of PMETAC brush incubated in AuNP suspension at pH 4 for 99 %rh. Data has been plotted in $R{\cdot}q^4$ representation for better visualization of features

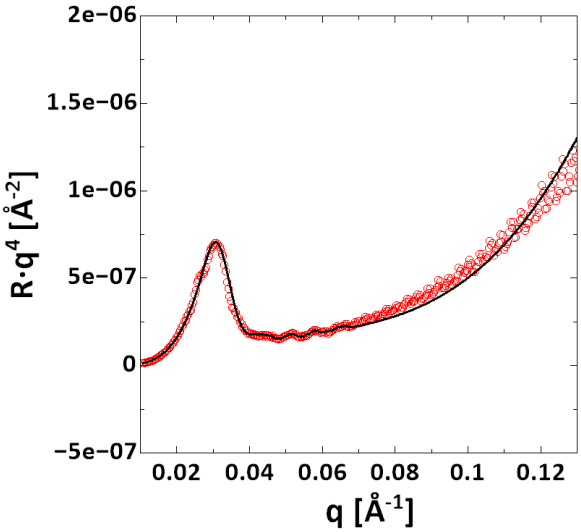

Figure 11.6: XRR data (symbols) and fits (line) for PMETAC/AuNP composite after incubation at pH 4 measured at 99 %r.h.. The data were fitted using a three-layer model. Reflectivity curves and fit are represented as $R{\cdot}q^4$ against q.

XRR data of PMETAC brush incubated in AuNP suspension at pH 4. Data has been fitted using a 2-layer model

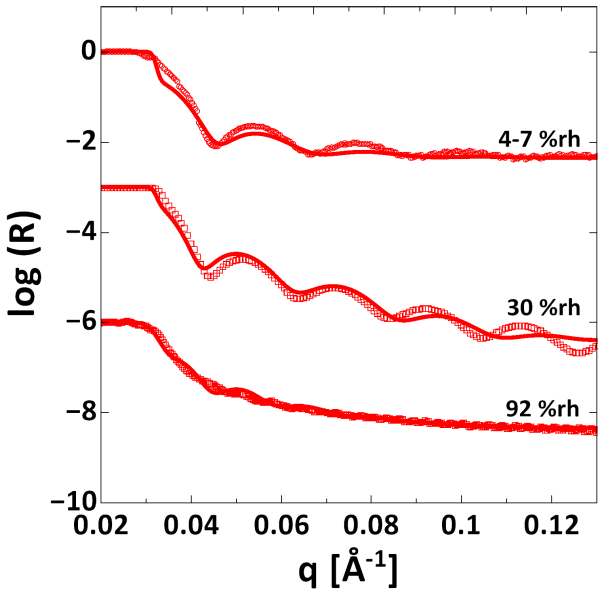

Figure 11.7: XRR data (symbols) and fits (line) for PMETAC/AuNP composite after incubation at pH 4 measured at different %r.h.. The data were fitted using a two-layer model. Reflectivity curves are shifted vertically for clarity

XRR data of PMETAC brushes incubated in AuNP suspension at pH 8. Data has been fitted with a three-layer model

In contrast to the aforementioned composites as well as to the neat PMETAC brush, PMETAC/AuNP composites after incubation at pH 8 show different electron density profiles across the entire brush (Fig. 11.8). Here, layer 1 has the highest electron density, which decreases with increasing humidity. Further, layer 1 has a higher thickness for the brush after AuNP incubation compared to the neat PMETAC brush at the same humidity value. The thickness of layer 1 increases with increasing humidity while the electron density decreases. The electron density for layer 2 is lower than for layer 1 and decreases as well with increasing humidity. Further, the thickness of layer 2 decreases with increasing humidity. The thicknesses and electron densities for layer 3 show no systematic behavior with changing of the humidity level. The sum of the thickness of layer 2 and 3 is smaller than the particle size, indicating less particle protrusion towards the vapor phase.

Table 11.1: Data for PMETAC/AuNP composites after incubation at pH 8 at different %r.h. obtained by XRR measured at room temperature.

	XRR Layer 1		XRR Layer 2		XRR Layer 3	
Humidity [%rh]	h_1 [nm]	ρ_e [Å^{-3}]	h_2 [nm]	ρ_e [Å^{-3}]	h_3 [nm]	ρ_e [Å^{-3}]
4-7	22.1	0.925	2.3	0.714	1.1	0.649
30	24.8	0.886	2.1	0.710	0.6	0.675
92	37.8	0.684	1.9	0.648	0.9	0.531

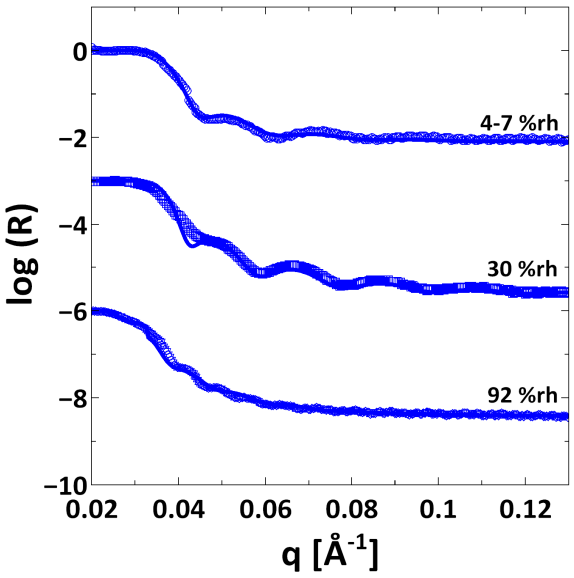

Figure 11.8: XRR data (symbols) and fits (line) for PMETAC/AuNP composite after incubation at pH 8 measured at different %r.h.. The data were fitted using a three-layer model. Reflectivity curves are shifted vertically against each other due to sake of clarity

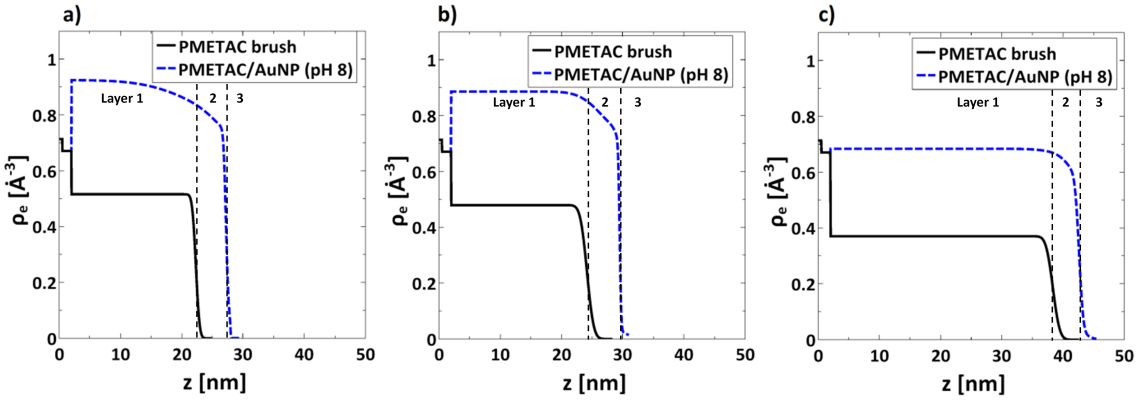

Figure 11.9: Electron density profiles in the z-direction from the substrate surface (z=0) for PMETAC/AuNP composite after incubation at pH 8 (blue broken lines) and neat PMETAC brush (black solid lines) measured at different r.h. for a) 4-7 %rh, b) 30 %rh, and c) 92 %rh

Appendix to chapter 8

AFM and SEM images of PNIPAM brush/AuNP composite materials

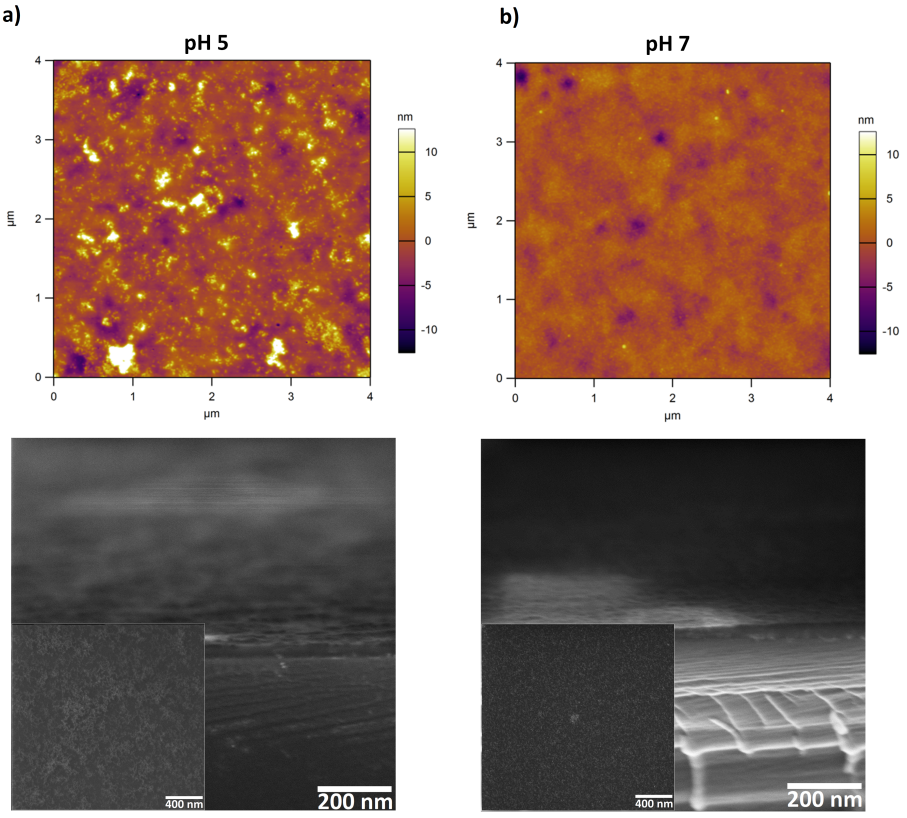

Figure 11.10: AFM height images (upper images) and SEM cross sections (lower images) of composite materials after incubation of PNIPAM brush in AuNP suspension at a) pH 5, and b) pH 7. The inset of each cross section shows a top-view of the composite materials. AFM height images were performed under water and at room temperature while SEM images were recorded in dry state at high vacuum.

Bibliography

[1] Hu, H.; Gopinadhand, M.; Osuji, C. O. *Soft Matter* **2014**, *10*, 3867–3889.

[2] Biesalski, M.; Rühe, J. *Macromolecules* **2003**, *36*, 1222–1227.

[3] Montemor, M. *Surf. Coat. Technol.* **2014**, *258*, 17–37.

[4] Uhlmann, P.; L. Ionov, N. H.; Nitschke, M.; Grundke, K.; Motornov, M.; Minko, S.; Stamm, M. *Prog. Org. Coat* **2006**, *55*, 168–174.

[5] Chen, W.-L.; Cordero, R.; Tran, H.; Ober, C. K. *Macromolecules* **2017**, *50*, 4089–4113.

[6] Azzaroni, O. *J. Polym. Sci. A Polym. Chem.* **2012**, *50*, 3225–3258.

[7] Cao, W.; Cudney, H. H.; Waser, R. *PNAS* **1999**, *96*, 8330–8331.

[8] Biesalski, M.; Johannsmann, D.; Rühe, J. *JCP* **2002**, *117*, 4988–4994.

[9] Willner, I.; Basnar, B.; Willner, B. *Adv. Funct. Mater.* **2007**, *17*, 702–717.

[10] Murdoch, T. J.; Humphreys, B. A.; Willot, J. D.; Prescott, S. W.; Nelson, A.; Webber, G. B.; Wanless, E. J. *J. Colloid Interface Sci.* **2017**, *490*, 869–878.

[11] Zhou, T.; Han, L.; Barbash, D.; Li, C. Y. *Nat. Commun.* **2016**, *7*, 1–8.

[12] Iacono, M.; Connolly, D.; Heise, A. *RSC Adv.* **2017**, *7*, 19976–19981.

[13] Wright, R. A. E.; Wang, K.; Qu, J.; Zhao, B. *Angew. Chem. Int. Ed. Commun.* **2016**, *55*, 8656–8660.

[14] Biesalski, M.; Rühe, J. *Macromolecules* **1999**, *32*, 2309–2316.

[15] Chen, Q. *Langmuir* **2014**, *30*, 8119–8123.

[16] Adiga, S. P.; Brenner, D. W. *J. Funct. Biomater.* **2012**, *3*, 239–256.

[17] Emilsson, G.; Xiong, K.; Sakiyama, Y.; Malekian, B.; Gagner, V. A.; Schoch, R. L.; Lim, R. Y. H.; Dahlin, A. B. *Nanoscale* **2018**, *10*, 4663–4669.

[18] Tokareva, I.; Minko, S.; Fendler, J. H.; Hutter, E. *J. Am. Chem. Soc.* **2004**, *126*, 15950–15951.

[19] Loschonsky, S.; Shroff, K.; Wörz, A.; Prucker, O.; Rühe, J.; Biesalski, M. *Biomacromolecules* **2008**, *9*, 543–552.

[20] Patel, A. K.; Sharma, P. S.; Prasad, B. B. *Mater. Sci. Eng. C* **2009**, *29*, 1545–1553.

[21] Shen, Y.; Li, G.; Ma, Y.; Yu, D.; Sun, J.; Li, Z. *Soft Matter* **2015**, *11*, 7502–7506.

[22] Zhou, F.; Huck, W. T. S. *Phys. Chem. Chem. Phys.* **2006**, *8*, 3815–3823.

[23] Wang, J.-S.; Matyjaszweski, K. *J. Am. Chem. Soc.* **1995**, *117*, 5614–5615.

[24] Xia, J.; Gaynor, S. G.; Matyjaszweski, K. *Macromolecules* **1998**, *31*, 5958–5959.

[25] Robinson, K. L.; Khan, M. A.; de Paz Báñez, M. V.; Wang, X. S.; Armes, S. P. *Macromolecules* **2001**, *34*, 3155–3158.

[26] Jones, D. M.; Huck, W. T. S. *Adv. Mater.* **2001**, *13*, 1256–1259.

[27] Huang, W.; Kim, J.-B.; Bruening, M. L.; Baker, G. L. *Macromolecules* **2002**, *35*, 1175–1179.

[28] Zhao, B.; Brittain, W. J. *Prog. Polym. Sci.* **2000**, *25*, 677–710.

[29] Turgman-Cohen, S.; Genzer, J. *Macromolecules* **2010**, *43*, 9567–9577.

[30] Higaki, Y.; Kobayashi, M.; Murakami, D.; Takahara, A. *Polym. J.* **2016**, *85*, 325–331.

[31] Kobayashi, M.; Terayama, Y.; Yamaguchi, H.; Terada, M.; Murakami, D.; Ishihara, K.; Takahara, A. *Langmuir* **2012**, *28*, 7212–7222.

[32] Guo, S.; Janczewski, D.; Zhu, X.; Quintana, R.; He, T.; Neoh, K. G. *J. Colloid Interface Sci.* **2015**, *452*, 43–53.

[33] Alexander, S. *J. Phys. France* **1977**, *38*, 983–987.

[34] Gennes, P. D. *J. Phys.* **1976**, *37*, 1445–1452.

[35] Gennes, P. D. *Macromolecules* **1980**, *13*, 1069–1075.

[36] Birshtein, T. M.; Zhulina, E. B. *Polymer* **1984**, *25*, 1453–1461.

[37] Halperin, A. *J. Phys. (Paris)* **1988**, *49*, 547–550.

[38] Halperin, A.; Zhulina, E. B. *Macromolecules* **1991**, *24*, 5393–5397.

[39] Zhulina, E. B.; Borisov, O. V.; Pryamitsyn, V. A.; Birshtein, T. M. *Macromolecules* **1991**, *24*, 140–149.

[40] Lai, P. Y.; Halperin, A. *Macromolecules* **1991**, *24*, 4981–4982.

[41] Milner, S. T.; Witten, T. A.; Cates, M. E. *Macromolecules* **1988**, *21*, 2610–2619.

[42] Milner, S. T. *EPL Europhys. Lett.* **1988**, *7*, 695.

[43] Milner, S. T.; Witten, T. A.; Cates, M. E. *Macromolecules* **1989**, *22*, 853–861.

[44] Skvortsov, A. M.; Pavlushkov, I. V.; Gorbunov, A. A.; Zhulina, Y. B.; Borisov, O. V.; Pryamitsyn, V. A. *Polym. Sci. U.S.S.R* **1988**, *30*, 1706–1715.

[45] Zhulina, Y. B.; Semenov, A. N. *Polym. Sci. U.S.S.R* **1989**, *31*, 196–205.

[46] Milner, S. T. *Science* **1991**, *251*, 905–914.

[47] Brittain, W. J.; Minko, S. *J. Polym. Sci. A* **2007**, *45*, 3505–3512.

[48] Dumont, E. L. P.; Belmast, H.; Hess, H. *Langmuir* **2013**, *29*, 15142–15145.

[49] Zhang, T.; Chen, T.; Amin, I.; Jordan, R. *Polym. Chem.* **2014**, *5*, 4790–4796.

[50] Biesalski, M.; Johannsmann, D.; Rühe, J. *JCP* **2004**, *120*, 8807–8814.

[51] Biesalski, M.; Rühe, J. *Macromolecules* **2002**, *35*, 499–507.

[52] Pincus, P. *Macromolecules* **1991**, *24*, 2912–2919.

[53] Mizutani, A.; Kikuchi, A.; Yamato, M.; Kanazawa, H.; Okano, T. *Biomaterials* **2008**, *29*, 2073–2081.

[54] Lian, C.; Wang, L.; Chen, X.; Han, X.; Thao, S.; Liu, H.; Hu, Y. *Langmuir* **2014**, *30*, 4040–4048.

[55] Louquet, S.; Rousseau, B.; Epherre, R.; Guidolin, N.; Goglio, G.; Mornet, S.; Duguet, E.; Lecommandoux, S.; Schatz, C. *Poly. Chem.* **2012**, *3*, 1408–1417.

[56] Jia, H.; Wildes, A.; Titmuss, S. *Macromolecules* **2012**, *45*, 305–312.

[57] Sudre, G.; Hourdet, D.; Creton, C.; Cousin, F.; Tran, Y. *Langmuir* **2014**, *30*, 9700–9706.

[58] de Groot, G. W.; Santonicola, M. G.; Sugihara, K.; Zambelli, T.; Reimhult, E.; Vörös, J.; Vancso, G. J. *ACS Appl. Mater. Inter.* **2013**, *5*, 1400–1407.

[59] Delcroix, M. F.; Demoustier-Champagne, S.; Dupont-Gillain, C. C. *Langmuir* **2014**, *30*, 268–277.

[60] Biesalski, M.; Rühe, J. *Macromolecules* **2004**, *37*, 2196–2202.

[61] Zhulina, E. B.; Leermakers, F. A. M. *Biophys. J.* **2007**, *93*, 1452–1463.

[62] Willot, J. D.; Murdoch, T. J.; Humphreys, B. A.; Edmondson, S.; Webber, G. B.; Wanless, E. J. *Langmuir* **2014**, *30*, 1827–1836.

[63] Beer, S. D.; Kutnyanszky, E.; Schön, P. M.; Vancso, G. J.; Müser, M. H. *Nat. Commun.* **2014**, *5*, 1–6.

[64] Lappala, A.; Mendiratta, S.; Terentjev, E. M. *Macromolecules* **2015**, *48*, 1894–1900.

[65] Karim, A.; Satija, S. K.; Douglas, J. F.; Ankner, J. F.; Fetters, L. J. *Phys. Rev. Lett.* **1994**, *73*, 3407–3410.

[66] Diamanti, S.; Arifuzzaman, S.; Genzer, J.; Vaia, A. *ACS Nano* **2009**, *3*, 807–818.

[67] Motornov, M.; Tam, T. K.; Pita, M.; Tokarev, I.; Katz, E.; Minko, S. *Nanotechnology* **2009**, *20*, 434006.

[68] Bajpai, A. K.; Shukla, S. K.; Bhanu, S.; Kankane, S. *Prog. Polym. Sci.* **2008**, *33*, 1088–1118.

[69] Galvin, C. J.; Genzer, J. *Prog. Polym. Sci* **2012**, *37*, 871–906.

[70] M. A. C. Stuart, W. T. H.; Genzer, J.; Müller, M.; Ober, C.; Stamm, M.; Sukhorukov, G. B.; Szleifer, I.; Tsukruk, V. V.; Urban, M.; Winnik, F.; Zauscher, S.; Luzinov, I.; Minko, S. *Nat. Mater.* **2010**, *9*, 101–113.

[71] Luzinov, I.; Minko, S.; Tsukruk, V. V. *Soft Matter* **2008**, *4*, 714–725.

[72] Amendola, V.; Pilot, R.; Frasconi, M.; Marago, O. M.; Iati, M. A. *J. Phys. Condens. Matter* **2017**, *29*, 203002.

[73] Peteiro-Cartelle, J.; Rodriguez-Pedreira, M.; Zhang, F.; Gil, P. R.; del Mercato, L. L.; Parak, W. J. *Nanomedicine* **2009**, *4*, 967–979.

[74] Batley, G. E.; Kirby, J. K.; McLaughlin, M. J. *Acc. Chem. Res.* **2013**, *46*, 854–862.

[75] Turkevich, J.; Stevenson, P. C.; Hillier, J. *Discuss. Faraday Soc.* **1951**, *11*, 55–75.

[76] Frens, G. *Nature: Phys. Sci.* **1973**, *241*, 20–22.

[77] Brust, M.; Walker, M.; Bethell, D.; Schiffrin, D. J.; Whyman, R. *J. Chem. Soc., Chem. Commun.* **1994**, *241*, 801–802.

[78] Sau, T. K.; Rogach, A. L.; Jäckel, F.; Klar, T. A.; Feldmann, J. *Adv. Mater.* **2010**, *22*, 1805–2185.

[79] Khlebtsov, N.; Dykman, L. *Chem. Soc. Rev.* **2011**, *40*, 1647–1671.

[80] Yeh, Y.-C.; Creran, B.; Rotello, V. M. *Nanoscale* **2012**, *4*, 1871–1880.

[81] Hu, M.; Chen, J.; Li, Z.-Y.; Au, L.; Hartland, G. V.; Li, X.; Marquez, M.; Xia, Y. *Chem. Soc. Rev.* **2006**, *35*, 1084–1094.

[82] Underwood, S.; Mulvaney, P. *Langmuir* **1994**, *10*, 3427–3430.

[83] Mie, G. *Ann. Phys. (Berl.)* **1908**, *330*, 377–445.

[84] Schmitt, J.; Mächtle, P.; Eck, D.; Möhwald, H.; Helm, C. A. *Langmuir* **1999**, *15*, 3256–3266.

[85] Ghosh, S. K.; Pal, T. *Chem. Rev.* **2007**, *107*, 4797–4862.

[86] Lupitskyy, R.; Motornov, M.; Minko, S. *Langmuir* **2008**, *24*, 8976–8980.

[87] Mulvaney, P. *Langmuir* **1996**, *12*, 788–800.

[88] Gehan, H.; Fillaud, L.; Chehimi, M.; Aubard, J.; Hohenau, A.; Felidj, N.; Mangeney, C. *ACS Nano* **2010**, *4*, 6491–6500.

[89] Yenice, Z.; Schön, S.; Bildirir, H.; Genzer, J.; von Klitzing, R. *J. Phys. Chem. B* **2015**, *119*, 10348–10358.

[90] Christau, S.; Thurandt, S.; Yenice, Z.; von Klitzing, R. *Polym. (Basel)* **2014**, *6*, 1877–1896.

[91] Christau, S.; Yenice, Z.; Genzer, J.; von Klitzing, R. *Langmuir* **2014**, *30*, 13033–13041.

[92] Solis, F. J.; Tang, H. *Macromolecules* **1996**, *29*, 7953–7959.

[93] Currie, E. P. K.; van der Gucht, J.; Borisov, O. V.; Stuart, M. A. C. *Langmuir* **1998**, *14*, 5740–5750.

[94] Currie, E. P. K.; van der Gucht, J.; Borisov, O. V.; Stuart, M. A. C. *Pure Appl. Chem.* **1999**, *71*, 1227–1241.

[95] Kim, J. U.; O'Shaughnessy, B. *Phys. Rev.* **2002**, *89*, 238301–1–238301–4.

[96] Kim, J. U.; O'Shaughnessy, B. *Macromolecules* **2006**, *39*, 413–425.

[97] Halperin, A.; Kröger, M.; Zhulina, E. B. *Macromolecules* **2011**, *44*, 3622–3638.

[98] Halperin, A.; Kröger, M. *Langmuir* **2009**, *25*, 11621–11634.

[99] Zhulina, E. B.; Rubinstein, M. *Macromolecules* **2014**, *47*, 5825–5838.

[100] Opferman, M. G.; Coalson, R. D.; Jasnow, D.; Zilman, A. *Phys. Rev. E* **2012**, *86*, 031806.

[101] Pileni, M. P. *Appl. Sur. Sci.* **2001**, *171*, 1–14.

[102] Paczesny, J.; Wojcik, M.; Sozanski, K.; Nikiforov, K.; Tschierske, C.; Lehmann, A.; Gorecka, E.; Mieczkowski, J.; Holyst, R. *J. Phys. Chem. C* **2013**, *117*, 24056–24062.

[103] Christau, S.; Möller, T.; Brose, F.; Genzer, J.; Soltwedel, O.; von Klitzing, R. *Polymer* **2016**, *98*, 454–463.

[104] Bhat, R. R.; Genzer, J.; Chaney, B. N.; Sugg, H. W.; Liebmann-Vinson, A. *Nanotechnology* **2003**, *14*, 1145–1152.

[105] Zhang, Z.; Sebe, G.; Wang, X.; Tam, K. C. *Carbohydr. Polym.* **2018**, *182*, 61–68.

[106] Fortin, N.; Klok, H.-A. *ACS Appl. Mater. Interfaces* **2015**, *7*, 4631–4640.

[107] Tokarev, I.; Tokareva, I.; Minko, S. *ACS appl. Mater. Interfaces* **2011**, *3*, 143–146.

[108] Ferhan, A. R.; Guo, L.; Zhou, X.; Chen, P.; Hong, S.; Kim, D.-H. *Anal. Chem.* **2013**, *85*, 4094–4099.

[109] Gupta, S.; Agrawal, M.; Uhlmann, P.; Simon, F.; Stamm, M. *Chem. Mater.* **2010**, *22*, 504–509.

[110] Laurent, P.; Souharce, G.; Duchet-Rumeau, J.; Portinha, D.; Charlot, A. *Soft Matter* **2012**, *8*, 715.

[111] Moya, S.; Azzaroni, O.; Kelby, T.; Donath, E.; Huck, W. *J. Phys. Chem. B* **2007**, *111*, 7034–7040.

[112] Christau, S.; Möller, T.; Genzer, J.; Köhler, R.; von Klitzing, R. *Macromolecules* **2017**, *50*, 7333–7343.

[113] Xue, L.; Agarwal, U. S.; Lemstra, P. J. *Macromolecules* **2002**, *35*, 8650–8652.

[114] Ivanov, M. R.; Bednar, H. R.; Haes, A. J. *ACS Nano* **2009**, *3*, 386–394.

[115] Reincke, F.; Kegel, W. K.; Zhang, H.; Nolte, M.; Wang, D.; Vanmaekelbergh, D.; Ohwald, H. M.; Möhwald, H. *Phys. Chem. Chem. Phys.* **2006**, *8*, 3828–3835.

[116] Balzer, B. N.; Micciulla, S.; Dodoo, S.; Zerball, M.; Gallei, M.; Rehan, M.; von Klitzing, R.; Hugel, T. *ACS Appl. Mater. Interfaces* **2013**, *5*, 6300–6306.

[117] Üzüm, C.; Hellwig, J.; Madaboosi, N.; Volodkin, D.; von Klitzing, R. *Beilstein J. Nanotechnol.* **2012**, *3*, 778–788.

[118] Heavens, O. S. *Rep. Prog. Phys.* **1960**, *23*, 1–65.

[119] Nelson, A. *J. Appl. Crystallogr.* **2006**, *39*, 273–276.

[120] Trapp, M.; Steitz, R.; Kreuzer, M.; Strobl, M.; Rose, M.; Dahint, R. *Rev. Sci. Instrum.* **2016**, *78*, 105112.

[121] Strobl, M.; Steitz, R.; Kreuzer, M.; Rose, M.; Herrlich, H.; Mezei, F.; Grunze, M.; Dahint, R. *Rev. Sci. Instrum.* **2011**, *82*, 055101.

[122] für Materialien und Energie, H.-Z. B. *JLSRF* **2017**, *3*, A114.

[123] Micciulla, S.; Gerelli, Y.; Campbell, R. A.; Schneck, E. *Langmuir* **2018**, *34*, 789–800.

[124] Schneck, E.; Schollier, A.; Halperin, A.; Moulin, M.; Härtlein, M. *Langmuir* **2013**, *29*, 14178–14187.

[125] Schneck, E.; Berts, I.; Halperin, A.; Daillant, J.; Fragneto, G. *Biomaterials* **2015**, *46*, 95–104.

[126] Parratt, L. G. *Phys. Rev.* **1954**, *95*, 359–369.

[127] Bhat, R. R.; Genzer, J. *Appl. Surf. Sci.* **2006**, *252*, 2549–2554.

[128] Sperling, R. A.; Parak, W. J. *Phil. Trans. R. Soc. A* **2010**, *368*, 1333–1383.

[129] Liu, X.; Atwater, M.; Wang, J.; Huo, Q. *Colloids Surf., B* **2007**, *58*, 3–7.

[130] Bhat, R. R.; Tomlinson, M. R.; Wu, T.; Genzer, J. *Adv. Polym. Sci.* **2006**, *198*, 51–124.

[131] Reinhard, M. B.; Siu, M.; Agarwal, H.; Alivisatos, A. P.; Liphardt, J. *Nano Lett.* **2005**, *5*, 2246–2252.

[132] Kizhakkedathu, J. N.; Janzen, J.; Le, Y.; Kainthan, R. K.; Brooks, D. E. *Langmuir* **2009**, *25*, 3794–3801.

[133] Bain, E. D.; Dawes, K.; Özcam, A. E.; Hu, X.; Gorman, C. B.; Srogl, J.; Genzer, J. *Macromolecules* **2012**, *45*, 3802–3815.

[134] Klok, H.-A.; Genzer, J. *ACS Macro Lett.* **2015**, *4*, 636–639.

[135] Gong, P.; Genzer, J.; Szleifer, I. *Phys. Rev. Lett.* **2007**, *98*, 1–4.

[136] Lim, I.-I. S.; Pan, Y.; Mott, D.; Ouyang, J.; Njoki, P. N.; Luo, J.; Zhou, S.; Zhong, C.-J. *Langmuir* **2007**, *23*, 10715–10724.

[137] Kesal, D.; Christau, S.; Krause, P.; Möller, T.; von Klitzing, R. *Polym. (Basel)* **2016**, *8*, 134.

[138] Dunlop, I. E.; Thomas, R. K.; Titmus, S.; Osborne, V.; Edmondson, S.; Huck, W. T. S.; Klein, J. *Langmuir* **2012**, *28*, 3187–3193.

[139] Krasteva, N.; Krustev, R.; Yasuda, A.; Vossmeyer, T. *Langmuir* **2003**, *19*, 7754–7760.

[140] Kobayashi, M.; Terayama, Y.; Hinzo, M.; Ishihara, K.; Takahara, A. *JPCS* **2009**, *184*, 012010.

[141] Ramos, J. J. I.; Moya, S. E. *Macromol. Rapid Commun.* **2011**, *32*, 1972–1978.

[142] Bolze, J.; Takahasi, M.; Mizuki, J.; Baumgart, T.; Knoll, W. *J. Am. Chem. Soc.* **2002**, *124*, 9412–9421.

[143] M. Zerball, A. L.; von Klitzing, R. *J. Phys. Chem. B* **2015**, *119*, 11879–11886.

[144] Patil, R.; Turgman-Cohen, S.; Šrogl, J.; Kiserow, D.; Genzer, J. *Langmuir* **2015**, *31*, 2372–2381.

[145] Yan, J.; Pan, X.; Wang, Z.; Zhang, J.; Matyjaszewski, K. *Macromolecules* **2016**, *49*, 9283–9286.

[146] Steels, B. M.; Koska, J.; Haynes, C. A. *J. Chromatogr. B* **2000**, *743*, 41–56.

[147] Hinterwirth, H.; Kappel, S.; Waitz, T.; Prohaska, T.; Lindner, W.; Lämmerhofer, M. *ACS Nano* **2013**, *7*, 1129–1136.

[148] Rodriguez-Loureiro, I.; Scoppola, E.; Bertinetti, L.; Barbetta, A.; Fragneto, G.; Schneck, E. *Soft Matter* **2017**, *13*, 5767–5777.

[149] Löhmann, O.; Micciulla, S.; Soltwedel, O.; Schneck, E.; von Klitzing, R. *Macromolecules* **2018**, *51*, 2996–3005.

[150] Andrieu-Brunsen, A.; Micoureau, S.; Tagliazucchi, M.; Szleifer, I.; Azzaroni, O.; Soler-Illia, G. J. A. A. *Chem. Mater.* **2015**, *27*, 808–821.

[151] Galvin, C. J.; Bain, E. D.; Henke, A.; Genzer, J. *Macromolecules* **2015**, *48*, 5677–5687.

[152] Li, Y.; Ko, Y.; Lin, Y.; Kiserow, D.; Genzer, J. *Macromolecules* **2017**, *50*, 8580–8587.

[153] Melzak, K. A.; Yu, K.; Bo, D.; Kizhakkedathu, J. N.; Toca-Herrera, J. L. *Langmuir* **2015**, *31*, 6463–6470.

[154] Kesal, D.; Christau, S.; Trapp, M.; Krause, P.; von Klitzing, R. *PCCP* **2017**, *8*, 134.

[155] Matyjaszewski, K.; Wei, M.; Xia, J.; Gaynor, S. G. *Macromol. Chem. Phys.* **1998**, *199*, 2289–2292.

[156] Zhang, H.; Klumperman, B.; Ming, W.; Fischer, H.; van der Linde, R. *Macromolecules* **2001**, *34*, 6169–6173.

[157] Chu, X.; Yang, J.; Liu, G.; Zhao, J. *Soft Matter* **2014**, *10*, 5568–5578.

[158] Galvin, C. J.; Dimitrious, M. D.; Satija, S. K.; Genzer, J. *J. Am. Chem. Soc.* **2014**, *136*, 12737–12745.

[159] Martinez, A. P.; Carrillo, J.-M.-Y.; Dobrynin, A. V.; Adamson, D. H. *Macromolecules* **2016**, *49*, 547–553.

[160] Adroher-Benitez, I.; Moncho-Jorda, A.; Dzubiella, J. *Langmuir* **2017**, *33*, 4567–4577.

[161] Z. Yenice, Z.; Schön, S.; Bildirir, H.; Genzer, J.; von Klitzing, R. *J. Phys. Chem. B* **2015**, *119*, 10348–10358.

[162] Jain, P. K.; El-Sayed, M. A. *Chem. Phys. Lett.* **2010**, *4-6*, 153–164.

[163] Lange, H.; Juarez, B. H.; Carl, A.; Richter, M.; Bastus, N. G.; Weller, H.; Thomsen, C.; von Klitzing, R.; Knorr, A. *Langmuir* **2012**, *28*, 8862–8866.

[164] Atay, T.; Song, J.-H.; Nurmikko, A. V. *Nano Lett.* **2004**, *4*, 1627–1631.

[165] Griffiths, D. J. *Introduction to Electrodynamics*, 3rd ed.; Prentice Hall: Upper Saddle River, New Jersey, 1999.

[166] Sih, B. C.; Wolf, M. O. *J. Phys. Chem. B* **2006**, *110*, 22298–22301.

[167] Jonsson, M.; Linse, P. *J. Chem. Phys.* **2001**, *115*, 3406–3418.

[168] Wallin, T.; Linse, P. *J. Phys. Chem. B* **1997**, *101*, 5506–5513.

[169] Wallin, T.; Linse, P. *J. Chem. Phys.* **1998**, *109*, 5089–5100.

[170] Jenkins, J. A.; Zhou, Y.; Thota, S.; Tian, X.; Zhao, X.; Zou, S.; Zhao, J. *J. Phys. Chem. C* **2014**, *118*, 26276–26283.

[171] Mitsuishi, M.; Koishikawa, Y.; Tanaka, H.; Sato, E.; Mikayama, T.; Matsui, J.; Miyashita, T. *Langmuir* **2007**, *23*, 7472–7474.

[172] Galvin, C. J.; Genzer, J. *Macromolecules* **2016**, *49*, 4316–4329.

[173] Leonforté, F.; Müller, M. *Macromolecules* **2016**, *49*, 5256–5265.

[174] Heine, D.; Wu, D. T. *J. Chem. Phys.* **2001**, *114*, 5313–5321.

[175] Weir, M. P.; Heriot, S. Y.; Martin, S. J.; Parnell, A. J.; Holt, S. A.; Webster, J. R. P.; Jones, R. A. L. *Langmuir* **2011**, *27*, 11000–11007.

[176] Cantini, E.; Wang, X.; Koelsch, P.; Preece, J. A.; Ma, J.; Mendes, P. M. *Acc. Chem. Res.* **2016**, *49*, 1223–1231.

[177] Dunderdale, G. J.; Fairclough, J. P. A. *Langmuir* **2013**, *29*, 3628–3635.

[178] Drummond, C. *Phys. Rev. Lett.* **2012**, *109*, 154302.

[179] Tugulu, S.; Klok, H.-A. *Biomacromolecules* **2008**, *9*, 906–912.

[180] Bratsch, S. G. *J. Phys. Chem. Ref. Data* **1989**, *18*, 1–12.

[181] Johansson, A.; Kollman, P.; Rothenberg, S.; McKelvey, J. *J. Am. Chem. Soc.* **1974**, *96*, 3794–3800.

[182] Lehmann, M.; Tabaka, W.; Oppermann, A.; Wöll, D.; Volodkin, D.; Wellert, S.; von Klitzing, R. *Langmuir* **2018**, *34*, 3597–3603.

[183] Backes, S.; Witt, M. U.; Roeben, E.; Kuhrts, L.; Aleed, S.; Schmidt, A. M.; von Klitzing, R. *Chem. Mater.* **2015**, *119*, 12129–12137.